Regulation of inflammatory TLR signalling by the BCAP adaptor

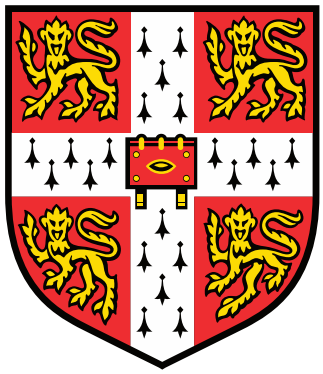

Johannes Uwe Lauenstein

Department of Biochemistry
University of Cambridge

This dissertation is submitted for the degree of
Doctor of Philosophy

Christ's College June 2019

Declaration

This thesis is the result of my own work except where specific reference is made to the work of others. This thesis also includes nothing which is the outcome of work done in collaboration except where specified in the text. This work has not been submitted in whole or in part to the University of Cambridge or any other university for the purpose of obtaining a degree or other qualification. This dissertation contains fewer than 60,000 words or 300 pages.

Johannes Uwe Lauenstein

June 2019

Abstract

BCAP is a PI3K adaptor protein in TLR, BCR and IL-1R and TCR signalling. In TLR signalling, BCAP acts as a negative regulator of inflammatory signalling. Regulation of TLR signalling is essential as overstimulation can cause excessive and pathological inflammation, which leads to serious illnesses such as sepsis and rheumatoid arthritis.

Through an N-terminal TIR domain, BCAP interacts with the MAL and MyD88 adaptors downstream of TLR activation. BCAP then recruits PI3K and PLC-$\gamma 2$ to the TLR signalosome. Although these proteins can facilitate negative regulation of TLRs by endocytosis, the mechanism by which BCAP dampens TLR signalling remains elusive. The first aim of this thesis is to determine the minimal domain requirements and stoichiometry of BCAP TIR domain interactions. The second aim is to characterise and further explore the BCAP interactome, in the context of TLR and BCR signalling. Identification of novel interaction partners and a more detailed understanding of existing interactions, including PI3K and PLC-$\gamma 2$, is crucial in understanding the function of BCAP in various signalling pathways.

An integrated structural and functional approach was used to study the mechanism of BCAP TIR domain interactions. Co-immunoprecipitation was used to show that the BCAP TIR domain associates with MAL, but does not dampen NF-κB signalling in reporter assays. For this negative regulation of TLR signalling, the BCAP DBB domain is essential. A crystal structure of the DBB domain in combination with SEC-MALS revealed that the DBB domain functions as a dimerisation region. First shown in NF-κB reporter assays, DBB domain dimerisation also prevents MAL TIR domain interactions *in vitro*. These results support a new model of steric inhibition of TIR domain interactions, by which BCAP negatively regulates TLR signalling.

An investigation of BCAP post-translational modifications revealed that the tyrosine kinases BTK, LYN and SYK, and the serine kinase CSNK2A1 contribute to BCAP hyperphosphorylation. A virotrap interaction screen identified a number of proteins including Grb2 and CRKL as new adaptor proteins in the BCAP interactome. Subsequent validation in mammalian cells via co-immunoprecipitation showed that Grb2 is a direct interaction partner of BCAP. Further characterization of all SH2 and SH3 domain-containing proteins in the BCAP interactome revealed an extensive network of SH2 and SH3 domain interactions as well as the specific interaction sites. In conclusion, these results indicate that BCAP is a complex hub that integrates multiple immune signalling pathways.

Table of Contents

List of Abbreviations

ABD	Adaptor-binding domain
ADPR	Adenosine diphosphate ribose
AIM2	Absent in melanoma 2
Akt	Protein kinase B
AMP	Adenosine monophosphate
ANK	Ankyrin repeat domain
AP-1	Activator protein 1
ASC	Apoptosis-associated speck-like protein containing a CARD
ATF3	AMP-dependent transcription factor 3
BANK1	B cell scaffold protein with ankyrin repeats
BCAP	B cell adaptor protein
$BCAP_L$	B cell adaptor protein, long isoform
$BCAP_S$	B cell adaptor protein, short isoform
BCR	B cell receptor
BSA	Bovine serum albumin
BTK	Bruton's tyrosine kinase
BTpA	Brucella TIR-containing protein A
Abl	Abelson-related gene
C-SH2	C-terminal Src homology 2 domain
CAMTA	Calmodulin-binding transcription activator
CARD	Caspase recruitment domain
CD	Cluster of differentiation
cGAS	Cyclic GMP-AMP synthase
CLR	C-type lectin receptors
Co-IP	Co-immunoprecipitation
CRKL	CT10 Regulator of kinase (Crk)-like protein
Cryo-EM	Cryo-electron microscopy
CSNK	Casein kinase
DAG	Diacylglycerol
DAMP	Danger associated molecular pattern
DAP12	DNAX-activation protein 12

DAPI	4′,6-diamidino-2-phenylindole
DBB	Dof/BCAP/BANK1 domain
DBD	DNA binding domain
DD	Death domain
DMSO	Dimethyl sulfoxide
dNTP	Deoxyribonucleotide triphosphate
DOCK2	Dedicator of cytokinesis 2
DSS	Dextran sodium sulphate
DTT	Dithiothreitol
Ebf1	Early B cell factor-1
eDHFR	*E. coli* dihydrofolate reductase
EDTA	Ethylenediaminetetraacetic acid
ER	Endoplasmic reticulum
ESCRT	Endosomal sorting complexes required for transport
FCS	Foetal calf serum
FoxO1	Forkhead box O1
FPLC	Fast protein liquid chromatography
GAG	Group-specific antigen
GMP	Guanosine monophosphate
GRB2	Growth factor receptor-bound 2
GSK-3	Glycogen synthase kinase-3
GST	Glutathione S-transferase
HEK	Human embryonic kidney
HEPES	4-(2-Hydroxyethyl)-1-piperazineethanesulfonic acid
HIN	Hematopoietic interferon-inducible nuclear antigens
HPLC	High-performance liquid chromatography
I3C	5-Amino-2,4,6-triiodoisophthalic acid
ICOS	Inducible T cell co-stimulator
IFN	Interferon
IKK	IκB kinase
IL	Interleukin
IL-1RAPL	Interleukin 1 receptor accessory protein like
IMAC	Immobilised metal affinity chromatography

IP3	Inositol-3-phosphate
IPTG	Isopropyl β-D-1-thiogalactopyranoside
IRAK	Interleukin-1 receptor-associated kinase
IRF	Interferon regulatory factor
ITK	IL2-inducible T cell kinase
IκB	I kappa B
kb	Kilobases
LB	Lysogeny broth
LIC	Ligation-independent cloning
LPS	Lipopolysaccharide
LRR	Leucin-rich repeat
LYN	Lck/Yes novel tyrosine kinase
MAL	MyD88-adaptor-like
MALDI	Matrix assisted laser desorption ionization
MALS	Multi-angle light scattering
MAPK	Mitogen-activated-protein kinase
MAVS	Mitochondrial antiviral-signalling
MBP	Maltose-binding protein
MD2	Myeloid differentiation 2
MDA5	Melanoma differentiation-associated protein 5
MS	Mass spectrometry
mTOR	Mammalian target of rapamycin
MW	Molecular weight
MyBP	Myelin basic protein
MyD88	Myeloid differentiation primary response protein 88
N-SH2	N-terminal Src homology 2 domain
NAD	Nicotinamide adenine dinucleotide
NAIP2	NLR family apoptosis inhibitory protein 2
NB	Nucleotide-binding
Nck	Non-catalytic region of tyrosine kinase adaptor protein
NF-κB	Nuclear factor-kappa B
NFAT	Nuclear factor of activated T cells
NK	Natural killer

NLR	NOD-like receptors
NOD	Nucleotide binding and oligomerization domain
NTA	Nitrilotriacetic acid
OAS	Oligoadenylate synthase
PAMP	Pathogen-associated molecular pattern
PBS	Phosphate-buffered saline
PCR	Polymerase chain reaction
PDK1	3-Phosphoinositide-dependent protein kinase-1
PEI	Polyethylenimine
PH	Pleckstrin homology domain
PI(3,4,5)P3	Phosphatidylinositol-3,4,5-trisphosphate
PI(3)P	Phosphatidylinositol-3-phosphate
PI(4,5)P2	Phosphatidylinositol-4,5-bisphosphate
PI3K	Phosphoinositide-3-kinase
PI4P	Phosphatidylinositol-4-phosphate
PIK3AP1	PI3K adaptor protein 1
PLC-γ2	Phospholipase C-γ2
PMA	Phorbol myristate acetate
PRR	Pattern recognition receptor
PTM	Post-translational modification
PVDF	Polyvinylidene difluoride
PYD	Pyrin domain
PYHIN	Pyrin and HIN domain-containing protein
Rac1	Ras-related C3 botulinum toxin substrate 1
RBD	Ras-binding domain
RE	Restriction enzyme
RHIM	Receptor interacting protein (RIP) homotypic interaction motif
Rho-GAP	Rho-GTPase- activating protein
RIG-I	Retinoic acid-inducible gene 1
RIPK	Receptor-interacting serine/threonine-protein kinase
RMSD	Root-mean-square deviation
RPMI	Roswell park memorial institute medium
RPS4	Resistant to *P. syringae* 4

RRS1	Resistant to *R. solanacearum* 1
SAD	Single-wavelength anomalous diffraction
SAM	Sterile α motif
SARM	Sterile α and armadillo-motif containing protein
SD	Standard deviation
SDS-PAGE	Sodium dodecyl sulphate polyacrylamide gel electrophoresis
SEC	Size-exclusion chromatography
SH	Src homology domain
SIGIRR	Single Ig IL-1-related receptor
SOC	Super optimal broth with catabolite repression
Src	Proto-oncogene tyrosine-protein kinase Src
SYK	Spleen tyrosine kinase
TAK1	Transforming growth factor beta-activated kinase
TBK1	TANK-binding kinase 1
TBS	Phosphate-buffered saline
TBST	Phosphate-buffered saline + Tween 20
TCEP	Tris-(2-carboxyethyl)phosphine
Tcp	TIR domain-containing protein
TCR	T cell receptor
TEC	Transient erythroblastopenia of childhood
TEV	Tobacco etch virus
TF	Transcription factor
Th	T helper
THP-1	Tamm-horsfall protein 1
TIG	Transcription factor Ig
TIR	Toll/interleukin-1 receptor
TLR	Toll-like receptor
TNF	Tumour necrosis factor
TNFAIP3	Tumour necrosis factor alpha-induced protein 3
TOF	Time of flight
Tollip	Toll-interacting protein
TOM1	Target of Myb protein 1
TRAF	TNF receptor associated factor

TRAM	TRIF-related adaptor molecule
TREM2	Triggering receptor expressed on myeloid cells 2
Triad3A	Triad domain-containing protein 3 variant A
TRIF	TIR domain-containing adaptor inducing interferon-β
TRIS	Tris(hydroxymethyl)aminomethane
tTLR4	Truncated TLR4
TYK2	Tyrosine kinase 2
UEVLD	UEV and lactate/malate dehydrogenase domains
UV	Ultraviolet
VLP	Virus-like particle
Vps34	Vacuolar protein sorting 34
VSV	Vesicular stomatitis virus

List of Figures

List of Tables

1 Introduction

The B cell adaptor protein (BCAP) is an important adaptor protein in immunity and plays a pivotal role in TLR, BCR, IL-R and TCR signalling. BCAP dampens TLR4 signalling by recruiting PI3K and PLC-γ2, both of which are key enzymes in phosphatidylinositol metabolism. The current literature on BCAP mainly describes the cellular and *in vivo* effects of the protein on the immune system. The precise molecular mechanism by which BCAP interacts with the TLR signalosome and downstream interaction partners of phosphatidylinositol metabolism is not understood. This study pursues an integrated approach drawing upon structural, biophysical and cell biological evidence to elucidate the mechanism of BCAP-mediated TLR regulation. This introduction chapter is divided into two main parts, of which the first describes the mechanisms of TLR activation with a focus on the upstream TIR domain-dependent signalling. The second part provides an overview of the cellular functions of BCAP in the immune system.

1.1 Pattern recognition receptors in innate immunity

Multicellular organisms have an innate immune system that provides an immediate first line of defence against infection by pathogenic micro-organisms. To accomplish this, these organisms use a number of pattern recognition receptors (PRRs) that recognise and respond to conserved microbial molecules, commonly referred to as pathogen-associated molecular patterns (PAMPs). PRRs also respond to endogenous ligands collectively termed damage-associated molecular patterns (DAMPs), which are released by damaged or dying cells.

There are distinct families of PRRs including the toll-like receptor (TLR) family of transmembrane receptors, the NOD-like receptors (NLR), the RIG-I-like receptor (RLR) family, the PYHIN family, the C-type lectin receptors (CLRs), oligoadenylate synthase (OAS) proteins and the related protein cyclic GMP-AMP synthase (cGAS) (Medzhitov, Preston-Hurlburt et al. 1997, Weis, Taylor et al. 1998, Girardin, Tournebize et al. 2001, Yoneyama, Kikuchi et al. 2004, Brehin, Casademont et al. 2009, Hornung, Ablasser et al. 2009, Wu, Sun et al. 2013). In response to infections, these receptors exhibit varying levels of functional overlap and redundancy to achieve microbial clearance (Monie, Bryant et al. 2009).

1.2 The role of Toll-like receptors in innate immunity

TLRs mediate immune responses to microbial stimuli such as bacterial lipids, lipoproteins and non-self nucleic acids. Since the first TLR was discovered, ten human TLR receptors and numerous ligands have been described (Medzhitov, Preston-Hurlburt et al. 1997). TLRs can be divided into two classes depending on their subcellular localisation. TLR1, TLR2, TLR4, TLR5, TLR6 and TLR10 recognise extracellular ligands and signal from the cell surface, while TLR3, TLR7, TLR8, and TLR9 recognise their respective ligands in the endosomal compartment.

TLR4 is activated by gram-negative bacterial LPS through the co-receptors MD2 and CD14 (Shimazu, Akashi et al. 1999). Triacyl and diacyl lipoproteins are recognised by heterodimers of TLR2 with TLR1 or TLR6, respectively (Jin, Kim et al. 2007, Kang, Nan et al. 2009). Bacterial flagellin protein induced activation and dimerisation of TLR5 (Yoon, Kurnasov et al. 2012). The most recent addition to the human TLR family, TLR10, is considered an orphan receptor. However, it has been shown to dimerise with TLR1 and TLR2 (Hasan, Chaffois et al. 2005). It is therefore possible that heterodimers containing TLR10 would recognise lipoproteins similar to the other TLR2 heterodimers (Hasan, Chaffois et al. 2005). The endosomal TLR9 responds to DNA with unmethylated CpG nucleotides, whereas TLR7 and TLR8 are activated by single-stranded RNA (Hemmi, Takeuchi et al. 2000, Diebold, Kaisho et al. 2004, Heil, Hemmi et al. 2004). Double-stranded viral RNA is recognised by TLR3 (Alexopoulou, Holt et al. 2001).

As single pass type I transmembrane receptors, TLRs are comprised of an extracellular leucine-rich repeat (LRR) domain for ligand detection and a cytoplasmatic TIR domain that initiates inflammatory signalling (Gay and Keith 1991). For a subset of TLR receptors, crystallographic receptor-ligand complexes revealed a remarkable plasticity of the LRR repeats to interact with a vast range PAMPs, with widely varying biophysical properties. TLR1-TLR2 heterodimers accommodate the Pam_3CSK_4 acyl chain in hydrophobic pockets at the top of the LRR heterodimer (Jin, Kim et al. 2007). TLR3 LRR dimers recognises dsRNA at multiple contact points at the top of the LRR, as well as inside the dimerisation interface (Liu, Botos et al. 2008). By contrast, the TLR4 ligand, LPS, has six acyl chains that are accommodated by the MD2 coreceptor, with limited LRR contacts that mainly interact with the lipid headgroup (Ohto, Fukase et al. 2007, Park, Song et al. 2009).

Extracellular ligand engagement induces receptor dimerisation and subsequent activation of the TIR domains. The activated receptor TIR domains act as a scaffold for the recruitment of the TIR domain-containing adaptor proteins, MyD88, MAL, TRIF, TRAM, SARM and BCAP (Figure 1) (Horng, Barton et al. 2001, Horng and Medzhitov 2001, Fitzgerald, Rowe et al. 2003, Oshiumi, Matsumoto et al. 2003, Couillault, Pujol et al. 2004, Troutman, Hu et al. 2012). TLRs, with the exception of TLR3, utilise a MyD88-dependent signalling pathway that relies on the recruitment of MAL to activated TLRs (Fitzgerald, Palsson-McDermott et al. 2001, Bonham, Orzalli et al. 2014). TLR3 signals through the TRIF adaptor protein, activating the MyD88-independent pathway (Yamamoto, Sato et al. 2003). This alternative pathway requires the endosomal membrane anchored adaptor protein TRAM (Fitzgerald, Rowe et al. 2003). TLR4 is unique in that it signals through both pathways. The MyD88-dependent pathway is activated by LPS stimulation at the cell surface, followed by receptor internalisation that activates the MyD88-independent pathway *via* TRAM and TRIF (Fitzgerald, Rowe et al. 2003). SARM and BCAP are negative regulators of TLR activation (Carty, Goodbody et al. 2006, Peng, Yuan et al. 2010, Ni, MacFarlane et al. 2012, Troutman, Hu et al. 2012).

1.3 Toll-like receptor signalling pathways

Ligand-induced TLR signalling results in the activation of immune cells. However, the precise cellular response depends on the combination of ligand and receptor. In innate immune cells like macrophages and dendritic cells, TLR signalling enhances bacterial clearance by phagocytosis and secretion of pro-inflammatory cytokines and chemokines. These signalling proteins encourage the recruitment and activation of additional immune cells. Pro-inflammatory signals also lead to the activation of the adaptive immune system, with the differentiation and activation of naïve T cells that do not express TLRs (Iwasaki and Medzhitov 2015). However, other cell types in the adaptive immune system do express TLRs. For example, B cells express a wide range of TLRs and ligand detection leads to increased proliferation, differentiation and expression of co-stimulatory molecules (Rawlings, Schwartz et al. 2012).

On a molecular level, these widely varying cellular responses are the result of transcription factor (TF) activation downstream of TLR signalling. Specifically, NF-κB, AP-1, and IRFs are activated downstream of TLR stimulation.

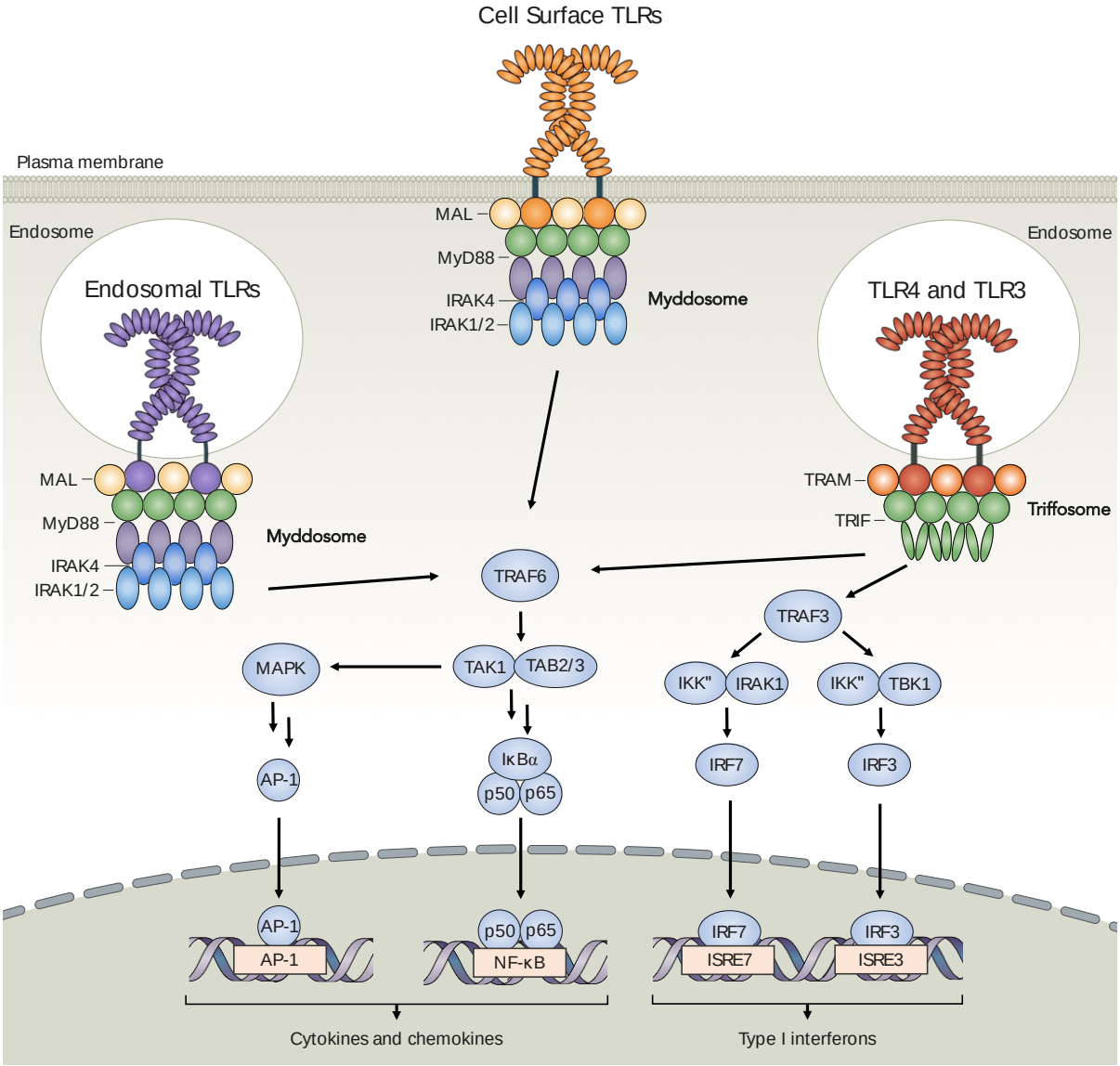

Figure 1. Overview of the TLR signalling pathway.

TLRs are present at the plasma membrane and in endosomal compartments. Upon the detection of microbial cell-wall components, non-self nucleic acids or DAMPS, TLRs activate the MyD88-dependent, or MyD88-independent signalling pathway. Through a complex signalling network and crosstalk with various other signalling pathways, TLR activation leads to the transcription of inflammatory cytokines, chemokines, and type I IFNs. MyD88-dependent myddosome formation activates TRAF6 resulting in the activation of NF-κB and MAPK-induced AP-1. The MyD88-independent triffosome activates IRF3 and IRF7 through TRAF3, and NF-κB *via* TRAF6.

In the MyD88-dependent pathway, MAL facilitates the recruitment of MyD88 to activated TLRs (Figure 1) (Fitzgerald, Palsson-McDermott et al. 2001). Subsequently, MyD88 will interact with the IRAK family proteins IRAK4, IRAK2 and IRAK1 to form the helical myddosome complex (Motshwene, Moncrieffe et al. 2009, Lin, Lo et al. 2010). IRAK phosphorylation then activates the E3 ubiquitin ligase TRAF6 that drives activation of the

NF-κB complex, and MAPKs through TAK1 (Wang, Deng et al. 2001). MAPK signalling subsequently leads to the activation of AP-1 (Wang, Deng et al. 2001).

Similarly, the MyD88-independent pathway is mediated by TIR domain-containing adaptor proteins (Figure 1). Recruitment of TRIF downstream of TLR3 and TLR4 promotes pro-inflammatory NF-κB and AP-1 signalling through TRAF6 (Konno, Yamamoto et al. 2009). Alternatively, TRIF and RIPK signalling results in caspase activation, which then leads to NF-κB signalling (Meylan, Burns et al. 2004). More distinctly though, the MyD88-independent pathway also results in the production of type I interferons following activation of IRF family transcription factors. TRIF signalling leads to the activation of TRAF3, subsequently activating TBK1 and IKK**ε** (Hacker, Redecke et al. 2006). This TBK1 and IKK**ε** complex then leads to IFN-β induction *via* IRF3 activation (Hacker, Tseng et al. 2011). IRF5 and IRF7 can be activated downstream of both MyD88-dependent and the MyD88-independent pathways through TRAF6 (Fitzgerald, Rowe et al. 2003, Kawai, Sato et al. 2004, Ouyang, Negishi et al. 2007).

1.4 Structure and function of TIR domains

Signalling mediated by TLRs is initially propagated by TIR domain adaptor proteins. TIR domain-containing proteins have been characterised in bacteria, plants and animals. In plants and animals, TIR domains are often found in multi-domain immune proteins. In bacteria, they often function as virulence factors that facilitate host immune evasion (Rana, Zhang et al. 2013).

In human TLR signalling, six TIR domain-containing adaptor proteins are involved in signal transduction. Of these six, MAL, MyD88, TRAM and TRIF are pro-inflammatory adaptor proteins that propagate the signal downstream of activated TLR dimers. BCAP and SARM are atypical adaptor proteins that negatively regulate inflammatory signalling (Carty, Goodbody et al. 2006, Troutman, Hu et al. 2012, Carlsson, Ding et al. 2016). Using x-ray crystallography and NMR, several receptor and adaptor TIR domain structures have been determined (Xu, Tao et al. 2000, Nyman, Stenmark et al. 2008, Ohnishi, Tochio et al. 2009, Valkov, Stamp et al. 2011, Enokizono, Kumeta et al. 2013, Snyder, Deredge et al. 2014, Halabi, Sekine et al. 2017). TIR domains typically span between 130-200 amino acids. Despite a low level of sequence similarity, all TIR domains are comprised of an α/β-fold with five α-helices surrounding a core of four or five parallel β-strands (Figure 2). The loops connecting these secondary structures have been shown to play a crucial role in signalling. For example, the loop connecting βB-sheet

and αB-helix (BB-loop) is crucial for the functioning of TIR domain adaptor proteins and receptor specificity (Figure 2) (Toshchakov, Basu et al. 2005). Mutations of critical residues in this loop have resulted in a loss-of-function phenotype in various adaptor proteins (Poltorak, He et al. 1998, Toshchakov, Basu et al. 2005). In TLR3, a point mutation in the BB-loop can even induce a shift from TRIF to MyD88-dependent signalling (Verstak, Arnot et al. 2013).

In plants, many TIR domains are found in the N-terminus of pathogen resistance proteins. These cytoplasmic nucleotide-binding (NB)/LRR resistance proteins recognise PAMPs and trigger a defence response known as the hypersensitive response (Dodds and Rathjen 2010). Other families of TIR domain-containing plant proteins are TIR-only (TIR-X) and TIR-NB (TIR-N) proteins (Meyers, Morgante et al. 2002). While the precise function of these last proteins is largely unknown, transient overexpression in *N. tabacum* and stable transgenics in *A. thaliana* have shown that TIR-X induces cell death and TIR-N enhances pathogen resistance (Nandety, Caplan et al. 2013).

In a wide range of bacterial species, TIR domains can be found as single domain proteins or in combination with other domains (Rana, Zhang et al. 2013). Most of the bacterial TIR domain-containing proteins are poorly characterised, but several instances of immunomodulatory functions have been described. TcpB and BTpA from *B. melitensis*, YpTIR1 from *Y. pestis* and TcpC from uropathogenic *E. coli CFT073* suppress TLR signalling by TIR domain interactions with host TIR domain-containing proteins, resulting in host immune evasion (Rana, Simpson et al. 2011, Waldhuber, Snyder et al. 2016, Nimma, Ve et al. 2017).

Even though TIR domains have been fairly well characterised with regard to their structural features, it remains unclear how various TIR domains activate and regulate inflammatory signalling.

1.5 The molecular mechanism of TIR domain signalling

Despite these structural insights and extensive mapping of various crucial protein interfaces, the mechanism of homotypic and heterotypic TIR domain interactions remains unclear. Consequently, the structure, stoichiometry and assembly of the full TLR signalosome is unknown.

Driven by ligand-induced TLR dimerisation and the early observation that MAL and MyD88 have the ability to self-associate *in situ* and *in vitro*, it was proposed that mammalian TIR

domains form dimers (Dunne, Ejdeback et al. 2003). These observations fuelled a search for TIR domain dimers and their dimerisation interfaces. Frequently, crystal contacts are proposed to represent dimerisation interfaces even though all known mammalian TIR domains are monomeric in solution (Xu, Tao et al. 2000, Khan, Brint et al. 2004, Nyman, Stenmark et al. 2008, Ohnishi, Tochio et al. 2009, Valkov, Stamp et al. 2011, Lin, Lu et al. 2012, Jang and Park 2014, Halabi, Sekine et al. 2017).

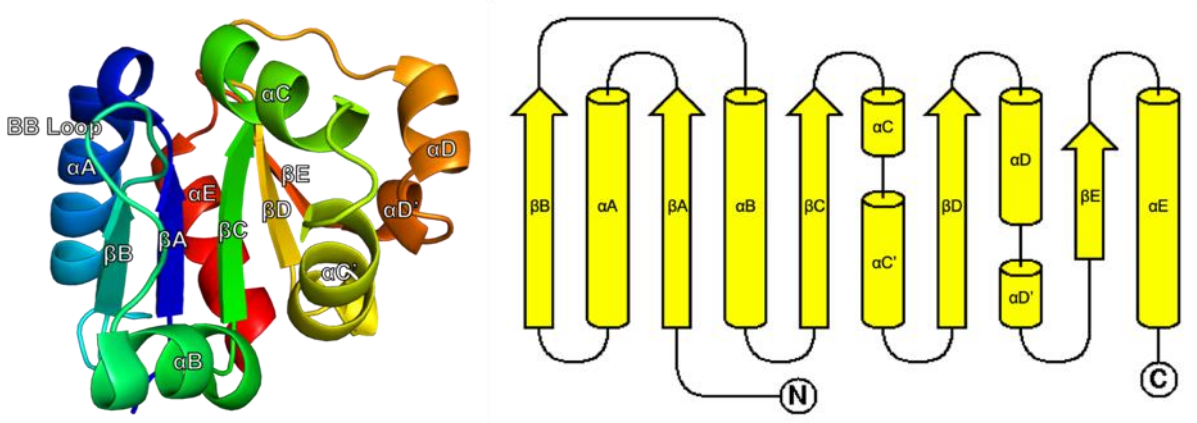

Figure 2. TIR domain structure and topology.

(A) Crystal structure of the BCAP TIR (BCAP^{TIR} domain) (PDB code 5FOR), illustrating the secondary structure features of a typical TIR domain with an α/β-fold containing five α-helices (αA-αE) surrounding a core of four or five parallel β-strands (βA-βE). (B) Topology diagram of the BCAP^{TIR} domain.

To date, the only evidence for TIR domain dimerisation has been found in plants and bacteria. In *A. thaliana*, a heterodimer between the TIR domains of the resistance proteins RRS1 and RPS4 was crystallised and confirmed to be dimeric in solution (Williams, Sohn et al. 2014). Other reports of dimeric plant TIR domain structures and homodimers are either based on inconclusive data or represent mere interpretations of crystal contacts that show little consistency with regard to dimerisation interfaces (Chan, Mukasa et al. 2010, Bernoux, Ve et al. 2011, Hyun, Lee et al. 2016, Zhang, Bernoux et al. 2017). By contrast, the bacterial TIR domain proteins YpTIR1 (*Y. pestis*), BtpA and TcpB (*B. melitensis)*, were shown to form dimers in solution (Rana, Simpson et al. 2011, Kaplan-Turkoz, Koelblen et al. 2013, Alaidarous, Ve et al. 2014).

In the absence of evidence for TIR dimerisation of mammalian proteins in solution, several extensive mutagenesis studies were conducted in order to map the relevant interface in MyD88, MAL, and TLR4 (Ohnishi, Tochio et al. 2009, Lin, Lu et al. 2012, Bovijn, Desmet et al. 2013, Loiarro, Volpe et al. 2013, Vyncke, Bovijn et al. 2016). In these studies, loss-of-function mutations of MAL and MyD88 are usually grouped in three or four interfaces that disrupt

NF-κB signalling and TIR domain oligomerisation. For the MAL TIR domain (MAL^{TIR}), three important interfaces contain the αC'-helix and DD-loop, the BC-loop and αC'-helix, and the DE-loop and αE-helix. Similarly, four important interfaces were identified in the MyD88 TIR ($MyD88^{TIR}$) domain and contained key residues in the BB-loop region, the αD-helix and αC-helix, the αE-helix, and DE-loop and EE-loop (Vyncke, Bovijn et al. 2016).

These loss-of-function mutations cover most of the TIR domain surface of the MAL and MyD88. Consequently, this data suggests that these protein interactions are more complex than simple homo- or heterodimerisation. However, these interfaces inspired several models of the TLR signalosome that are based on *in silico* docking techniques (Bovijn, Desmet et al. 2013, Guven-Maiorov, Keskin et al. 2015, Guven-Maiorov, Keskin et al. 2015, Vyncke, Bovijn et al. 2016). These models remain highly speculative, since the proposed interfaces are inconsistent between different publications and dimerisation of mammalian TIR domains remains a mere hypothesis. Moreover, all models fail to bridge stoichiometric mismatch between receptor dimerisation and myddosome formation, where MyD88 adopts a helical conformation with about four units per turn.

1.6 Filament formation in innate immune signalling

In the search for the TLR signalosome structure and TIR domain oligomerisation interfaces, the field has pivoted towards the study of larger signalling complexes. Many PRRs tend to cluster and form filamentous complexes that subsequently induce activation of downstream effector proteins (Hauenstein, Zhang et al. 2015, Vajjhala, Ve et al. 2017). This sequential recruitment and oligomerisation of adaptor proteins by activated PRRs often involves a co-operative assembly mechanism that builds on an initial nucleation event (Lu, Magupalli et al. 2014, Xu, He et al. 2014, Lu, Li et al. 2016). These phenomena have been observed in NLR and PYHIN inflammasomes, MAVS and RLR receptors, and the myddosome and triffosome downstream of TLR signalling (Figure 3) (Kagan, Magupalli et al. 2014, Vajjhala, Ve et al. 2017, Latty, Sakai et al. 2018).

NLR inflammasome activation initiates the assembly of large specks containing ASC filaments and effector caspases (Figure 3) (Lu, Magupalli et al. 2014, Man, Hopkins et al. 2014). NLRP1, NLRP3 and NAIP2/NLRC4 are known to form this type of inflammasome through initial receptor oligomerisation. NAIP2 and NLRC4 assemble into an oligomeric ring upon ligand binding (Hu, Zhou et al. 2015, Zhang, Chen et al. 2015). This results in proximity-induced

oligomerisation of receptor CARD domains and subsequent recruitment of the ASC CARD domain. ASC is recruited downstream of both CARD and PYD domain-containing NLRs and forms large filamentous structures by PYD domain filament formation (Lu, Magupalli et al. 2014, Sborgi, Ravotti et al. 2015). The ASC PYD domain filaments are thought to be crosslinked by ASC CARD domain interactions and activation of effectors caspases. Crosslinking drives condensation of the protein complexes and results in the typical macromorphological inflammasome speck (Lu, Magupalli et al. 2014, Dick, Sborgi et al. 2016). The resulting activation of caspase 1 drives proteolytic activation of IL-1β and gasdermin D, which leads to pyroptotic cell death (Shi, Zhao et al. 2015).

ASC is also involved in the activation of DNA-recognising PRRs. For example, the PHYRIN protein family member AIM2 recognises dsDNA *via* its HIN domain (Figure 3) (Jin, Perry et al. 2013). This induces clustering of the AIM2 PYD domain that results in the recruitment of ASC and subsequent inflammasome formation with caspase activation (Lu, Magupalli et al. 2014).

Another group of filament-forming proteins are the cytosolic RLR family members RIG-I and MDA5 that recognise viral RNA (Figure 3) (Andrejeva, Childs et al. 2004, Yoneyama, Kikuchi et al. 2004). RIG-I and MDA5 form a ring-like filament around dsRNA, leaving their CARD domains to interact with MAVS that then forms CARD domain filaments on the outer mitochondrial membrane (Hou, Sun et al. 2011, Jiang, Ramanathan et al. 2011, Kowalinski, Lunardi et al. 2011, Reikine, Nguyen et al. 2014, Yu, Qu et al. 2018). Through TRAF2/3 and TBK1, the MAVS signalosome activates IRF3 and IRF7, resulting in expression of type I IFNs (West, Shadel et al. 2011). Alternatively, TRAF6-dependent activation of RIPK1 can lead to NF-κB signalling (West, Shadel et al. 2011).

TLR3 signalling through TRIF, RIPK1 and caspase 8 involves the formation of TRIF-containing filaments (triffosome) (Figure 3) (Gentle, McHenry et al. 2017). TRIF filament formation is also supported by preliminary data suggesting TRIF filaments can assemble *in vitro* (Unpublished data, Gay group). TRIF oligomerisation is likely driven by the TIR domain and the RHIM motif, which is essential for filament formation in RIPK1 and RIPK3 (Li, McQuade et al. 2012). RIPK1 and RIPK3 kinases then interact with FADD through DD interactions, and induce caspase 8-dependent cell death (Kaiser and Offermann 2005).

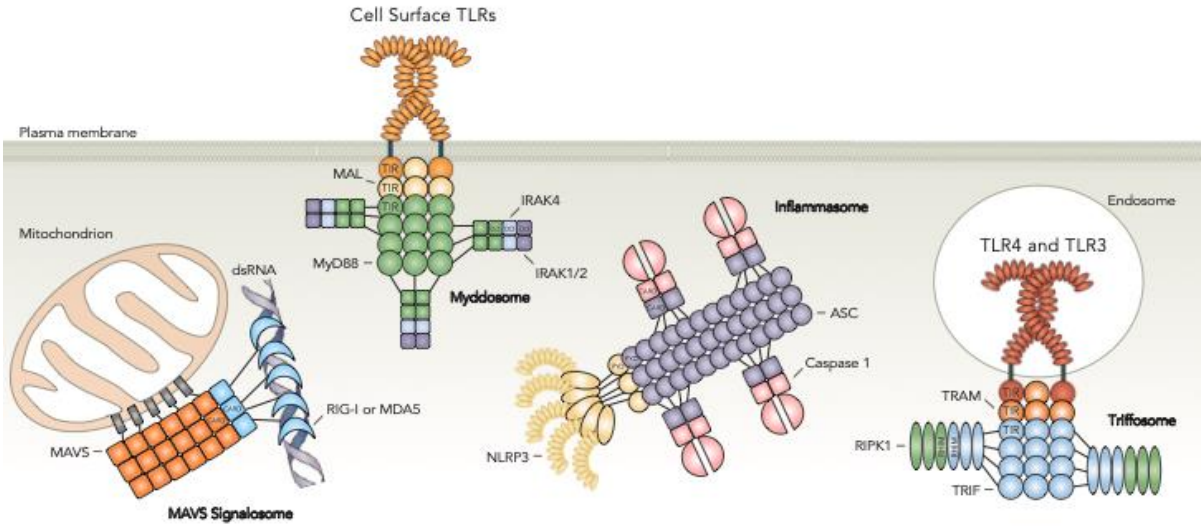

Figure 3. Overview of filament formation in innate immunity signalosomes.

Depicted are the well-characterised innate immunity signalosomes that utilise filament formation to amplify inflammatory signalling. The figure does not represent the exact stoichiometry or domain arrangements for proteins in each signalosome. LPS (not shown) binding to TLR4 through MD2 induces receptor dimerisation that leads to the assembly of the TIR domain-containing signalosome. Sequential recruiting and activation of MAL and MyD88 leads to myddosome formation through MyD88 death domains (DDs), resulting in the recruitment of IRAK kinases that initiate the activation of NF-κB. Engagement of RIG-I and MDA5 by dsRNA activates CARD domains that form a nucleation point for MAVS CARD domain oligomerisation on the outer mitochondrial membrane. Through TRAF proteins, the MAVS signalosome activates IRF3, IRF7 and NF-κB. NLRP3 or AIM2 (not shown) inflammasome activation is initiated by DAMPs resulting in a conformational rearrangement of the PYR domains that nucleates ASC PYR domain oligomerisation. Subsequent activation of ASC CARD domains results in the recruitment of caspase 1 that activates pro-IL-1β through proteolysis. TLR3 recognises dsRNA, inducing receptor dimerisation. Subsequent TIR domain activation leads recruitment of TRAM and TRIF adaptor proteins through TIR domain interactions. The TRIF adaptor protein can then induce RIPK1 activation *via* RHIM domain oligomerisation. Triffosome activation and signalling *via* RIPK1 leads to caspase 8-dependent cell death.

1.7 Filament formation in TLR signalling

With numerous examples of filament formation and higher-order oligomerisation in other PRRs, these concepts are now being adopted in the field of TLR signalling and TIR domain adaptor proteins (Latty, Sakai et al. 2018).

Downstream of TLRs, MyD88-dependent signalling leads to the formation of the myddosome *via* MyD88 DD interactions with IRAK kinases (Motshwene, Moncrieffe et al. 2009). The crystal structure of this DD complex reveals an assembly similar to ASC PYD and MAVS CARD domain filaments (Lin, Lo et al. 2010). Although the precise mechanism of myddosome assembly is unknown, it is likely that MyD88 presents activated DD complexes that act as a platform for sequential recruitment of four IRAK4 and four IRAK2 DDs (Unpublished data,

Gay group). This brings the IRAK kinase domains in proximity causing activation and cross-phosphorylation (Ferrao, Zhou et al. 2014).

The role of TIR domains in the formation of myddosomes remains elusive. However, it was recently discovered that MAL^{TIR} and $MyD88^{TIR}$ domains can form large filamentous structures *in vitro* (Ve, Vajjhala et al. 2017). The MAL^{TIR} domain was shown to form temperature reversible filaments composed of twelve protofilaments that associate laterally, each containing two parallel strands of TIR domains. The filament forms a hollow tube with an inner diameter of 130 Å, which is in contrast to other PRR filaments that tend to contain 3-4 subunits within each cross-sectional segment (Ve, Vajjhala et al. 2017). The MAL^{TIR} domains contained in the filamentous structure were found to have substantial conformational differences compared to the NMR and crystal structures, due to participation of flexible regions and loops in the filament packing (Valkov, Stamp et al. 2011, Hughes, Lavrencic et al. 2017).

This large MAL filament represents the first structural evidence of homotypic TIR domain interactions, and contains valuable information regarding TIR domain interaction interfaces. The intrastrand interactions are comprised of head-to-tail contacts between TIR domains and involve the BB-loop residues, called BB-surface, and the EE-surface of the next subunit, comprised of the βD- and βE-strands. Herein, the conserved BB-loop residues P125 and G126 are buried in a pocket of the βE-strand. Each subunit of the protofilament interacts with two other subunits of the adjacent strand. These interstrand interactions are composed of the BC-surface, containing the αB- and αC-helices of one subunit, and the CD-surface with the αD-helix and the CD-loop of the opposite MAL^{TIR} domain subunit. The contacts that make up the interfaces between protofilaments primarily consist of salt bridges. Mutations of key residues showed that substitution of most interstrand and intrastrand residues abolished MAL filament formation *in vitro* (Ve, Vajjhala et al. 2017). Altogether, the interfaces contained in the MAL filament match the results of previous site-directed mutagenesis studies (Lin, Lu et al. 2012, Bovijn, Desmet et al. 2013, Ve, Vajjhala et al. 2017).

Viewing these earlier results from mutagenesis studies in the light of this novel filamentous model explains how numerous mutations of residues and interfaces spread throughout the TIR domain surface all lead to loss-of-function in signalling assays. Given the conserved structure of TIR domains, it is highly probable that all TIR domains form or participate in higher oligomeric structures to amplify pro-inflammatory signalling. Moreover, the binding interfaces are almost certainly identical among all TIR domains, since it is unlikely that such small domains encode for multiple independent ways of oligomerisation.

1.8 The role of dimerisation in TIR domain interactions

Despite the discovery of higher order TIR domain assemblies and the absence of evidence for TIR domain dimers, indirect dimerisation still plays an important role in TIR domain signalling. In several instances, TIR-adjacent domains play a crucial role in signalling. Ligand-induced dimerisation of the TLR ectodomain causes rearrangements and activation of the cytosolic TIR domains. Similarly, the MyD88 DD drives dimerisation of the full-length protein, bringing TIR domains into close proximity (Ohnishi, Tochio et al. 2009). The atypical TLR adaptor SARM is the best-studied example of this indirect dimerisation. Forced dimerisation of SARM TIR ($SARM^{TIR}$) domain in chimeric constructs results in TIR domain activation (Gerdts, Brace et al. 2015, Summers, Gibson et al. 2016). In the full-length protein, the TIR domain is followed by sterile alpha motif (SAM) domains that drive dimerisation (Gerdts, Summers et al. 2013).

The $SARM^{TIR}$ domain has been shown to have a unique catalytic activity causing depletion of axonal NAD^+. This NADase activity leads to pathological axonal degradation, and is dependent on protein dimerisation (Gerdts, Summers et al. 2013, Essuman, Summers et al. 2017). The products of this enzymatic reaction are ADPR and cyclic ADPR, with variable ratios in different species. The glutamic acids residues E596 and E642 are essential to the reaction and were proposed as catalytic residues (Summers, Gibson et al. 2016, Essuman, Summers et al. 2017). However, as a $SARM^{TIR}$ domain crystal structure is not available, the precise active site remains to be determined. The TIR domains of MyD88 and TLR4 did not exhibit such enzymatic activity, and SARM is therefore likely unique among TIR domain-containing proteins (Essuman, Summers et al. 2017). However, the example of SARM illustrates that induced proximity, but not necessarily dimerisation *sensu stricto* plays an important role in TIR domain activation.

The TLR adaptor protein BCAP contains a TIR domain followed by a DBB and ANK domain that have been linked to dimerisation (Battersby, Csiszár et al. 2003, Halabi, Sekine et al. 2017). However, the effect of BCAP dimerisation on TIR domain interactions and TLR signalling has not been investigated.

1.9 Negative regulation of TLR signalling

Signalling pathways require a delicate balance of activation and inhibition. Excessive TLR signalling leads to pathological inflammatory signalling that can result in sepsis, where detrimental amounts of proinflammatory cytokines pose a life-threatening risk. Cells have

evolved a multitude of strategies to regulate TLR signalling, ranging from negative feedback loops to ubiquitin-dependent protein degradation, targeting of protein-protein interactions, competing signalling pathways and protein sequestration (Liew, Xu et al. 2005, Hamerman, Pottle et al. 2016). This regulatory network has a high level of redundancy throughout several checkpoints and illustrates the complexity of inflammatory signalling.

For example, soluble TLR2 and TLR4 isoforms inhibit signalling by blocking ligand binding to full-length TLRs (Liew, Xu et al. 2005). Equally, cytosolic TIR domain-containing proteins can inhibit TLR signalling by interfering with the TIR domain signalosome. This category of proteins includes orphan receptors like SIGIRR, ST2, and IL-17RD, or soluble adaptors, such as SARM and BCAP (Brint, Xu et al. 2004, Carty, Goodbody et al. 2006, Troutman, Hu et al. 2012, Mellett, Atzei et al. 2015). TNFAIP3 and IRAK-M are cytosolic proteins that inhibit key signalling steps downstream of the myddosome (Kobayashi, Hernandez et al. 2002, Catrysse, Vereecke et al. 2014). Regulation is also provided at the transcriptome level. Examples of which are the transcription factors ATF3 and FoxO1, which negatively regulate the transcription of proinflammatory genes (Fan, Morinaga et al. 2010, Hamerman, Pottle et al. 2016). Furthermore, parallel signalling pathways such as TREM2/DAP12 can inhibit TLR responses by modulating the activation of MAPKs by competing for downstream adaptors and transcription factors (Guven-Maiorov, Keskin et al. 2015, Hamerman, Pottle et al. 2016). Lastly, the concentration of active TLRs is controlled by a complex trafficking network, where a balance of secretion and endocytosis cycles cell surface receptors between endosomes and the plasma membrane (Gay, Symmons et al. 2014, Liaunardy-Jopeace, Bryant et al. 2014). Endocytosis can also lead to receptor degradation in lysosomes (Saitoh 2009). For TLR4 and TLR9, this proteolytic degradation is ubiquitin dependent *via* the E3 ubiquitin-protein ligase Triad3A (Chuang and Ulevitch 2004).

TLR4 internalisation and MyD88-independent signalling have been shown to depend on PLC-γ2 and degradation of phosphatidylinositol-(4,5)-bisphosphate (PI(4,5)P2) (Kagan, Su et al. 2008, Zanoni, Ostuni et al. 2011, Aksoy, Taboubi et al. 2012). This process of PLC-γ2-dependent endocytosis also requires CD14 and SYK tyrosine kinase (Zanoni, Ostuni et al. 2011). Furthermore, PI3K was also found to induce internalisation of TLR4 by converting PI(4,5)P2 into phosphatidylinositol-(3,4,5)-trisphosphate (PI(3,4,5)P3) (Aksoy, Taboubi et al. 2012). Conversion of PI(4,5)P2 depletes membrane binding sites for MAL, inducing its release from the plasma membrane and subsequent degradation (Aksoy, Taboubi et al. 2012). The proteases calpain and caspase-1 contribute to MAL degradation (Miggin, Palsson-McDermott

et al. 2007, Aksoy, Taboubi et al. 2012). The mechanisms by which PI3K and PLC-γ2 are recruited to activated TLR signalosomes remain poorly understood. Several PI3K overexpression studies claim to have shown that the p85 regulatory subunit of PI3K can bind directly to TLR2, TLR3, TLR5, MAL and MyD88 (Arbibe, Mira et al. 2000, Sarkar, Peters et al. 2004, Rhee, Kim et al. 2006, Laird, Rhee et al. 2009, Santos-Sierra, Deshmukh et al. 2009). However, these experiments should be interpreted with caution, as either the appropriate SH2 domain binding sites for p85 were not present in these TLRs and adaptor proteins, or the motifs were non-essential for the observed PI3K interaction. Therefore, BCAP has been proposed to bridge MyD88-dependent TLR signalling to PI3K and PLC-γ2 (Halabi, Sekine et al. 2017). Since BCAP contains multiple YxxM binding sites for p85 subunit and is known to interact with PLC-γ2, it provides a credible link between TLR signalling and phosphatidylinositol metabolism.

1.10 The function of BCAP in B lymphocytes

BCAP is an important negative regulator of inflammatory TLR signalling. BCAP was first characterised in chicken B cells. Here, a pull-down assay was performed using p85 N-SH2 domain as bait, and revealed BCAP as an interaction partner (Okada, Maeda et al. 2000). Physiologically, BCAP is recruited to the activated B cell receptor (BCR) complex by the adaptor protein Nck (Castello, Gaya et al. 2013). BCR ligation in DT40 cells leads to BCAP phosphorylation, which results in the recruitment and activation of PI3K (Okada, Maeda et al. 2000). BCAP also links PI3K to the BCR co-receptor CD19, in chicken and mouse B cells (Inabe and Kurosaki 2002, Aiba, Kameyama et al. 2008). This PI3K activation downstream of CD19, was found to be more dependent on the BCAP YxxM motifs than those of CD19 (Inabe and Kurosaki 2002). Altogether, these results suggest that BCAP and CD19 have partially overlapping functions in BCR-mediated PI3K activation. However, it is unclear how BCAP would be recruited to the CD19 co-receptor.

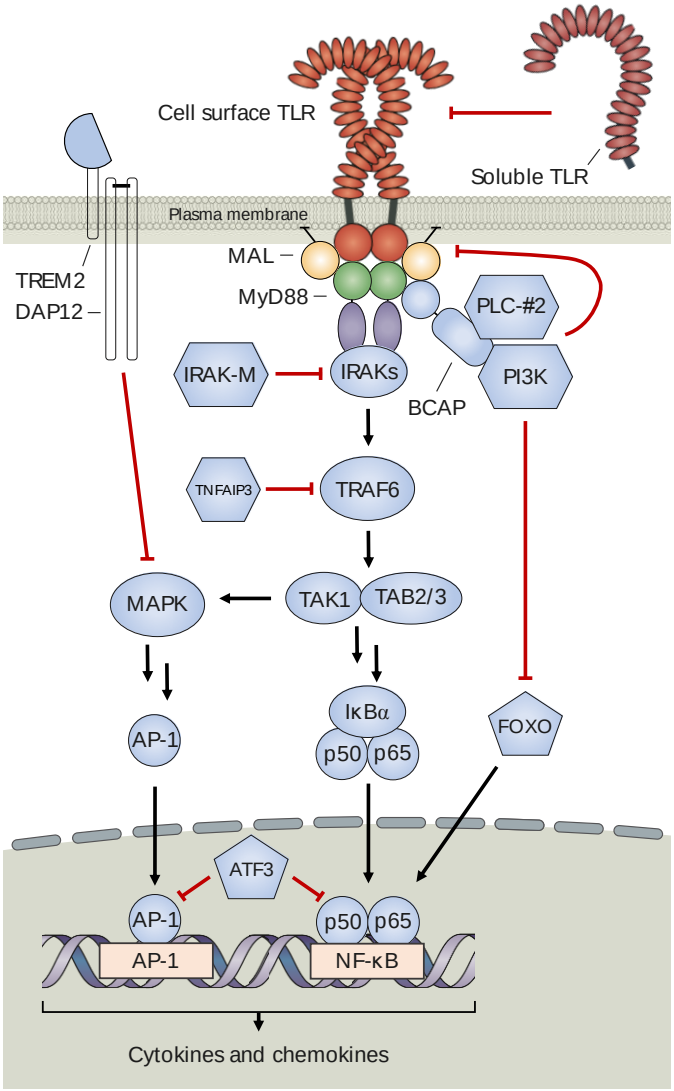

Figure 4. Overview of negative regulation of TLR signalling.

Depicted is a simplified overview of the TLR signalling pathways with a selected points of negative regulation. Extracellularly, soluble isoforms of surface TLRs can block ligand binding. Transmembrane receptors like TREM2-DAP12 inhibit TLR signalling by reducing MAPK activation. The TIR signalosome can be disrupted by phosphatidylinositol metabolism of PI3K and PLC-γ2, which results in a loss of MAL anchoring sites and leads to TLR4 endocytosis. IRAK-M and TNFAIP3 block signalling steps downstream of the TIR signalosome. At the transcription factor level, ATF3 dampens transcription of inflammatory genes through recruitment of histone deacetylases to the promoter region of inflammatory genes. FoxO transcription factors are phosphorylated and exported from the nucleus upon PI3K-Akt activation, terminating the transcription of inflammatory genes.

PI3K activity is particularly important for B cell development, activation and differentiation. B cells from BCAP-deficient mice show a decreased ability to mature and proliferate, while producing less immunoglobulin and being more susceptible to apoptosis (Yamazaki, Takeda et al. 2002). The mechanism of these loss-of-function phenotypes is not always clear, as BCAP deletion in mice did not lead to altered PI3K activity in B cells. BCAP-deficient B cells also exhibit impaired NF-κB activity through reduced expression of the NF-κB family member

c-Rel (Yamazaki, Takeda et al. 2002, Yamazaki and Kurosaki 2003). This is somewhat unexpected since BCAP is a negative regulator of TLR signalling (Troutman, Hu et al. 2012). Furthermore, BCAP-deficient mice exhibited reduced calcium mobilisation, likely due to insufficient PLC-γ2 activation (Yamazaki, Takeda et al. 2002). This mechanism is supported by the finding that PLC-γ2 associates with BCAP in HEK293T cells (Halabi, Sekine et al. 2017).

In conclusion, BCAP is involved in a wide range of B cell signalling pathways, and BCAP deficiency leads to numerous phenotypes, some of which are yet to be explained on a molecular level.

1.11 The role of BCAP in NK cells and T lymphocytes

After the initial discovery in B cells, BCAP was also found to be crucial in other areas of the immune system. For example, BCAP is strongly expressed in natural killer (NK) cells (MacFarlane, Yamazaki et al. 2008). NK cells from BCAP-deficient mice exhibited increased IFN-γ production, matured faster and were more resistant to apoptosis (MacFarlane, Yamazaki et al. 2008). This gain of function phenotype in NK cells is driven by defective PI3K-Akt signalling, which is in contrast to the loss-of-function phenotypes described in B cells.

Although there is little research regarding BCAP in T lymphocytes, PI3K signalling is essential for the proper clonal expansion of activated antigen-specific T cells (Shi, Cinek et al. 1997). The mechanism underlying this PI3K signalling in T cell activation and proliferation is not fully understood. For example, it is not clear whether the YxxM motif of the T cell co-receptor CD28 is required for PI3K recruitment *in vivo*, since mutation or deletion of this motif shows little effect *in vivo* (Pagan, Pepper et al. 2012). It was recently observed that BCAP, although not expressed in naïve T cells, was rapidly up-regulated in $CD8^+$ T cells upon activation (Singh, Ni et al. 2018). BCAP-deficient $CD8^+$ T cells show reduced CD3-dependent PI3K activation, which results in impaired clonal expansion and T cell differentiation *in vivo* (Singh, Ni et al. 2018). This suggests the BCAP is part of the T cell receptor (TCR) signalosome. This hypothesis is supported by a recent study that identified BCAP in a mass spectrometry screen of TCR-associated proteins (Unpublished data, Okkenhaug group, Department of Pathology, University of Cambridge).

BCAP was also found to propagate PI3K signalling downstream of IL-1R in T cells (Deason, Troutman et al. 2018). BCAP signals downstream of IL-1R and IL-18R in CD4+ T cells, where

it is required for optimal differentiation of Th1 and Th17 lineage cells (Deason, Troutman et al. 2018). This IL-1R association was shown to be TIR domain dependent and might be facilitated through MyD88 or the receptor TIR domain. These recent reports illustrate that BCAP is an important signalling adaptor in T cells, regulating T cell expansion and activation downstream of TCR and the IL-1R family.

1.12 The function of BCAP in myeloid cells

After the initial characterisation of BCAP in B cells and adaptive immunity, focus also shifted to the role of BCAP in myeloid cells and innate immunity. This was driven by the observation that BCAP-deficient B cells exhibit defective c-Rel NF-κB activation (Yamazaki, Takeda et al. 2002, Yamazaki and Kurosaki 2003). Supporting a role for BCAP in innate immunity, the protein is expressed in macrophages, dendritic cells and in hematopoietic progenitor cells (Matsumura, Oyama et al. 2010, Song, Chew et al. 2011). In these stem cells, BCAP acts as a negative regulator of myeloid cell development (Duggan, Buechler et al. 2017).

In myeloid cells, BCAP was first shown to be phosphorylated and upregulated upon LPS stimulation of mouse macrophages (Matsumura, Oyama et al. 2010, Song, Chew et al. 2011). BCAP-deficient mice have a hypersensitive innate immune system, with increased inflammation upon infection with *S. typhimurium* and a more severe form of DSS-induced colitis (Troutman, Hu et al. 2012). Mouse macrophages deficient in BCAP also have an increased production of the cytokines IL-6, IL-10 and IL-12 in response to TLR2, TLR4 and TLR9 stimulation (Matsumura, Oyama et al. 2010, Ni, MacFarlane et al. 2012). (Troutman, Hu et al. 2012). Further studies then revealed that BCAP contains a TIR domain that enables recruitment to the TLR signalosome where it acts as a negative regulator (Ni, MacFarlane et al. 2012, Troutman, Hu et al. 2012). The N-terminal TIR domain enables interaction with MAL, MyD88, and potentially TLR2 and TLR4 (Troutman, Hu et al. 2012, Halabi, Sekine et al. 2017). The molecular mechanism of BCAP-mediated negative regulation of TLR signalling is highly contentious. Multiple mechanisms have been proposed, but they fall short of addressing all aspects of BCAP signalling.

A first hypothesis suggests that BCAP facilitates endocytosis of activated TLR4 receptors through recruitment of PLC-γ2 and PI3K (Halabi, Sekine et al. 2017). TLR4 endocytosis leads to a shift from MyD88-dependent NF-κB signalling to anti-inflammatory TRAM-TRIF signalling (Figure 5). This mechanism relies on the observation that BCAP interacts with

PLC-γ2 and PI3K, which both regulate TLR4 endocytosis (Aksoy, Taboubi et al. 2012). Although this mechanism fits negative regulation of surface TLRs, it does not address the BCAP inhibition of TLR9 (Troutman, Hu et al. 2012). In mouse macrophages, negative regulation of TLR9 signalling by BCAP is dependent on PI3K activity as shown by the use of wortmannin (Ni, MacFarlane et al. 2012). However, this result is somewhat contradictory and wortmannin is a broad inhibitor of PI3K-related protein kinases (De Matteis and Godi 2004). Moreover, there is no apparent function for class I PI3Ks in TLR9 endosomes, since these compartments are enriched in PI(3)P and PI(3,5)P2 (van Meer, Voelker et al. 2008, Bissig and Gruenberg 2013).

A second hypothesis suggests that BCAP-mediated activation of PI3K leads to an Akt-dependent phosphorylation and nuclear export of the FoxO1 transcription factor (Eijkelenboom and Burgering 2013). FoxO1 residues T24, S256 and S319 are the targets of Akt phosphorylation, and S256 phosphorylation is significantly reduced in BCAP-deficient mouse macrophages (Hamerman, Pottle et al. 2016). Nuclear export of FoxO1 could then cause the termination of FoxO1-mediated transcription of pro-inflammatory genes such as IL-12, IL-6 and IL-1β (Su, Coudriet et al. 2009, Fan, Morinaga et al. 2010, Brown, Wang et al. 2011).

Thirdly, it cannot be ruled out that BCAP might engage in TIR domain-mediated inhibition of TLR signalosomes. TIR domains of MAL and MyD88 inhibit TLR signalling in overexpression models (Fitzgerald, Palsson-McDermott et al. 2001, Horng and Medzhitov 2001, Yamamoto, Sato et al. 2002). Moreover, indirect dimerisation of TIR domains might obstruct the assembly of TIR domain filaments by steric hindrance.

Recent reports have also suggested a novel function for BCAP in plasmacytoid dendritic cells. BCAP PI3K activation was found to be an essential link in TLR7 and TLR9-dependent IFN-α production (Chu, Ni et al. 2019). In this signalling pathway, BCAP is proposed to be localised at the plasma membrane, where its TIR domain interacts with DOCK2 to activate Rac1. Rac1 is then required for IKKα phosphorylation that drives IRF7-dependent IFN-α transcription. Evidence for the BCAP-DOCK2 interaction comes from co-immunoprecipitation experiments in HEK293T cells. However, dependence on the $BCAP^{TIR}$ domain suggests that this might be an indirect interaction through endosomal TLR signalosomes.

Given the increasing importance for BCAP in immune signalling with involvement in a wide range of pathways and cell types, further research is required to elucidate the mechanism, and protein interactions that facilitates this negative regulation of TLR signalling.

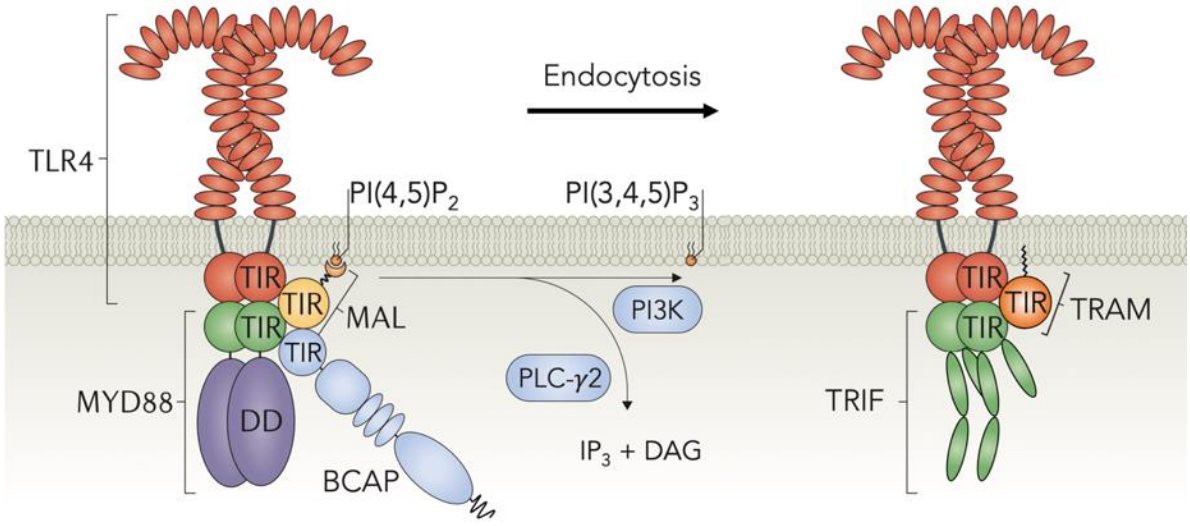

Figure 5. Displacement of MAL by PI(4,5)P2 depletion drives TLR4 endocytosis.

Schematic representation of TLR4 endocytosis through BCAP-induced activation of PI3K and PLC-γ2. The figure does not represent the exact stoichiometry of the proteins involved in this negative regulation of TLR signalling. BCAP is recruited to the TLR4 signalosome through TIR domain interactions. *Via* SH3 and SH2 domain interactions, PI3K and PLC-γ2 form a complex with BCAP. Activation of PI3K and PLC-γ2 leads to a depletion of the PI(4,5)P2 pool required for MAL membrane localisation. A loss of MAL membrane association initiates endocytosis and the activation of TRAM and TRIF that induce IRF signalling.

1.13 Structure of BCAP

The *PIK3AP1* gene encodes two variants of BCAP, generated by alternative initiation or splicing (Okada, Maeda et al. 2000). The larger isoform corresponds to the full-length protein ($BCAP_L$), whereas the shorter isoform lacks the N-terminal TIR domain ($BCAP_S$). Despite the expression of only two isoforms, endogenous BCAP from myeloid and lymphoid cells appears as four to six bands on western blot (Okada, Maeda et al. 2000, MacFarlane, Yamazaki et al. 2008, Ni, MacFarlane et al. 2012). The post-translational modifications (PTM) that cause both BCAP isoforms to each appear as two or more bands are poorly understood, and might contain valuable information towards the function and regulation of BCAP.

The existence of the N-terminal TIR domain (residues 1-142) was first proposed following the observation that BCAP negatively regulates TLR signalling in NF-κB luciferase assays (Troutman, Hu et al. 2012). A crystal structure later confirmed the TIR domain fold and revealed structural similarity with the TIR domains of TLR2, IL-1RAPL, MAL and TLR10 despite sequence identities below 20% (Halabi, Sekine et al. 2017). However, in contrast to MAL^{TIR}, the $BCAP^{TIR}$ domain contains no disulphide bonds and the BB-loop is relatively short and well-defined in the crystal structure.

A linker of approximately 40 amino acid residues connects the TIR domain to an adjacent domain (residues 181-317) that was previously annotated as a transcription factor-Ig (TIG) domain followed by a 3-α-helix region (Figure 6) (Troutman, Hu et al. 2012). Due to the conservation of this region between the *D. melanogaster* protein Dof, BCAP and BANK1 this domain was later named DBB domain (Battersby, Csiszár et al. 2003). TIG domains from transcription factors (TIG^{TF}) play an important role in protein dimerisation and DNA binding (Muller, Rey et al. 1995, Chen, Glover et al. 1998). Similarly, a yeast two-hybrid screen revealed that the BCAP DBB domain drives protein oligomerisation (Battersby, Csiszár et al. 2003).

The DBB domain is followed by three ankyrin repeats (ANK) (residues 322-403) referred to as ANK domain. Ankyrin repeats are approximately 33 amino acid residues and adopt a helix-loop-helix fold with antiparallel α-helices followed by a β-hairpin/loop (Mosavi, Cammett et al. 2004). Similar to the DBB domain, the ANK domain has been suggested to contribute to BCAP dimerisation (Halabi, Sekine et al. 2017). However, for both domains no structural information is available.

The C-terminal half of BCAP is predicted to be unstructured, with the exception of a coiled-coil motif (residues 605-665). This unstructured region contains several important protein binding motifs. For example, three proline-rich regions (residues 530-537, 775-790 and 797-805) provide binding sites for SH3 domain-containing proteins like Nck (Figure 6) (Castello, Gaya et al. 2013). Based on sequence specificity, other proteins including Src tyrosine kinases, PLC-γ2 and GRB2 SH3 domains were predicted to interact with the BCAP proline-rich regions (Sparks, Rider et al. 1996). The C-terminal region also contains a variety of tyrosine motifs that enable SH2 domain interactions. Four YxxM motifs provide the putative binding sites for PI3K (Figure 6) (Okada, Maeda et al. 2000, Matsumura, Oyama et al. 2010, Ni, MacFarlane et al. 2012).

1.14 BCAP tyrosine phosphorylation

BCAP-SH2 domain interactions like those with p85 and PLC-γ2 require tyrosine phosphorylation of BCAP tyrosine binding motifs. The tyrosine kinase c-Abl was shown to phosphorylate BCAP at several sites in the C-terminal unstructured region, when co-expressed in HEK293T cells (Maruoka, Suzuki et al. 2005). However, the physiological relevance of these phosphorylations remains unclear.

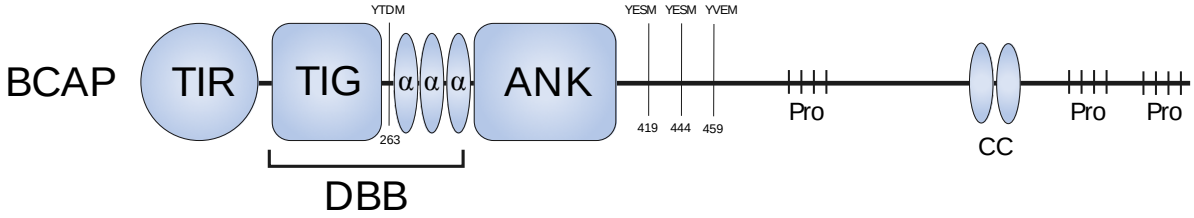

Figure 6. Domain architecture of human BCAP.

Depicted are the BCAP domains and other relevant protein sequences. Starting from the N-terminus, the TIR domain is followed by a transcription factor-Ig (TIG) domain with three α-helices (α). These features form the DBB domain, which is followed by the ankyrin repeat domain (ANK). The C-terminal unstructured region contains a coiled-coil motif (CC) and several protein interaction sites. The four YxxM motifs and proline-rich regions (Pro) are important binding sites for SH2 and SH3 domain interactions.

In chicken B cells, the kinases SYK and to a lesser extent BTK, were shown to contribute to BCAP tyrosine phosphorylation, as determined in knock-out cell lines (Okada, Maeda et al. 2000). In mouse macrophages however, SYK was not required for BCAP phosphorylation (Ni, MacFarlane et al. 2012). In fact, BCAP tyrosine phosphorylation in mouse macrophages is increased in the absence of SYK. Similarly, B cells deficient in LYN tyrosine kinase, showed increased BCAP phosphorylation (Okada, Maeda et al. 2000). However, LYN was later shown to be essential for BCAP phosphorylation downstream of mouse CD19, which was ectopically expressed in chicken B cells (Inabe and Kurosaki 2002). Further overexpression studies in HEK293T cells suggest that SYK plays a role in phosphorylation of BCAP YxxM motifs (Matsumura, Oyama et al. 2010). Similarly, overexpression in HEK293T cells showed that BCAP interacts with both SYK and LYN, and provided indications for LYN phosphorylation on BCAP (Inabe and Kurosaki 2002, Halabi, Sekine et al. 2017).

Given these somewhat conflicting findings, it remains unclear which kinases are responsible for BCAP tyrosine phosphorylation in various cell types, and a deeper analysis using *in vitro* kinase assays or appropriate inhibitors is required. Moreover, the precise phosphorylation sites and redundancies between YxxM motifs are yet to be determined.

1.15 Structure and function of the BCAP homolog BANK1

The BCAP homolog BANK1 has a domain arrangement highly similar to BCAP (Troutman, Hu et al. 2012). An N-terminal TIR domain shows 33% sequence identity with the $BCAP^{TIR}$ domain (Halabi 2015). Like BCAP, the BANK1 TIR domain is followed by DBB and ANK domains, as well as an unstructured C-terminal region. The latter, similar to BCAP contains a

coiled-coil motif and two proline-rich regions, but lacks the YxxM motifs for PI3K interaction. Genome-wide studies have implicated BANK1 in various diseases. For example, several BANK1 single nucleotide polymorphisms are associated with a susceptibility to systemic lupus erythematosus and systemic sclerosis (Kozyrev, Abelson et al. 2008, Rueda, Gourh et al. 2010, Bae, Lee et al. 2017, Martinez-Bueno, Oparina et al. 2018, Jiang, Athanasopoulos et al. 2019). Despite the structural similarities with BANK1, BCAP seems to fulfil a somewhat different role in immune cells as it has not been linked to pathologies.

Like BCAP, BANK1 has been associated with BCR and TLR signalling. BANK1 is expressed in B cells and tyrosine phosphorylated upon BCR stimulation (Yokoyama, Su Ih et al. 2002). BANK1 is also important in BCR-induced calcium mobilisation through interaction with PLC-γ2 and LYN-mediated tyrosine phosphorylation of the calcium channel inositol-1,4,5-trisphosphate receptor (Yokoyama, Su Ih et al. 2002, Bernal-Quiros, Wu et al. 2013). The tyrosine kinases BLK, SYK and LYN have been associated with this BANK1-mediated regulation of calcium signalling and interaction with PLC-γ2 in B cells (Bernal-Quiros, Wu et al. 2013). In the context of TLR signalling in B cells, BANK1 was shown to control TLR7-mediated type I interferon (Wu, Kumar et al. 2016). BANK1 was also linked to TLR9, since BANK1 deficiency in mice leads to a reduction in p38 phosphorylation and IL-6 secretion (Wu, Kumar et al. 2013). Overall, little is known about the role of BANK1 in these signalling pathways, but structural and functional similarities with BCAP may contribute to a better mechanistic understanding of this multi-domain adaptor protein.

1.16 PI3K

Based on structure and substrate specificity, PI3K enzymes have been categorised into three classes, denoted class I, II and III. PI3Ks are important in both innate and adaptive immune signalling, where they can both activate or regulate inflammation depending on the cell type or specific signalling pathway.

Class I PI3Ks catalyse the phosphorylation of plasma membrane-localised PI(4,5)P2 to generate the secondary messenger PI(3,4,5)P3 (Okkenhaug 2013). Class II PI3Ks can phosphorylate phosphatidylinositol (PI) and phosphatidylinositol-4-phosphate (PI4P) *in vitro*, and are involved in T cell signalling (Srivastava, Di et al. 2009). The Class III PI3K Vps34 phosphorylates PI to generate phosphatidylinositol-3-phosphate (PI3P), which is important for phagocytosis, autophagy and vesicle trafficking (Engelman, Luo et al. 2006, Okkenhaug 2013).

Class I PI3Ks and their downstream pathways are of significant importance to TLR, BCR and TCR signalling. This broad link with immunity and the interaction with BCAP makes class I PI3Ks of particular interest in this thesis.

Class I PI3Ks consists of a p110 catalytic subunit that associates with a p85 regulatory subunit (Figure 7). The catalytic subunits are further subdivided into class IA (p110α, p110β and p110δ) enzymes that associate with a regulatory subunit, and class IB (p110γ) enzymes that function as a monomer (Engelman, Luo et al. 2006, Vanhaesebroeck, Guillermet-Guibert et al. 2010). The p85 regulatory subunits (p85α, p55α, p50α, p85β and p55) vary in length and domain architecture, but all contain SH2 and SH3 domains that regulate the kinase activity of the catalytic subunit (Figure 7) (Fruman 2010).

In resting cells, the catalytic p110 subunit is kept in an inactive state by the regulatory subunit. The protein complex is recruited to activated signalling complexes through p85 SH2 domain interactions, which interact with phosphorylated YxxM motifs (Fruman 2010). The presence of two regulatory SH2 domains leads to a preferential binding of tandem YxxM motifs spaced by limited distance of 10-20 residues (Fruman 2010, Burke, Vadas et al. 2011). These SH2 domain interactions induce a conformational change in the PI3K complex, resulting in the release of kinase inhibition (Yu, Wjasow et al. 1998). The PI(3,4,5)P3 signalling molecule then recruits proteins containing pleckstrin homology (PH) domains such as PDK1 and Akt, which results in a phosphorylation cascade that ultimately activates downstream effectors including mTOR and FoxO transcription factors (Engelman, Luo et al. 2006, Hedrick 2009).

1.17 PLC-γ2

PLC-γ2 is another important protein in phosphoinositide metabolism. PLC-γ2 is an enzyme of the phospholipase C family that catalyses the hydrolysis of phospholipids to yield diacylglycerol (DAG) and inositol-1,4,5-trisphosphate (IP3). The secondary messenger IP3 in turn acts on the endoplasmic reticulum-localised IP3 receptor, resulting in a cytosolic influx of calcium ions (Baba and Kurosaki 2011). Several members of the PLC family play a role in the innate and adaptive immune system. PLC-γ2 in particular has been linked to TLR and BCR signalling, with an expression pattern limited to immune cells.

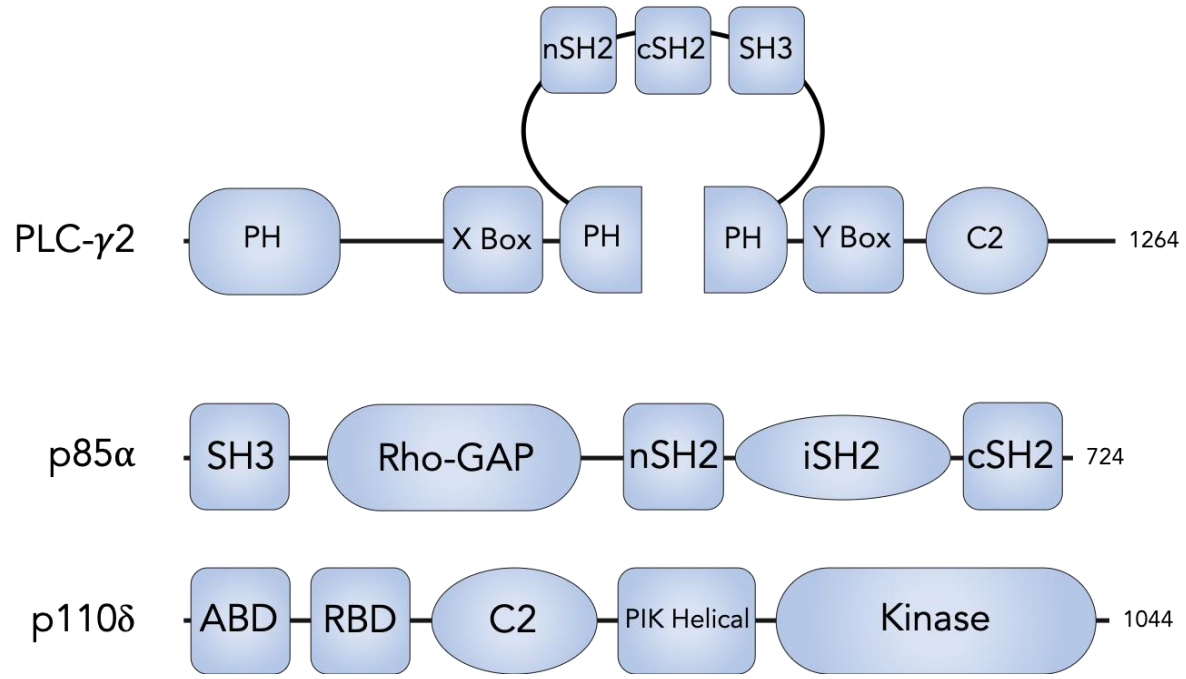

Figure 7. Domain architecture of human PI3K and PLC-γ2.

(A) The PLC-γ2 catalytic activity is driven by a split catalytic domain (X box and Y box), which converts PI(4,5)P2 into diacylglycerol (DAG) and inositol 1,4,5-trisphosphate (IP3). Catalytic activity is regulated by SH2 and SH3 domains. Membrane localisation of PLC-γ2 is driven by two pleckstrin homology domains (PH) and a C2 domain. (B) A typical Class I PI3K is comprised of a regulatory subunit, as represented by p85α, and a second catalytic subunit, represented by p110δ. p85 isoforms have a core domain structure containing two SH2 domains spaced by an inter-SH2 region (iSH2) responsible for p110 binding. Outside of the core region, p85 contains an SH3 and a Rho-GAP binding domain. The p110 catalytic subunits contain an adaptor-binding domain (ABD), a Ras binding domain (RBD), a C2 domain, a PIK helical domain and a catalytic kinase domain that converts PI(4,5)P2 into PI(3,4,5)P3.

PLC-γ2 is phosphorylated upon stimulation of TLR9 and induces TNFα secretion (Rao, Liu et al. 2013). Similarly, downstream of TLR2 and TLR4, PLC-γ2 contributes to IL-6 and TNFα expression (Aki, Minoda et al. 2008). PLC-γ2 is also crucial for the TLR2 and TLR4-mediated calcium flux that leads to IκB-α phosphorylation (Aki, Minoda et al. 2008). These pro-inflammatory roles of PLC-γ2 are contrasted by its role in negative regulation of inflammatory TLR4 signalling by endocytosis (Zanoni, Ostuni et al. 2011). The mechanisms by which PLC-γ2 is recruited to activated TLR signalling complexes are not fully understood. However, interactions with BCAP and BANK1 are likely to facilitate some of these functions (Bernal-Quiros, Wu et al. 2013, Halabi, Sekine et al. 2017).

PLC-γ2 is a multidomain protein with a catalytic domain and several regulatory domains that target the enzyme to its substrates and regulate the catalytic activity (Figure 7). The enzymatic activity of PLC-γ2 is located in a split catalytic triose phosphate isomerase barrel comprised of

two halves (X and Y boxes) (Essen, Perisic et al. 1996). In both PLC-γ isozymes (PLC-γ1 and PLC-γ2), an X/Y linker region connecting the catalytic domains contains two SH2 domains and one SH3 domain (Gresset, Hicks et al. 2010). These Src homology domains facilitate the interaction with proteins in receptor signalling complexes, and regulate the PLC-γ2 catalytic activity through auto-inhibition, similar to PI3K (Gresset, Hicks et al. 2010). The kinases involved in the SH2 domain-dependent activation of PLC-γ2 are likely context dependent, but SYK and BTK have been associated with PLC-γ2 activation in B cells (Kurosaki and Tsukada 2000, Chiang, Veckman et al. 2012). The N-terminal PH domain targets PLC-γ2 to membranes containing PI(3,4,5)P3 (Falasca, Logan et al. 1998, Pawelczyk and Matecki 1999). The C2 domain is another membrane binding domain that recruits the protein to negatively charged membranes in a calcium-dependent manner (Murray and Honig 2002).

In summary, PLC-γ2 plays an important role in TLR signalling and BCAP is a likely candidate to bridge this interaction. Moreover, the BCAP association with tyrosine kinases and its binding sites for SH2 and SH3 domain interactions may facilitate PLC-γ2 activation.

2 Thesis aims

Publications on the role of BCAP in TLR signalling suggest that the BCAP DBB domain may contribute to the negative regulation of TLR signalling. The first aim of this thesis is to elucidate the role of the DBB domain with regard to TIR domain interactions and inhibition of pro-inflammatory TLR signalling.

The second aim is to obtain structural information of the DBB and ANK domains, to further elucidate the function of these domains and their influence on TIR domain interactions. Moreover, a DBB domain structure would allow for the investigation of the intriguing structural similarities between the TIG fold of the DBB domain and transcription factors.

Previous results in the literature also lead to the hypothesis that BCAP hyperphosphorylation causes the appearance of multiple bands on western blot. Consequently, the third aim is to identify the nature of BCAP post-translation modifications, and to determine the kinases responsible for BCAP phosphorylation.

The fourth aim of this project is to further characterise existing BCAP interactions, and to identify novel BCAP interaction partners that could depend on extensive BCAP phosphorylation. Additional interaction partners would also enable a more precise mapping of BCAP in immune signalling networks and could help to explain the mechanism of TLR regulation.

3 Results

3.1 The role of the BCAP DBB domain in TIR domain interactions

3.1.1 Background

As mentioned, TIR domain interactions remain poorly characterised despite extensive research. Reports of putative mammalian TIR domain homodimers and related oligomerisation interfaces are abundant in the literature without direct experimental evidence. The N-terminal $BCAP^{TIR}$ domain has been claimed to interact with MAL and MyD88 through TIR domain interactions (Troutman, Hu et al. 2012). Through co-immunoprecipitation (Co-IP), these authors were able to show that various BCAP constructs interact with MAL and MyD88. $BCAP_S$, lacking the TIR domain, failed to interact with MAL and MyD88 under these conditions. NF-κB reporter assays gave similar results, suggesting that BCAP constructs containing the TIR domain are able to dampen inflammatory NF-κB signalling in HEK293 cells.

While these results highlight the importance of the $BCAP^{TIR}$ domain, they fail to outline the domains required for TIR domain interactions and signalling. Moreover, the authors imply the use of a $BCAP^{TIR}$ domain construct in their experiments, while using a construct spanning residues 1-321. These domain boundaries include the BCAP TIR and DBB domains. Consequently, the DBB domain may play an important role in facilitating TIR domain interactions and the negative regulation of TLR signalling.

Validation of TIR domain interactions and signalling assays as outlined by Troutman *et alia* (Troutman, Hu et al. 2012) should help to elucidate these contradictions. By comparing BCAP constructs containing strict TIR domain boundaries to longer constructs containing the DBB and ANK domains, the functional importance of these TIR-adjacent domains can be assessed.

3.1.2 The $BCAP^{TIR}$ domain interacts with MAL but not MyD88 *in situ*

A Co-IP experiment was conducted in order to assess the importance of the BCAP TIR and DBB domains for heterotypic TIR domain interactions. The FLAG-tagged BCAP constructs FLAG-TIR (1-143), FLAG-TIR-TIG2α (1-288) FLAG-TIR-DBB (1-309), FLAG-TIR-DBB-ANK (1-447), FLAG-tagged $BCAP_L$ and FLAG-MyD88 were overexpressed in HEK293T cells and probed for interaction with Myc-MAL and Myc-MyD88 by immunoprecipitation with anti-FLAG antibody.

As previously described, FLAG-BCAP and FLAG-TIR-DBB were able to pull down Myc-MAL and Myc-MyD88. However, while FLAG-TIR was able to interact with Myc-MAL, a Myc-MyD88 interaction was not detected. These results suggest that the $BCAP^{TIR}$ domain is sufficient for MAL interaction, whereas MyD88 association requires the full-length dimeric DBB domain as further discussed in Section 3.2.7.

The $BCAP^{TIR}$-MAL interaction is unexpected, since the $BCAP^{TIR}$ domain was previously found to be monomeric and therefore inactive in solution (Halabi, Sekine et al. 2017). Moreover, these results do not align with the widespread assumption that dimers are the functional units of TIR domain interactions. Instead, given recent reports on TIR domain filaments (Ve, Vajjhala et al. 2017), it is likely that the $BCAP^{TIR}$ domain interacts with MAL^{TIR} and $MyD88^{TIR}$ filaments.

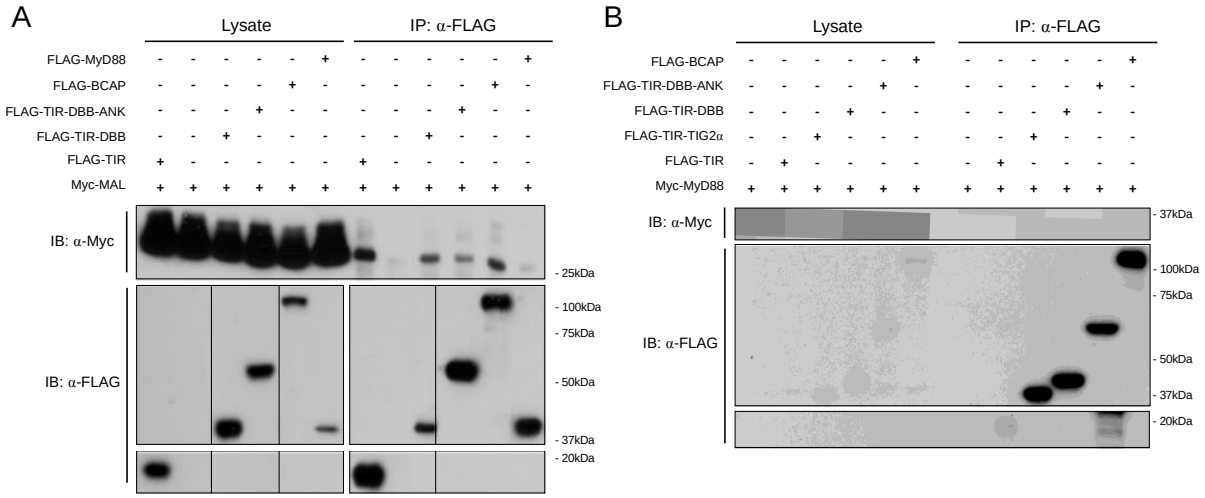

Figure 8. Co-immunoprecipitation reveals that the $BCAP^{TIR}$ domain interacts with MAL.
HEK293T cells were transiently transfected with FLAG-TIR (1-143), FLAG-TIR-TIG2α (1-288), FLAG-TIR-DBB (1-309), FLAG-TIR-DBB-ANK (1-447), FLAG-MyD88 and (A) Myc-MAL or (B) Myc-MyD88. At 24 h post-transfection, cells were lysed and subjected to immunoprecipitation with anti-FLAG antibody. Precipitates were split and assayed for precipitation of FLAG-tagged BCAP constructs or co-precipitation of Myc-tagged MAL and MyD88 by western blotting.

3.1.3 The BCAP DBB domain is required for TIR domain signalling

Since there might be a disconnect between TIR domain interactions and negative regulation of TLR signalling, an NF-κB reporter assays was used to evaluate the functional contribution of the DBB domain. Despite the caveats of studying TLR signalling in non-immune cells such as HEK293T cells, this type of NF-κB reporter assay based on overexpression of adaptor proteins has been well-established (Fitzgerald, Palsson-McDermott et al. 2001, Bin, Xu et al. 2003, Fitzgerald, Rowe et al. 2003, Troutman, Hu et al. 2012).

Similar to the Co-IP in HEK293T cells (Figure 8), BCAP constructs of various lengths were tested for their ability to dampen MAL and MyD88 overexpression-induced NF-κB signalling.

Myc-BCAP$_L$ (1-805), Myc-TIR-DBB-ANK (1-447) and Myc-TIR-DBB (1-309) constructs were able to dampen MAL inflammatory NF-κB signalling (Figure 9A). This is in agreement with previously published results (Troutman, Hu et al. 2012). However, Myc-TIR (1-143), and FLAG-TIR-TIG2α (1-288) were unable to dampen inflammatory signalling. In fact, a significant increase in NF-κB signalling was observed when Myc-TIR and Myc-MAL were co-transfected.

Whereas MAL overexpression resulted in a 10-fold increase in NF-κB signalling, MyD88 overexpression consistently resulted in a >100-fold induction (Figure 9). This MyD88-induced NF-κB signalling was inhibited by Myc-BCAP$_L$, Myc-TIR-DBB, Myc-TIR-DBB-ANK and Myc-TIR-TIG2α (Figure 9B). Unexpectedly, Myc-TIR again induced a large increase in NF-κB signalling (Figure 9B).

The different degree of NF-κB induction upon MyD88 and MAL expression has been observed in previous studies (Troutman, Hu et al. 2012), and may be caused by the fact that MAL overexpression relies on endogenous MyD88 for myddosome formation and subsequent NF-κB activation. MyD88 overexpression on the other hand should directly increase the rate of myddosome formation, leading to higher NF-κB signalling.

Altogether, these results illustrate that the BCAP^{TIR} domain is unable to negatively regulate TLR signalling. These results also suggest that the DBB domain plays a crucial role in these experiments. The presence of both the BCAP TIR and DBB domains seems to dampen inflammatory NF-κB signalling in these experiments. Removal of the last DBB α-helix in the TIR-TIG2α construct may suggest a for dimerisation in the context of MAL-induced NF-κB signalling, as further discussed in Section 3.2.7. Though somewhat preliminary, these results may also explain why previous studies included the DBB domain in constructs that were annotated as TIR domains (Troutman, Hu et al. 2012). Although the interaction between the BCAP^{TIR} domain and MAL is independent of the DBB domain, it is essential for negative regulation of NF-κB signalling.

The increase of MAL and MyD88-induced NF-κB signalling in the presence of the BCAP^{TIR} domain is an unexpected observation. Western blot analysis of Myc-MAL and Myc-MyD88 expression shows that the increase in NF-κB signalling is not caused by higher expression of MAL or MyD88 (Figure 9C). It can there be hypothesised that the BCAP^{TIR} domain is able to maximise the competency of MyD88 autoactivation and myddosome formation. This

observation may contribute to the mechanistic understanding of the TLR signalosome as further discussed in section 4.1.

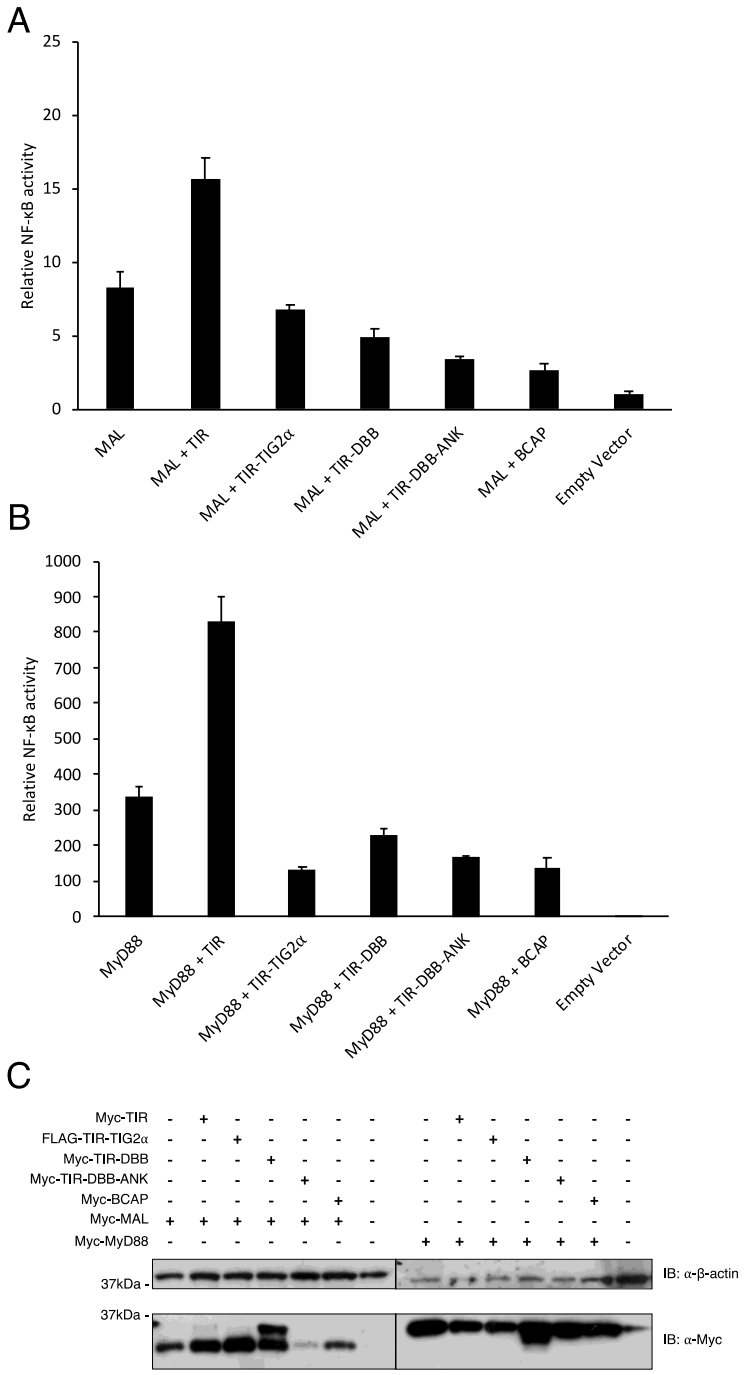

Figure 9. The BCAP DBB domain is required for negative regulation of TLR signalling.

HEK293T cells were transiently transfected with pNF-κB-luc (NF-κB inducible firefly luciferase reporter), phRG-TK (constitutive *Renilla* luciferase reporter) and a combination of, Myc-TIR, FLAG-TIR-TIG2α, Myc-TIR-DBB and Myc-TIR-DBB-ANK, Myc-BCAP$_L$ and (A) Myc-MAL or (B) Myc-MyD88 as indicated. At 24 h post-transfection, cells were lysed and the NF-κB-induced luciferase activity was measured *via* a luminescence read-out. Relative NF-κB activation represents the ratio of firefly luciferase over *Renilla* luciferase activity. Data is represented as mean ±SD of five technical repeats and the images shown represent three independent experiments. (C) Immunoblotting of (A) and (B) NF-κB reporter assay conditions.

3.1.4 Dimeric $BCAP_L$ prevents MAL filament formation *in vitro*

In order to better understand the interplay of $BCAP^{TIR}$ domain with MAL filaments, an *in vitro* interaction assay was conducted. Observations from an *in vitro* system may contribute to our understanding of TIR domain interactions, and help elucidate the apparent disconnect between $BCAP^{TIR}$ domain interactions and negatively regulating the TLR signalosome.

In this experiment, the MAL^{TIR} domain (residues 79-221) was cloned, expressed in *E. coli* and purified as described in Sections 5.3.1 and 5.4. This construct can be purified as a monomeric and soluble TIR domain, but has the ability to form temperature reversible filaments (Ve, Vajjhala et al. 2017).

BCAP constructs with various domain boundaries were expressed in *E. coli* and purified as further described in section 3.2.4 and 3.2.7. $BCAP_L$ (residues 2-805) was expressed in Expi293F cells as described in section 5.3.2. Purified TIR-TIG2α (7-288), TIG2a (179-288), DBB-ANK and $BCAP_L$ were then combined with the MAL^{TIR} domain to evaluate filament formation. Filament formation was detected by localising the MAL^{TIR} domain in the soluble supernatant or insoluble pellet fractions after incubation at 30 °C (Figure 10).

In the negative control, the MAL^{TIR} domain is exclusively located in the insoluble pellet fraction after incubation. Addition of the TIG2α, TIR-TIG2α or DBB-ANK constructs did not influence filament formation. Interestingly, each of these BCAP constructs was also present in the pellet fraction, suggesting an interaction with the MAL^{TIR} domain filaments. However, this was independent of the presence of the $BCAP^{TIR}$ domain in these constructs, indicative of an unspecific interaction. Upon the addition of dimeric $BCAP_L$ to MAL^{TIR} domains, no filament formation could be observed. This implies that dimeric $BCAP_L$ is able to inhibit MAL^{TIR} domain filament formation *in vitro*. The functional difference between monomeric TIR-TIG2α and dimeric $BCAP_L$ further suggests that dimerisation is an important property for BCAP-MAL interactions as discussed in section 3.2.7.

In order to further characterise the interaction between $BCAP_L$ and the MAL^{TIR} domain, the samples were analysed by analytical gel filtration. This resulted in two separate peaks corresponding to monomeric MAL^{TIR} domain and dimeric $BCAP_L$ (Figure 11). Moreover, the BCAP peak did not shift to a higher molecular weight compared to the control that only contained BCAP, indicating that no complex formation was present under these conditions.

The absence of complex formation on gel filtration suggests a low-affinity interaction, an interaction with a fast off rate, or the absence of a BCAP-MAL interaction altogether. The fact

that BCAP prevents MAL interactions at a 1:10 sub-stoichiometric ratio suggests that some level of interaction is taking place. In comparison to the HEK293T Co-IP (Figure 8), these results suggest that *in situ* other proteins are necessary to stabilise BCAP-MAL interactions. Since BCAP is also known to interact with MyD88, it may be possible that simultaneous interaction with endogenous MyD88 stabilises BCAP-MAL interactions.

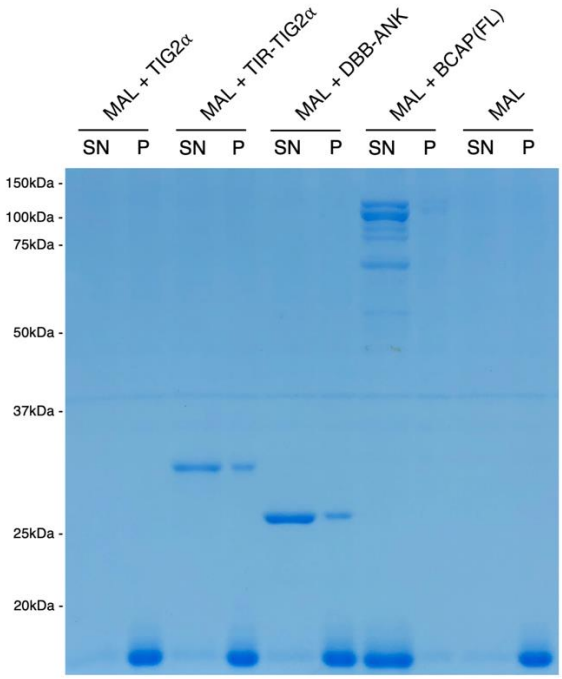

Figure 10. Dimeric BCAP prevents MAL filament formation *in vitro*.
Purified MAL^{TIR} domain and various BCAP constructs (TIG2α, TIR-TIG2α, DBB-ANK, $BCAP_L$) were mixed in a 10:1 molar ration and incubated at 30 °C for 30 min to induce MAL filament formation. Soluble (supernatant, SN) and insoluble fraction (pellet, P) were separated by centrifugation and analysed by SDS-PAGE.

3.1.5 Limitations to the interpretation of the BCAP DBB domain function

Collectively, the results presented in this chapter support the hypothesis that the DBB domain plays an important role in $BCAP^{TIR}$ domain signalling. On the other hand, the results from some individual experiments are somewhat preliminary. Results from the NF-κB reporter assay have to be interpreted with caution, since it is difficult to conclude a significant reduction in NF-κB signalling for TIR-TIG2α and TIR-DBB based on the current data. Statistical tests such as a student T-test shows a significant reduction of MAL-induced NF-κB signalling by Myc-TIR-DBB, however, since only five technical repeats can be compared, these tests have little meaning.

To further validate the role of the DBB domain in NF-κB reporter assay, the amount of TIR-TIG2α and TIR-DBB construct DNA could be systematically increased in this

experimental setup. A concentration dependent reduction of NF-κB signalling, or the absence thereof, would then give more confidence to the conclusion that TIR-TIG2α or TIR-DBB negatively regulate inflammatory signalling.

3.2 Structural analysis of the BCAP DBB and ANK domains

3.2.1 Background

The aim of this section was to express and purify recombinant protein to milligram quantities for biophysical and structural studies. Chapter 3.1 described how the BCAP DBB domain plays an important role in negative regulation of TLR signalling. A structural model of the DBB and ANK domains would provide valuable information to understand the mechanisms through which the DBB domain acts on TIR interactions. Moreover, a structural model and further biophysical characterisation would provide valuable insight into the BCAP dimerisation regions.

Despite the definition of DBB domain characteristics by Battersby *et alia* (Battersby, Csiszár et al. 2003), no structural information is available to date. However, based on the initial domain characterisation of BCAP and secondary structure predictions, the DBB domain is expected to be comprised of a TIG fold followed by three α-helices.

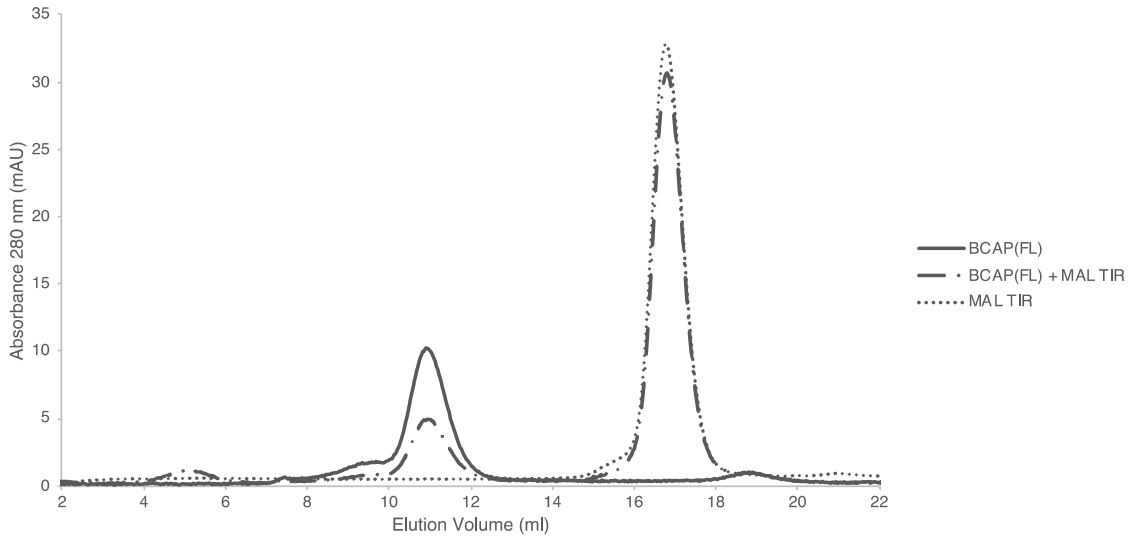

Figure 11. $BCAP_L$ and MAL^{TIR} domain do not form a stable complex during gel filtration.

Analytical size exclusion chromatography of purified MAL^{TIR} domain and $BCAP_L$ as indicated. $BCAP_L$ and to MAL^{TIR} domain were mixed in a molar ratio of 1:10. Samples were incubated at 30 °C for 1 h before analysis on a Superdex 200 10/300 GL column.

3.2.2 Expression and purification on the BCAP DBB and ANK domains

Based on secondary structure predictions, BCAP constructs of various lengths were designed and cloned into a pMCSG7 vector resulting in an N-terminal His-tag followed by a TEV protease cleavage site (Figure 12). Initial constructs used the $BCAP_S$ start codon as N-terminal boundary, whereas various C-terminal boundaries were selected (Table 4). The C-termini were located at the end of annotated domains, and were systematically moved by several amino acids to allow for potential mistakes in domain annotations.

All resulting DBB and DBB-ANK constructs were expressed in *E. coli* cells as described in section 5.3.1. After overnight expression, all constructs showed a clear overexpression band on SDS-PAGE (Figure 13). With the goal to evaluate the stability of various constructs, each construct was purified by nickel affinity purification, followed by gel filtration.

3.2.3 DBB domain purification revealed protein degradation

Initial nickel IMAC resulted in significant amounts of target protein with few bacterial contaminants (Figure 14A-B). On SDS-PAGE, however, the His-tagged DBB constructs appeared as multiple bands that were not evident in the lysate fraction. Subsequent gel filtration (Figure 14C) or anion exchange (not shown) did not result in homogeneous samples, as contamination bands at a higher and lower molecular weight (MW) were persistent (Figure 14D). Since all DBB constructs behaved identically to the DBB313 purification shown in Figure 14, they did not meet the requirements for crystallisation trials.

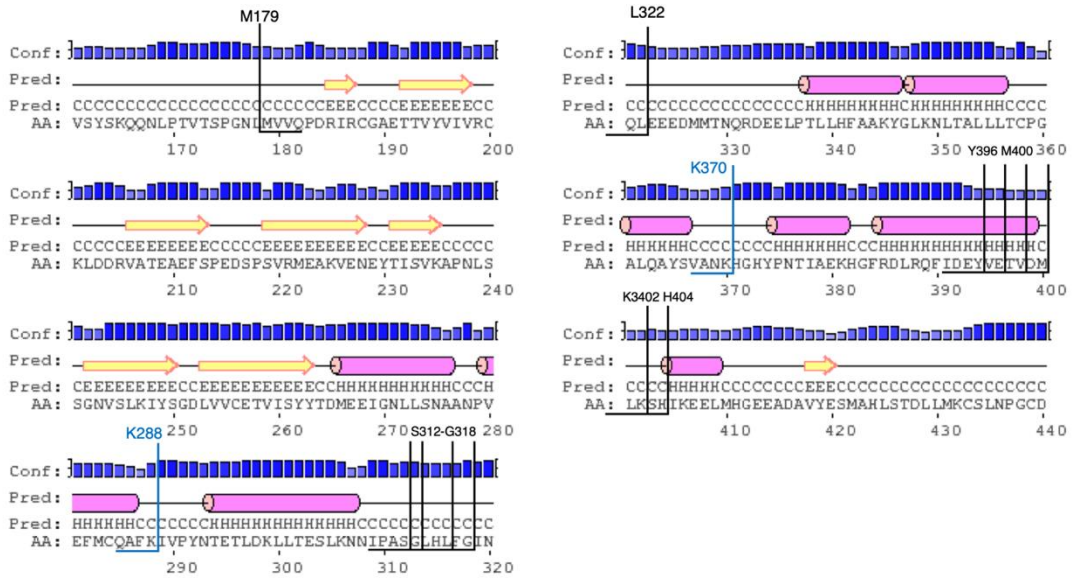

Figure 12. Overview of DBB and DBB-ANK construct domain boundaries.

(A) *PSIPRED* (Buchan and Jones 2019) schematic representation of the BCAP DBB and ANK domains with their respective secondary structure features. Black lines indicate initial N- and C-terminal boundaries for the DBB and ANK constructs. Blue lines indicate C-terminal domain boundaries that were later derived from the initial set by limited proteolysis.

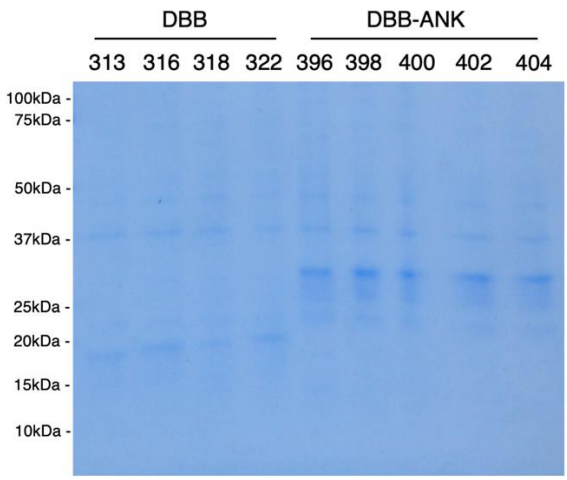

Figure 13. Test expression of DBB and DBB-ANK constructs.

Samples from the Rosetta2(DE3) test expression of DBB and DBB-ANK constructs as referred to by their C-terminal residue number. Bacterial cultures for test expression were grown in auto-induction medium at 37 °C for 4 h after which the temperature was reduced to 20 °C for protein expression overnight. Samples were lysed and the soluble fractions were analysed on SDS-PAGE.

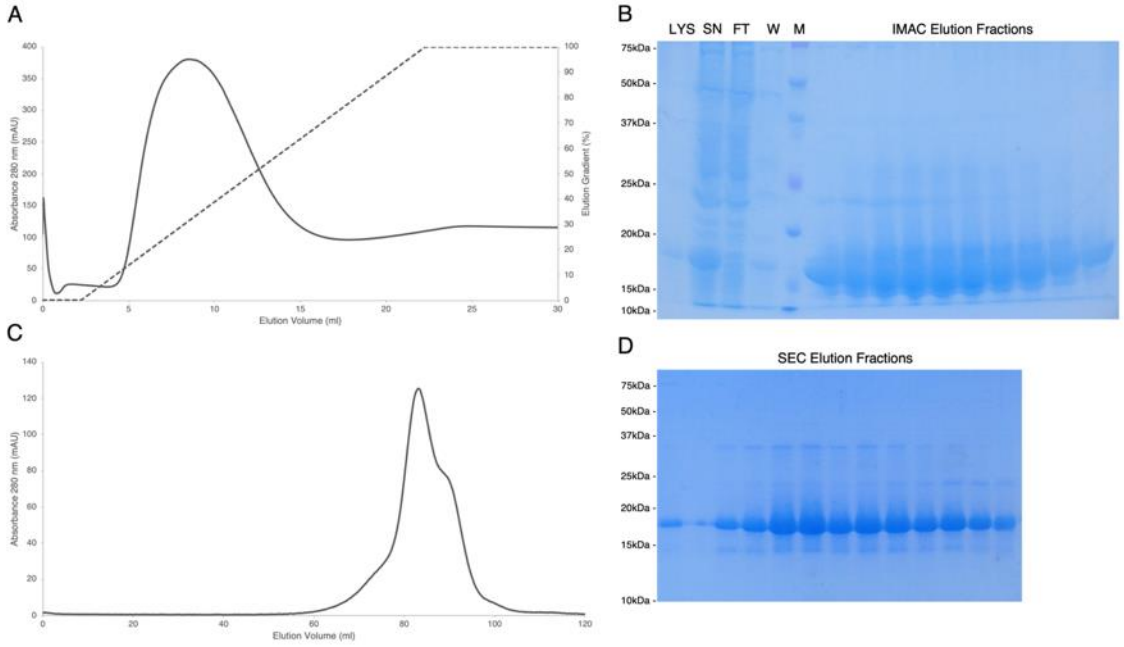

Figure 14. Purification of DBB constructs *via* nickel affinity chromatography and gel filtration.

(A) Nickel IMAC elution profile of DBB313 from a 1 ml Chelating HP column. (B) SDS-PAGE was used to analyse the lysate (LYS), supernatant (SN), flowthrough (FT), wash (W) and elution fractions from the DBB313 nickel IMAC purification. (C) Size exclusion chromatography of DBB313 using a HiLoad 16/600 Superdex 200 column. (D) SDS-PAGE analysis of peak elution fractions from DBB313 gel filtration. M indicates the marker.

3.2.4 DBB-ANK domain purification yielded pure and stable protein

Given the poor stability of the DBB domain constructs, efforts were focused on larger DBB-ANK constructs. All DBB-ANK constructs with C-terminal residues 396-404 were processed

with an initial nickel IMAC purification, followed by TEV protease cleavage and a second nickel IMAC purification step to remove the His-tagged TEV protease and uncut protein. Subsequently, gel filtration was used as a buffer exchange and final purification step.

All DBB-ANK constructs behaved identically during purification. With DBB-ANK396 as an example, nickel IMAC (Figure 15A) resulted in a relatively pure sample on SDS-PAGE that ran as one band without visible contaminants (Figure 15B). IMAC elution fractions were then pooled and treated with TEV protease. Subsequently, samples were passed over a second nickel IMAC column, and the resulting flowthrough was concentrated and loaded onto a Superdex 200 16/60 column. Gel filtration resulted in a symmetric peak, with negligible amounts of impurities on SDS-PAGE (Figure 15C-D).

Similarly to all shorter DBB-ANK constructs, the DBB-ANK404 purification resulted in a symmetric peak on gel filtration (Figure 16A), without any visible contaminants on SDS-PAGE (Figure 16B). Fractions from gel filtration were pooled for further analysis. On native-PAGE, the protein migrated as a single band, indicative of a monodisperse sample (Figure 16C).

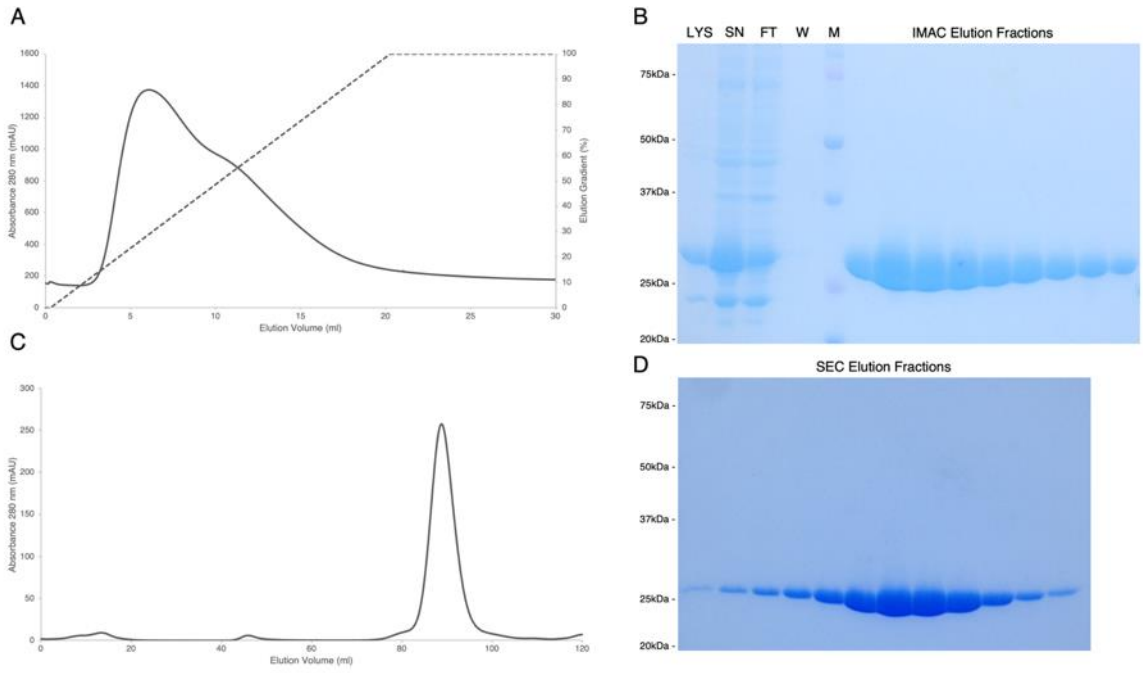

Figure 15. Purification of DBB-ANK constructs *via* nickel affinity chromatography and gel filtration.
Purification strategy of DBB-ANK396 representative of the purification of all DBB-ANK constructs. (A) Nickel IMAC elution profile of DBB-ANK396 from a 1 ml Chelating HP column. (B) SDS-PAGE was used to analyse the lysate (LYS), supernatant (SN), flowthrough (FT), wash (W) and elution fractions from the DBB-ANK396 nickel IMAC purification. (C) Size exclusion chromatography of DBB-ANK396 using a HiLoad 16/600 Superdex 200 column. (D) SDS-PAGE analysis of DBB-ANK396 gel filtration peak elution fractions. M indicates the marker.

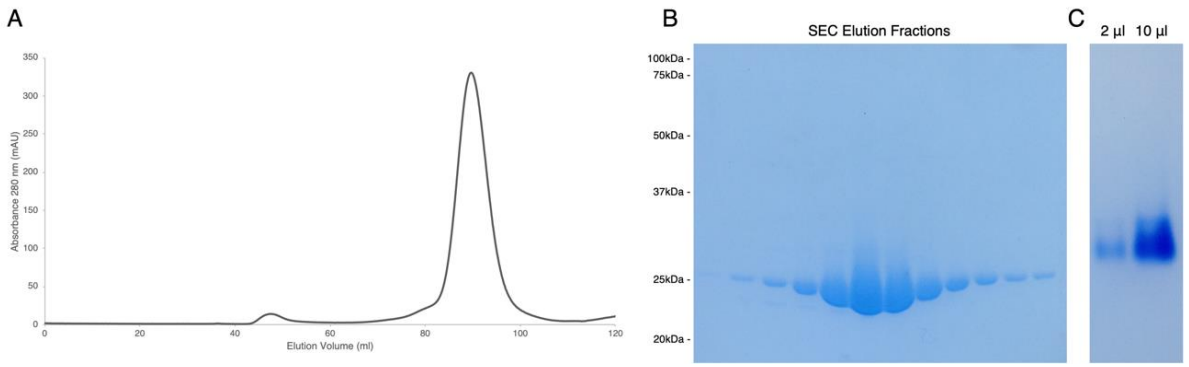

Figure 16. Assessment of DBB-ANK404 purity after gel filtration.

(A) HiLoad 16/600 Superdex 200 size exclusion chromatography of DBB-ANK404 following nickel IMAC purification and TEV cleavage. (B) SDS-PAGE analysis of DBB-ANK404 gel filtration peak elution fractions. (C) Native-PAGE analysis of DBB-ANK404 after gel filtration. Volumes refer to the amount of sample loaded in each lane.

Crystallisation of DBB-ANK constructs

Starting with the DBB-ANK396, several commercial crystallisation screens were set up at protein concentrations ranging from 6-10 mg/ml as described in section 5.6.1. No crystallisation hits nor phase separation, or otherwise interesting precipitation were observed after drop equilibration.

With the DBB-ANK404 construct, another set of commercial crystallisation screens was set up at a concentration of 9 mg/ml as described in Section 5.6.1. Crystals appeared overnight in conditions containing the organic acids malonate (1.1 M malonate, 0.5% jeffamine ED-2003 and 0.1 M HEPES pH 7.5), citrate (1 M Na citrate, 0.1 M HEPES pH 7.0) and tartrate (1.2 M Na/K tartrate, 0.1 M TRIS pH 8.0) (Figure 17A). The crystals were subjected to UV-imaging to confirm protein crystallisation (Figure 17B). The rod-shaped crystals did absorb UV light, but they exhibited a faint signal due to the absence of tryptophan residues in the DBB and ANK domains. Crystals from all three crystallisation conditions were cryo-protected using 20% (v/v) glycerol and screened for diffraction using the in-house Icarus (Bruker) X-ray source. After 60 s exposure no diffraction was detected.

In order to improve the crystal diffraction properties, an extensive set of optimisation screens was conducted based on the malonate-containing crystallisation condition. Two-dimensional screens were prepared, in which the malonate (0.8-1.3 M) and jeffamine (0.3-0.5%) concentrations were systematically varied over 96 wells, while keeping the HEPES buffer concentration constant. Using this setup, the initial crystallisation condition was reproducible and small crystals appeared overnight, independent of the jeffamine concentration. Crystals from this screen again showed no diffraction on the inhouse X-ray source, but did diffract up

to 30 Å with synchrotron radiation (Diamond Light Source i04). Similarly, optimisation screens that varied the pH (pH 6.0-9.0) did not improve diffraction, nor change the crystal morphology.

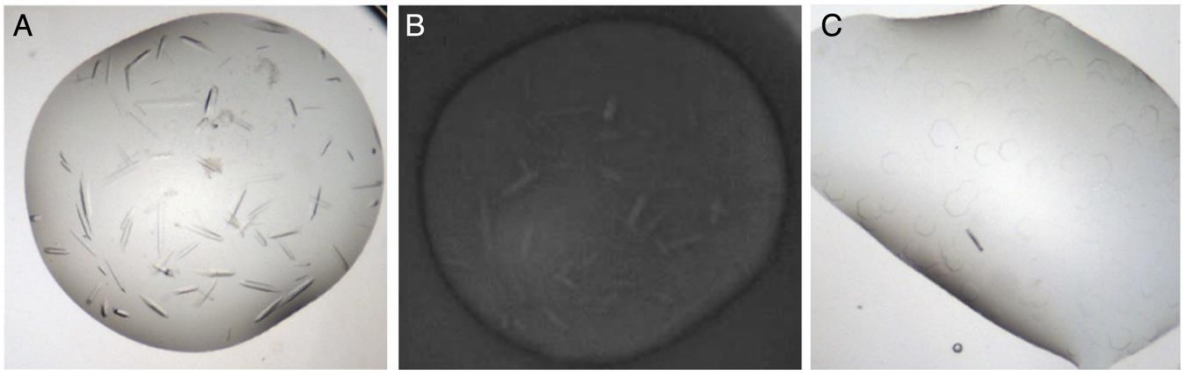

Figure 17. DBB-ANK404 crystallisation in the presence of malonate.
(A) Crystals in the shape of monoclinic styloids appeared overnight in the presence of 1.1 M malonate, 0.5% jeffamine ED-2003 and 0.1 M HEPES pH 7.5. (B) UV absorbance of (A). (C) Upon the addition of 10 mM TCEP to the original malonate-containing crystallisation condition, flat hexagonal crystals appeared overnight.

To screen a wider range of compounds, an additive screen was conducted with the initial malonate-containing hit. In 18 of 96 conditions, crystals of varying size appeared after one to three days (Table 1). Notably, crystals grown in the presence of the reducing agent TCEP had a flat hexagonal shape (Figure 17C). A manual optimisation screen with a hanging drop setup was used to increase the drop volume in order to enhance the size of the hexagonal crystals. Selected crystals (grown in 1.1 M malonate, 0.5% jeffamine ED-2003, 0.1 M HEPES, 10 mM TCEP pH 7.0) were cryo-protected in 20% glycerol before freezing in liquid nitrogen. Since the presence of glycerol significantly slowed down crystal growth, another hanging drop screen was conducted with increasing concentrations of glycerol (3-20%). Crystals appeared in up to 16% glycerol, and were directly frozen for diffraction testing.

Diffraction screening on the in-house X-ray source revealed that only rod-shaped crystals grown in the presence of glycerol diffracted up to about 9 Å. Crystals grown in identical conditions were later screened using synchrotron radiation (i02, Diamond Light Source), where diffraction did not exceed 7 Å. Based on test images at this resolution, the space group was determined to be P4 with predicted lattice dimensions of 222.54 × 222.54 × 461.66 Å, and angles of 90.00°.

An optimisation screen where increasing amounts of glycerol (3-20%) were added to the initial hits containing citrate and tartrate resulted in crystals that diffracted up to 10 Å (Diamond Light Source i04). Similar to malonate-containing screens, manual pH optimisation (pH 6.0-9.0) did not improve crystal diffraction. In the presence of up to 10 mM TCEP, hexagonal crystal forms

were observed in tartrate and citrate-containing conditions but these crystals did not diffract with synchrotron radiation (Diamond Light Source i04).

Table 1. Crystallisation conditions in the DBB-ANK404 additive screen.

Additive	Crystal morphology*	Day of appearance
0.1 M Barium chloride dihydrate	3	2
0.1 M Strontium chloride hexahydrate	3	2
0.1 M Yttrium(III) chloride hexahydrate	1	2
1.0 M Ammonium sulphate	3	2
2.0 M Sodium chloride	1	2
0.5 M Sodium fluoride	3	2
1.0 M Potassium sodium tartrate tetrahydrate	2	2
1.0 M Sodium citrate tribasic dihydrate	1	2
1.0 M Sodium malonate pH 7.0	2	1
30% w/v 6-Aminohexanoic acid	3	2
30% w/v 1,5-Diaminopentane dihydrochloride	3	2
0.1 M TCEP hydrochloride	3	2
30% w/v Dextran sulphate sodium salt (Mr 5000)	2	2
30% w/v D-Sorbitol	2	1
30% v/v Glycerol	3	3
2.0 M NDSB-211	3	2
0.15 mM CYMAL®-7	3	2
30% w/v Trimethylamine N-oxide dihydrate	2	1

* Crystal morphology score
1 - Shower
2 - Microcrystals
3 - Macrocrystals

3.2.5 Further optimisation of DBB-ANK crystallisation

One strategy to improve protein crystallisation or diffraction is the reduction of surface entropy. In practice this can be accomplished by site-directed mutagenesis of flexible surface residues such as lysine or glutamate, or by chemical modification (Walter, Meier et al. 2006). The latter is less laborious and does not perturb the protein fold. Lysine dimethylation is one such technique that was successfully used to crystallise TLR adaptor proteins in the past (Snyder, Deredge et al. 2014, Halabi, Sekine et al. 2017). DBB-ANK404 was lysine methylated using formaldehyde and dimethylamine-borane complex as described in Section 5.5.1. Subsequent gel filtration resulted in a slight shift in retention volume indicative of a successful chemical modification (Figure 18). Crystallisation trials with methylated DBB-ANK404 did not result in positive hits, including the previous crystallisation conditions containing organic acids.

A second approach to obtain structural information on the DBB-ANK domain was to design new constructs leveraging the stable C-terminal domain boundary. For this purpose, a TIR-DBB-ANK404 construct (residues 7-404) was cloned into pMCSG7. Additionally, a DBB-ANK (residues 179-405) construct of the mouse BCAP protein (Mm404) was cloned into pMCSG7, using domain boundaries equivalent to the DBB-ANK404 construct. Both

TIR-DBB-ANK404 (Figure 19) and Mm404 (Figure 20) were purified as described for human DBB-ANK404 and resulted in pure and monodisperse protein.

Crystallisation trials of TIR-DBB-ANK404 did not result in positive hits. However, Mm404 produced spherulites in a condition containing 2.5 M NaCl, 0.1 M imidazole and 0.2 M zinc acetate pH 8.0 (Figure 20E). Unfortunately, these spherulites were not reproducible in further optimisation screens.

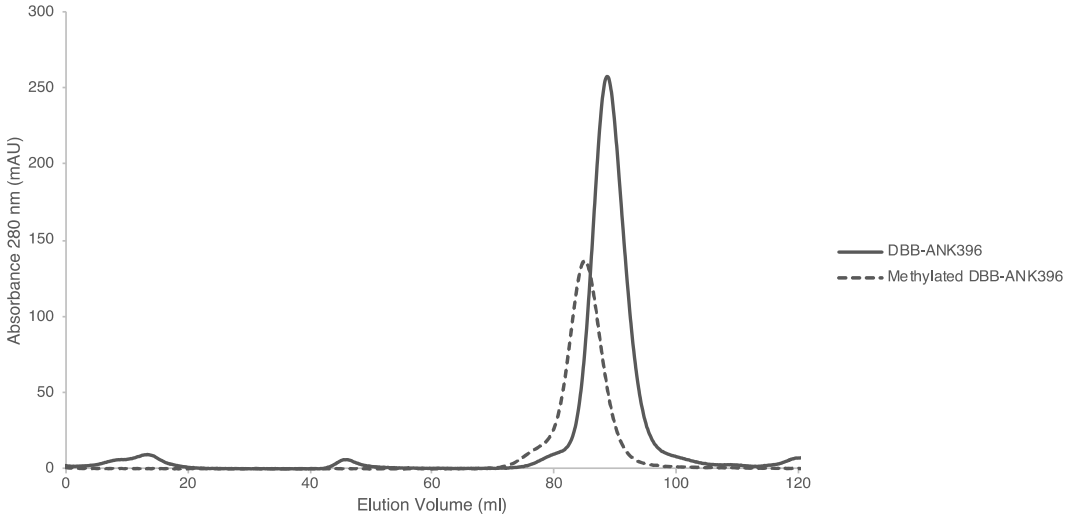

Figure 18. Lysine methylation of DBB-ANK396 results in a noticeable shift on gel filtration.
Before and after lysine methylation, DBB-ANK396 was analysed by gel filtration using a HiLoad 16/600 Superdex 200 column.

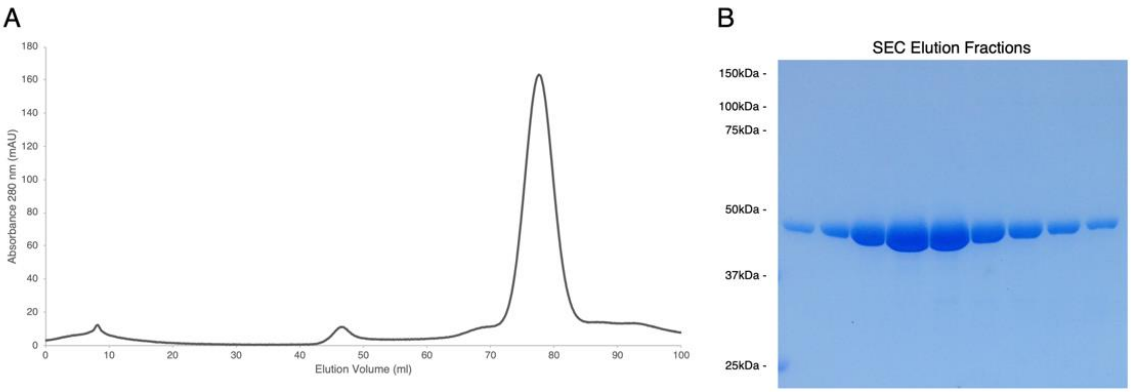

Figure 19. Purification of TIR-DBB-ANK404 construct *via* gel filtration.
(A) HiLoad 16/600 Superdex 200 size exclusion chromatography of TIR-DBB-ANK404 following nickel IMAC purification and TEV cleavage. (B) SDS-PAGE analysis of TIR-DBB-ANK404 gel filtration peak elution fractions.

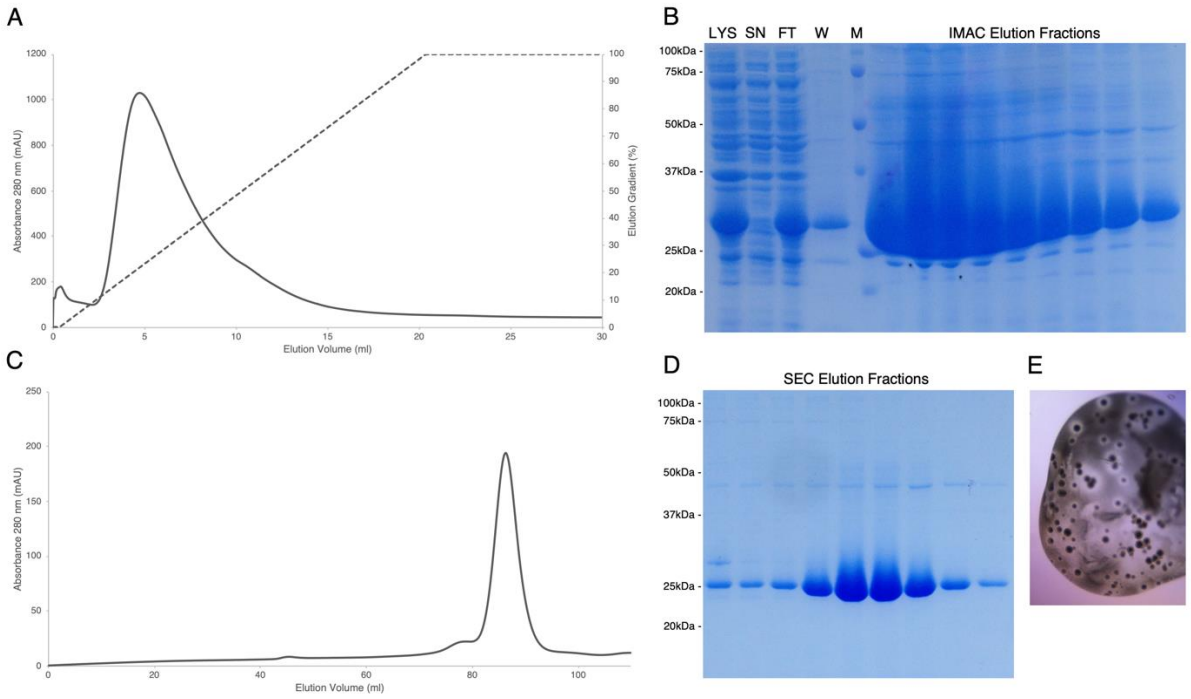

Figure 20. Purification of Mm404 constructs *via* nickel affinity chromatography and gel filtration leading to spherulites in crystallisation trials.

(A) Nickel IMAC elution profile of Mm404 from a 1 ml Chelating HP column. (B) SDS-PAGE was used to analyse the lysate (LYS), supernatant (SN), flowthrough (FT), wash (W) and elution fractions from the Mm404 nickel IMAC purification. (C) Size exclusion chromatography of Mm404 using a HiLoad 16/600 Superdex 200 column. (D) SDS-PAGE analysis of Mm404 gel filtration peak elution fractions. (E) Spherulites observed in crystallisation condition containing 2.5 M NaCl, 0.1 M imidazole and 0.2 M zinc acetate pH 8.0. M indicates the marker.

3.2.6 Optimisation of the DBB-ANK constructs using limited proteolysis

Due to the unsuccessful attempts to improve the diffraction of DBB-ANK404 crystals, the protein was subjected to limited proteolysis, to remove potentially flexible regions and identify a rigid core that may allow for better crystal packing and diffraction. DBB-ANK404 was seperately incubated with different concentrations of sequence-grade trypsin (Promega) and sequence-grade chymotrypsin (Promega) (Figure 21A-B). Minutes after exposure to protease, two bands above 20 kDa appeared on SDS-PAGE. Both proteases also revealed a fragment of approximately 12 kDa that was stable for up to 3 h. The three major degradation products of trypsin proteolysis were subjected to MALDI peptide mass fingerprinting (Figure 21C). With the full-length DBB-ANK404 as a reference with 89% coverage, mass spectrometry revealed that the top-most degradation band had been subject to C-terminal cleavage at K370. The second degradation band contained an N-terminal cleavage site around R221 or K225. Lastly, the most stable degradation product around 12 kDa was a DBB domain fragment cleaved at K288.

Constructs containing the new C-terminal domain boundaries (DBB-ANK370 containing residues 179-370 and DBB288 containing residues 179-288) were cloned into pMCSG7 vectors and expressed as described in Section 5.1 and Section 5.3.1, respectively. Purification of DBB-ANK370 resulted in relatively pure and stable protein similar to previous DBB-ANK constructs (Section 3.2.4). Although slight degradation was visible on SDS-PAGE (Figure 22), crystallisation trials were performed. However, no positive hits were obtained after drop equilibration in these screens.

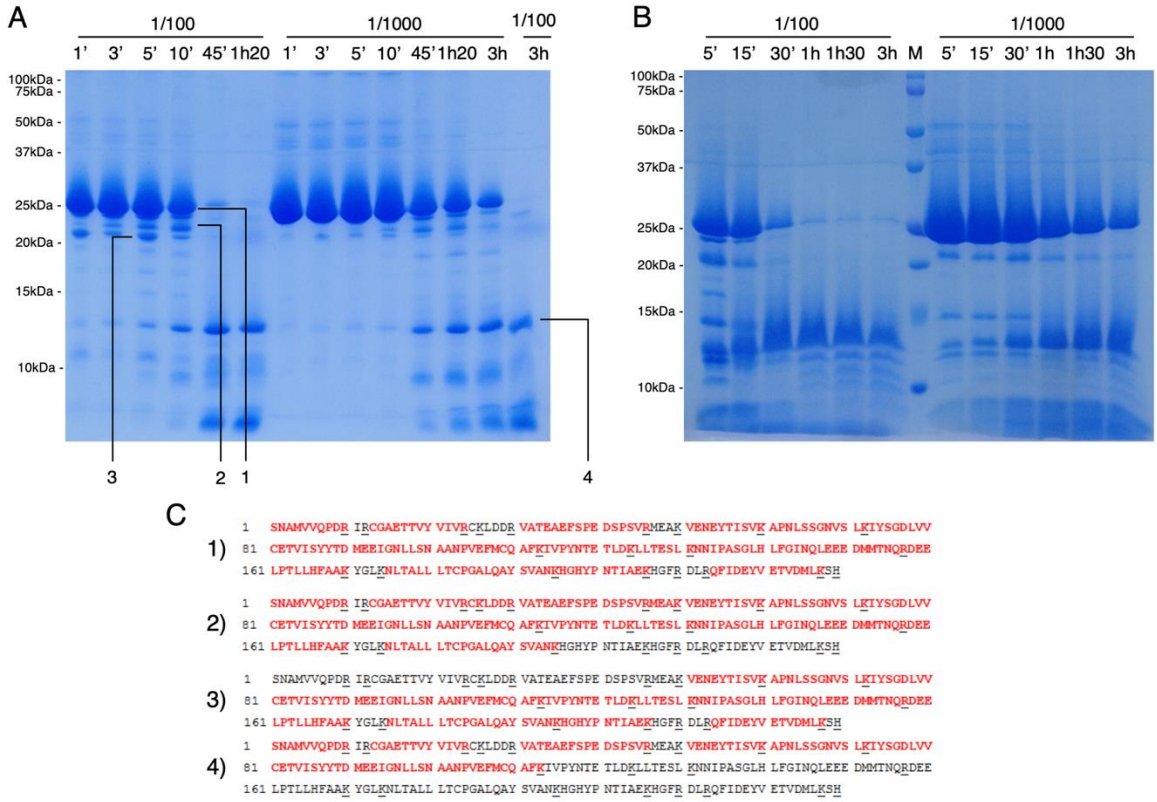

Figure 21. Limited proteolysis of DBB-ANK404 results in multiple stable fragments.

(A) Trypsin limited proteolysis of DBB-ANK404, with the protease dilution and time of digestion as indicated. (B) Chymotrypsin limited proteolysis of DBB-ANK404. (C) MALDI peptide mass fingerprinting of the full-length DBB-ANK as reference. Underlined amino acids represent theoretical trypsin cleavage sites. Residues marked in red were part of peptides that were detected during the analysis. M Indicates the marker.

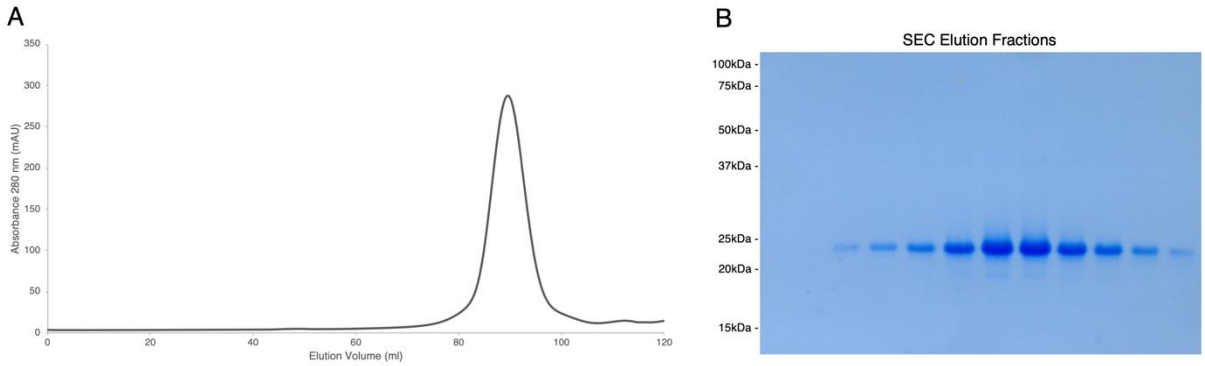

Figure 22. Purification of DBB-ANK370 construct *via* gel filtration.

(A) HiLoad 16/600 Superdex 200 size exclusion chromatography of DBB-ANK370 following nickel IMAC purification and TEV cleavage. (B) SDS-PAGE analysis of DBB-ANK370 gel filtration peak elution fractions.

3.2.7 Purification and characterisation of the DBB domain

The DBB288 construct was expressed in *E. coli* as described in Section 5.3.1. Purification was analogous to the DBB-ANK protocol with an initial nickel IMAC step, followed by TEV protease digestion and a second nickel IMAC step. Nickel IMAC yielded large amounts of protein with limited degradation indicated by a band around 12 kDa (Figure 23A-B).

The final gel filtration purification step resulted in a pure protein as assessed by SDS-PAGE, with minute higher MW contaminants (Figure 23D). However, the protein eluted as an asymmetrical peak with a longer trailing edge (Figure 23C). Protein fractions were pooled to avoid the trailing edge, and concentrated to 2 mg/ml for further biophysical analysis.

The BCAP DBB domain has previously been associated with BCAP oligomerisation (Battersby, Csiszár et al. 2003, Halabi, Sekine et al. 2017). In order to assess the oligomerisation propensity of DBB288 compared to DBB-ANK404, and to determine a possible contribution of the ANK domain to BCAP dimerisation, purified proteins were analysed with SEC-MALS as described in Section 5.6.3.

To obtain a purified ANK domain required for this experiment, DNA coding for BCAP residues 333-467 was cloned into pMCSG7. Following expression and cell lysis as described in sections 5.3.1 and 5.3.3, no soluble protein expression was obtained. An MBP-tag was chosen to enhance expression and solubility, since MBP is a stable monomeric protein that should not interfere with SEC-MALS measurements (Reuten, Nikodemus et al. 2016). DNA coding for the ANK domain was cloned into a pMCSG9 His-MBP-tagged expression vector and again expressed in *E. coli*. Nickel IMAC purification yielded plenty of protein that was further purified *via* gel filtration without removing the MBP-tag (Figure 24A-B). Gel filtration resulted in a two separate elution peaks that both contained pure MBP-ANK with a slight contaminant

around the MW of the MBP-tag (Figure 24C-D). The elution peak around 85 ml corresponds to monomeric or dimeric protein, whereas the peak around 60 ml likely represents aggregates (>300 kDa), since this peak was not observed during subsequent SEC-MALS.

Using SEC-MALS, DBB-ANK404 was determined to be dimeric in solution with a measured molecular weight of 47.9 kDa (Figure 25A). This measurement falls within the expected experimental error for a theoretical dimeric MW of 51.1 kDa. The MW of the DBB288 construct was determined to be 13.22 kDa and is consistent with a monomeric DBB288 domain, which has a predicted MW of 12.4 kDa (Figure 25B). Consequently, this measurement reveals that DBB288 is monomeric in solution at the given concentration of 2 ml/mg before injection. MBP-ANK measurements were inconsistent and the measured MW strongly varied along an asymmetrical elution peak (Figure 25C). The leading-edge shoulder was not observed during the purification process, and was likely hidden by the lower resolution of the HiLoad 16/600 Superdex 200 column. The average MW over the peak was about 90 kDa. With a predicted monomeric and dimeric MWs of 56.7 and 113.4 kDa, respectively, the oligomerisation state of MBP-ANK in solution could not be robustly identified.

Previous results showed that the full-length DBB domain, which contains all three C-terminal α-helices, is dimeric in solution (Halabi, Sekine et al. 2017). Removal of the last DBB α-helix (DBB288) in this experiment now shows the importance of the last DBB α-helix for dimerisation. Independent of the ANK domain contribution to BCAP dimerisation, the C-terminal α-helix is the driver of BCAP dimerisation.

These results also have implications for the previous NF-κB reporter assays described in Section 3.1.3. This assay showed that only constructs containing both the TIR and full DBB domains can dampen MAL-induced inflammatory signalling. Removal of the last α-helix results in loss-of-function with regard to signalling. It can therefore be concluded that the DBB domain facilitates TIR domain signalling through dimerisation.

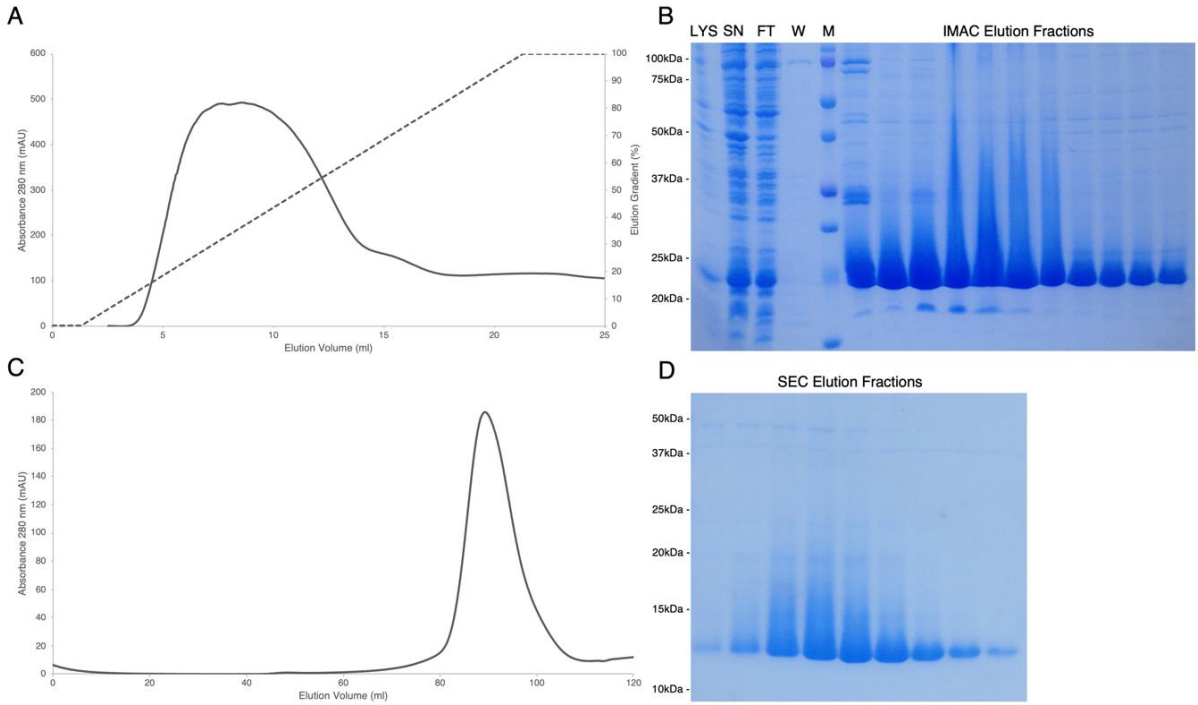

Figure 23. Purification of DBB288 constructs *via* nickel affinity chromatography and gel filtration.

(A) Nickel IMAC elution profile of DBB288 from a 1 ml Chelating HP column. (B) SDS-PAGE was used to analyse the lysate (LYS), supernatant (SN), flowthrough (FT), wash (W) and elution fractions from the DBB288 nickel IMAC purification. (C) Size exclusion chromatography of DBB288 using a HiLoad 16/600 Superdex 75 clomun. (D) SDS-PAGE analysis of peak elution fractions from the DBB288 gel filtration. M indicates the marker.

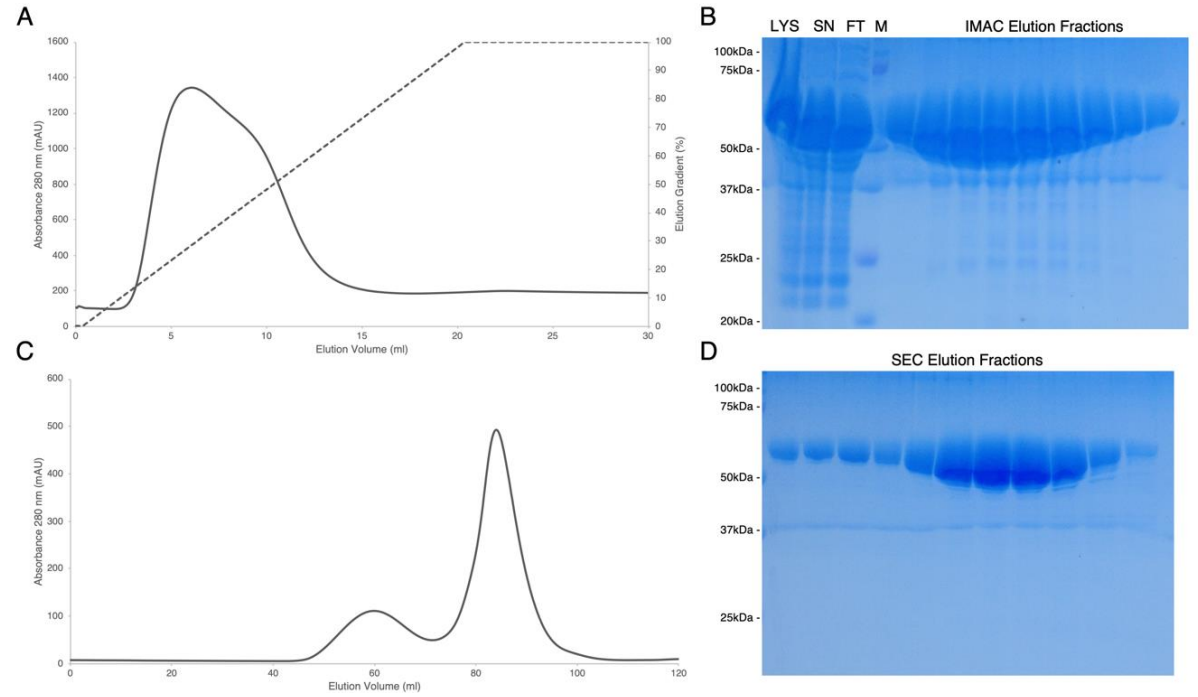

Figure 24. Purification of the BCAP ANK domain *via* nickel affinity chromatography and gel filtration.

(A) Nickel IMAC elution profile of MBP-ANK from a 1 ml Chelating HP column. (B) SDS-PAGE was used to analyse the lysate (LYS), supernatant (SN), flowthrough (FT) and elution fractions from the MBP-ANK nickel IMAC purification. (C) Size exclusion chromatography of MBP-ANK using a HiLoad 16/600 Superdex 200. (D) SDS-PAGE analysis of MBP-ANK elution fractions from both gel filtration peaks. M indicates the marker.

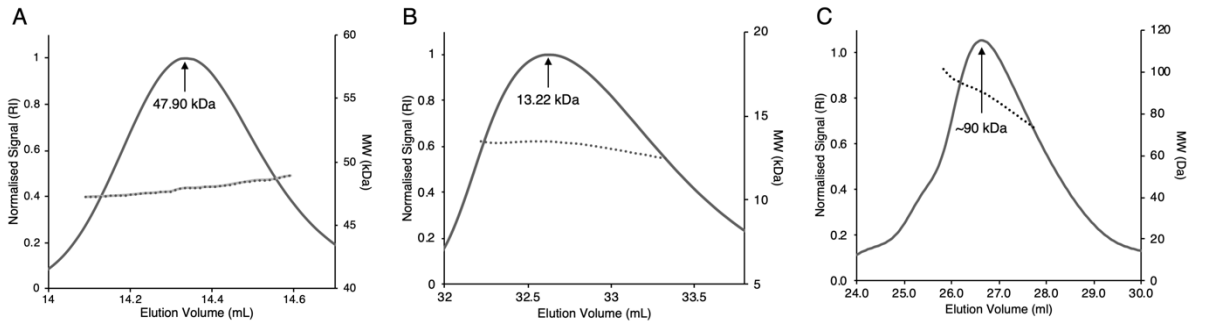

Figure 25. SEC-MALS analysis of DBB-ANK404 and DBB288.

Size exclusion chromatography in combination with multi-angle light scattering (SEC-MALS) of DBB-ANK404 (A), DBB288 (B) and MBP-ANK (C). Samples were loaded onto a Superdex 200 Increase 10/300 GL column at a concentration of 2 mg/ml. Plots show normalised refractive index and weight-averaged molecular weight variation across the peaks.

3.2.8 Crystallisation of the DBB domain

Commercial crystallisation screens were set up for DBB288 at 5.5 mg/ml as described in Section 5.6.1. Crystals appeared overnight in three conditions of the Wizard 1 & 2 screen that contained phosphate buffers (Figure 26). Selected crystals were cryo-protected with 20% (v/v) glycerol and tested for diffraction using synchrotron radiation (Diamond Light Source, i04), where crystals diffracted up to 3.5 Å. Subsequently, this crystallisation condition was further optimised with gradients of NaH_2PO_4 (0.5-1.3 M) and K_2HPO_4 (0.5-1.5 M) that were systematically varied over a 96-well plate. The concentration of acetate buffer was kept constant at 0.1 M and pH 4.5. Crystals were reproducible, and conditions with large crystals were further optimised in a manual hanging drop screen, where the concentrations of NaH_2PO_4 (0.7-1.3 M) and K_2HPO_4 (0.7-1.3 M) were further refined. A crystal from a condition containing 1.3 M NaH_2PO_4, 0.7 M K_2HPO_4 and 0.1 M sodium acetate pH 4.5 was cryo-protected in 25% (v/v) glycerol and a full dataset was collected at a resolution of 3 Å (ID30A-3, ESRF). Data collection statistics are summarised in Table 2.

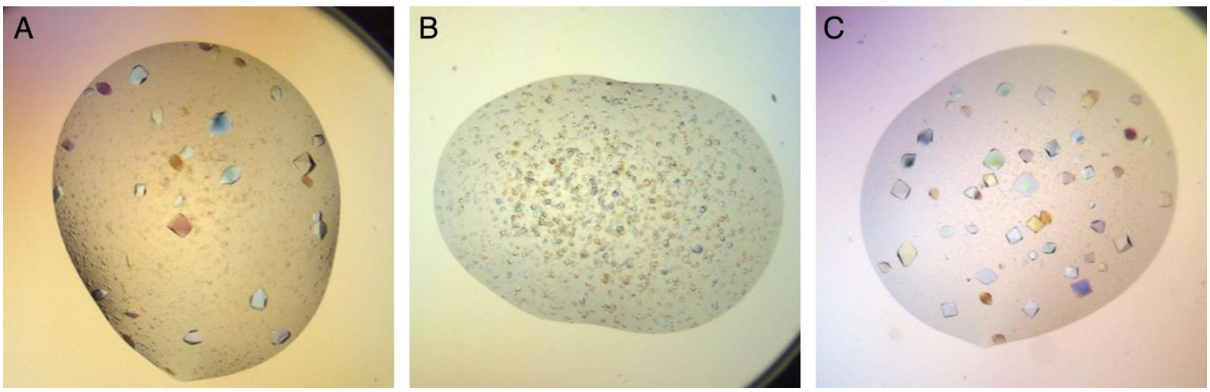

Figure 26. DBB288 crystallises in several condition containing phosphate buffers.

(A) DBB288 crystals appeared overnight in a condition containing (A) 1.2 M NaH_2PO_4, 0.8 M K_2HPO_4, 0.2 M $LiSO_4$ and 0.1 M CAPS pH 10.5, (B) 0.4 M NaH_2PO_4, 1.6 M K_2HPO_4, 0.2 M NaCl and 0.1 M imidazole pH 8, and (C) 0.8 M NaH_2PO_4, 1.2 M KH_2PO_4 and 0.1 M Na acetate pH 4.5. Drops contained a total volume of 400 nl before equilibration.

3.2.9 Experimental phasing of the BCAP DBB domain

Due to the low sequence similarity between the BCAP DBB domain and other TIG domains (<15%), no homologous model was available for phasing. In an attempt to use single-wavelength anomalous diffraction (SAD) phasing, DBB288 was co-crystallised in the presence of 5-Amino-2,4,6-triiodoisophthalic acid (I3C). At a wavelength of 0.987 Å, diffraction varied between 3-3.5 Å, but the anomalous signal was limited to 10 Å (ERSF ID30A-3). As I3C co-crystallisation relies on hydrogen bonds rather than covalent binding, like various heavy metals used for phasing, low I3C occupancy was likely contributing to this low-resolution anomalous signal.

In order to increase the anomalous scattering signal, selenomethionine-containing DBB288 was produced. DBB288 was expressed in minimal medium supplemented with selenomethionine as described in Section 5.3.1. Purification and crystallisation were identical to the native protein. Crystals grown in 0.9 M NaH_2PO_4, 0.9 M KH_2PO_4 and 0.1 M sodium acetate pH 4.5 were cryoprotected in 25% (v/v) glycerol for data collection. From these crystals, a 4 Å SAD dataset was collected (Proxima 2A, Soleil) with the kind help of Allister Crow (Department of Pathology, University of Cambridge). Data collection statistics are summarised in Table 2. Selenomethionine-containing and native crystals exhibited identical unit cell parameters.

The precise resolution of the native and SAD datasets was determined by a cut-off at $I/\sigma > 2$ and R-meas < 0.7. Initially, the three space groups $P4_1\ 2\ 2$, $P4_3\ 2\ 2$, and $P4_3\ 2_1\ 2$ fit the data and were processed in parallel. Model building and refinement later revealed that $P4_3\ 2\ 2$ gave the best refinement statistics.

Table 2. Crystallography data collection and refinement statistics.

	Native	Anomalous
Data collection Statistics		
Beamline	ERSF ID30A-3	SOLEIL PROXIMA 2A
Wavelength	0.9677	0.979
Resolution range	29.96 - 3.0 (3.107 - 3.0)	19.97 - 4.0 (4.142 - 4.0)
Space group	P 43 2 2	P 43 2 2
Unit cell	87.169 87.169 234.075 90 90 90	86.728 86.728 232.968 90 90 90
Total reflections	155114 (15856)	284327 (27827)
Unique reflections	18777 (1823)	8008 (788)
Multiplicity	8.3 (8.7)	35.5 (35.3)
Completeness (%)	99 (100)	99 (100)
Mean I/sigma(I)	17.80 (2.28)	31.31 (8.24)
Wilson B-factor	94.35	136.98
R-merge	0.0728 (0.8961)	0.1252 (0.6221)
R-meas	0.07764 (0.9538)	0.127 (0.6311)
CC1/2	0.999 (0.747)	1 (0.979)
CC*	1 (0.925)	1 (0.995)
Refinement		
Reflections used in refinement	18773 (1823)	
Reflections used for R-free	1876 (182)	
R-work	0.1849 (0.3637)	
R-free	0.2451 (0.4048)	
CC(work)	0.957 (0.714)	
CC(free)	0.945 (0.431)	
Number of non-hydrogen atoms	4160	
Protein residues	541	
RMS(bonds)	0.009	
RMS(angles)	1.22	
Ramachandran favored (%)	88	
Ramachandran allowed (%)	8.8	
Ramachandran outliers (%)	3.2	
Rotamer outliers (%)	1	
Clashscore	9.1	
Average B-factor	104.57	

Using the 4 Å SAD dataset, a phase estimate was obtained for an initial model of the 3 Å native dataset (Figure 27A). Despite successful phasing, automated model building at this low resolution proved challenging and had to be repeated manually. A carbon backbone skeleton model was built into long tubular sections of electron density. Large aromatic sidechains were then used as reference points in further iterative model building and refinement (Figure 27B). After numerous rounds of refinement, 97% of the DBB288 sequence could be mapped to the electron density. A few residues at the C-terminal helix of one chain could not be modelled,

and a large electron density could not be accounted for (Figure 27C). The resulting refinement statistics are summarised in Table 2.

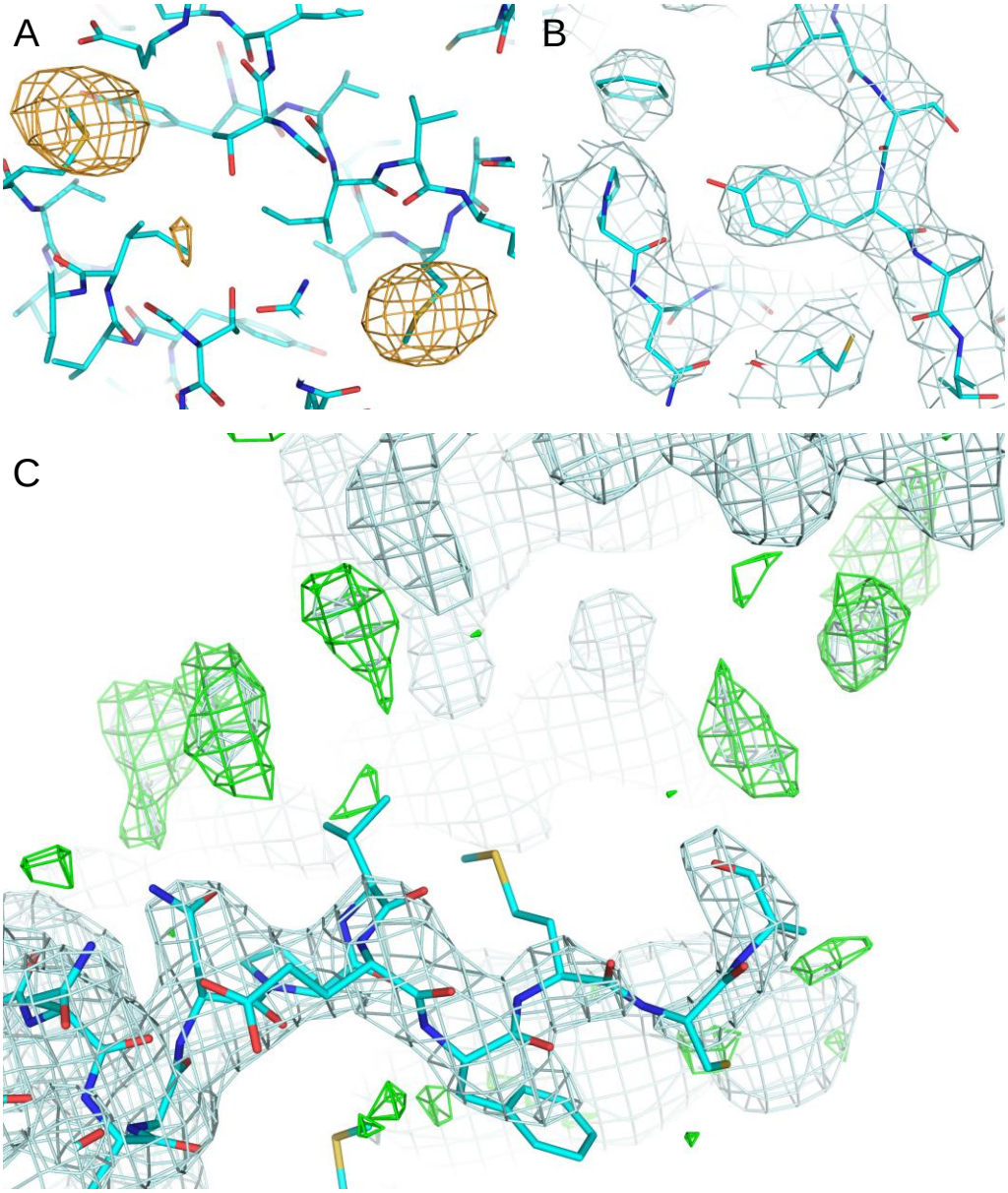

Figure 27. Features of the DBB288 electron density map.

(A) Electron density of the anomalous signal from selenomethionine residues matched to location of methionine residues in the DBB288 model. (B) Representative view of the 3 Å DBB288 electron density map, where large aromatic sidechains were used as anchoring points during early model building. (C) Electron density map around the C-terminal α-helix, with electron density that could not be accounted for in the final DBB288 model.

3.2.10 Structure of the BCAP DBB domain

The BCAP DBB domain adopts a typical TIG fold (TIG^{BCAP}) followed by three α-helices, two of which are contained in this structure (Figure 28A). The TIG^{BCAP} is comprised of seven β-strands (βA-βH) that make up a C-type Ig fold (Figure 28B). Structurally, TIG^{BCAP} exhibits striking similarity with a number of TIG^{TF} domains (Figure 30). TIG^{BCAP} shares an identical

topology with NF-κB p50, NFAT, CAMTA1 and Ebf1 TIG domains, with Cα RMSD values down to 1.6 Å. This similarity is striking since the DBB288 structure was obtained using experimental phases that are independent of the TIG^{TF} structures.

The DBB α-helices make contacts with α-helices from adjacent chains, and form a hypothetical dimer (Figure 28A). Herein, the first α-helix (αA) provides the largest contribution as it makes lateral contacts with the αA from the closest adjacent protomer. The second α-helix (αB) makes contacts with several symmetry-related units. These αB interactions are likely defined by crystal packing and may not reflect a physiological dimer.

The asymmetric unit of the DBB288 protein contains five copies of the DBB domain, two of which share substantial interactions between the TIG^{BCAP} and 3α regions (interface 1, 946 $Å^2$) (Figure 29). The remaining three subunits contact this hypothetical DBB dimer through TIG^{BCAP} loop interactions (interface 2, 566 $Å^2$ and interface 3, 617 $Å^2$) or αA (interface 4, 419 $Å^2$) (Figure 29). Even though the DBB288 construct was determined to be monomeric in solution (Figure 25), interface 1 between the TIG^{BCAP} and 3α regions likely represents a biologically relevant dimer. The interactions are comprised of residues from βA2, βB, βE and βD (ABED β-sheet) that interact with the other subunit as a dyad *via* a 2-fold rotational axis (Figure 28A). The interface consists of a hydrophobic centre surrounded by extensive polar interactions. Comparable ABED β-sheet dimerisation interfaces are found in NFAT5, NF-κB p50 and Ebf1 TIG domain structures (Ghosh, van Duyne et al. 1995, Stroud, Lopez-Rodriguez et al. 2002, Treiber, Treiber et al. 2010) (Figure 31). Moreover, structural comparison between the hypothetical interface 1 and TIG^{TF} domains reveals RMSD values as low as 2.2 Å. The size of these TIG^{TF} ABED β-sheet interfaces varies between 460-680 $Å^2$ (Table 3).

Similar to the BCAP DBB domain, Ebf1 dimerisation is driven by the α-helical region containing three α-helices located at the C-terminus of the TIG domain (Figure 32) (Hagman, Gutch et al. 1995, Treiber, Treiber et al. 2010). This supports previous SEC-MALS results that emphasise the importance of the α-helical region for DBB dimerisation (Figure 25). Overall, the conformational similarity to TIG^{TF} dimers and the importance of the α-helical region in Ebf1 suggest that interface 1 represents a physiological relevant DBB domain dimer.

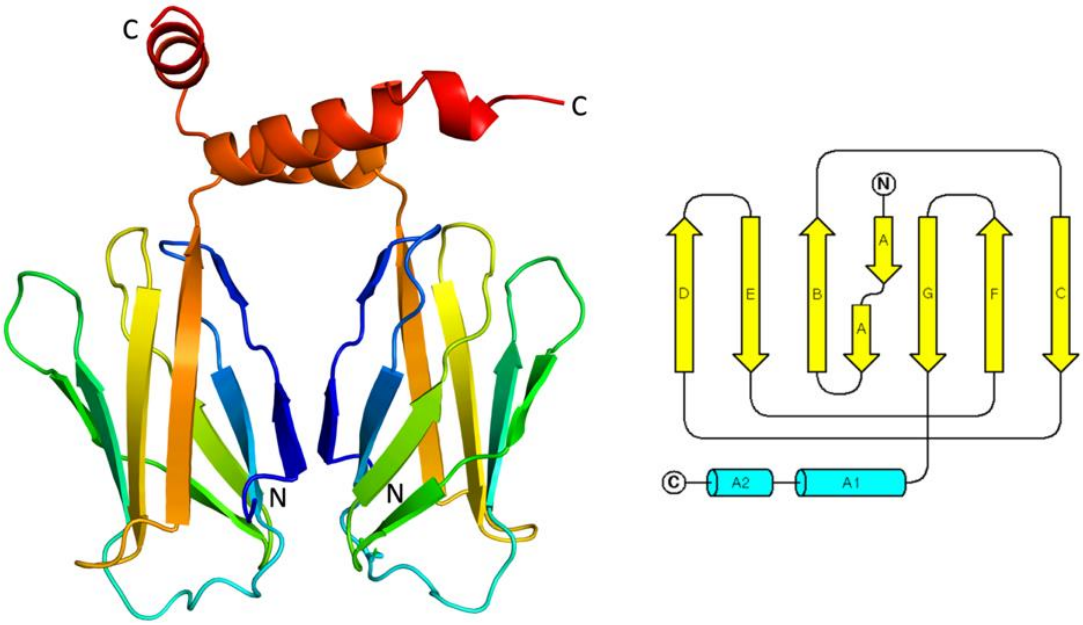

Figure 28. Crystallographic structure of the BCAP DBB domain.

(A) Crystallographic model of the BCAP DBB domain (DBB288). The structure is comprised of a core TIG fold, followed by two C-terminal α-helices. (B) Topology diagram of the BCAP DBB domain structure, depicting a C-type Ig fold with a broken βA strand.

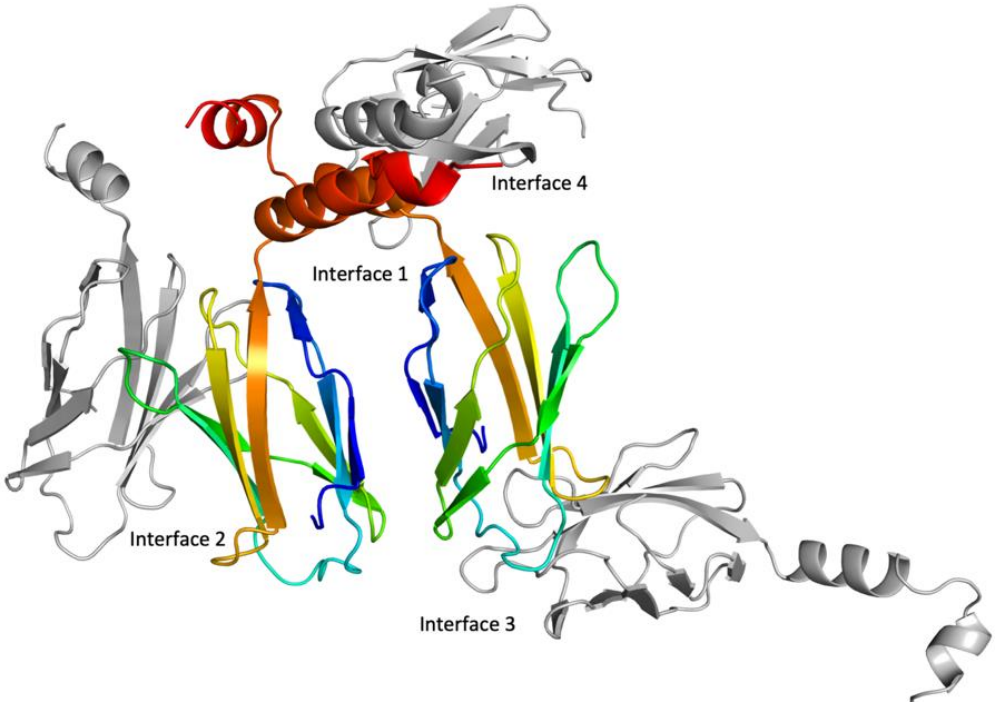

Figure 29. Asymmetric unit of the DBB288 structure.

The asymmetric unit of the DBB288 crystal contains five protomers that make contacts *via* four main interfaces as indicated. The pair with the largest dimerisation interface is shown in colours. Protomers participating in smaller interfaces are coloured in grey.

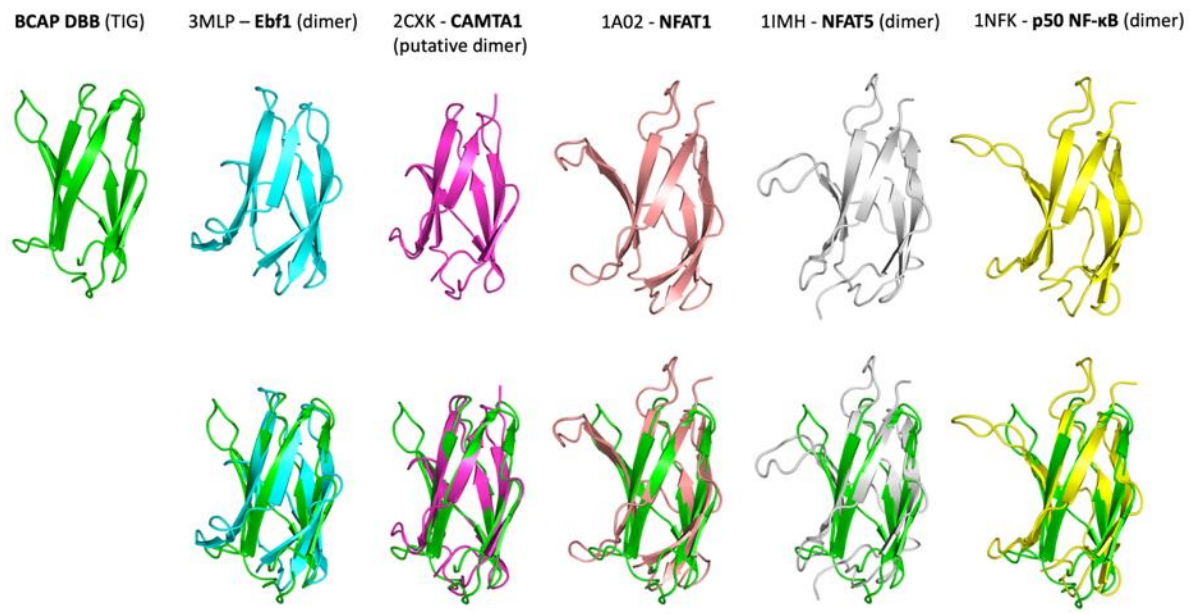

Figure 30. Structural comparison of BCAP TIG^{TF} domain monomers.

(A) Overview of TIG^{TF} domains with similar domain topology as TIG^{BCAP} domain (green). (B) Structural alignment of various TIG^{TF} domains with the TIG^{BCAP} domain (green): Ebf1 (teal, PDB:3MLP), CAMTA1 (pink, PDB:2CXK), NFAT1 (orange, PDB:1A02), NFAT5 (grey, PDB:1IMH), NF-κB p50 (yellow, PDB:1NFK).

Table 3. Overview of structural similarities between BCAP DBB288 and TIG^{TF} domains.

	PDB Code	BCAP Sequence Identity(%)	Monomer RMSD (Å)	Dimer RMSD (Å)	Dimer Interface (Å^2)
Transcription factors					
NFAT5 (dimer)	1IMH	13.2	2.2	2.3	596
NFAT1	1A02	8.6	2.1		
p50 NF-κB (dimer)	1NFK	13.4	2.4	3.3	683
Ebf1 (dimer)	3MLP	14.8	2.8	3.6	463
CAMTA1 (putative dimer)	2CXK	12.8	1.6	2.2	598

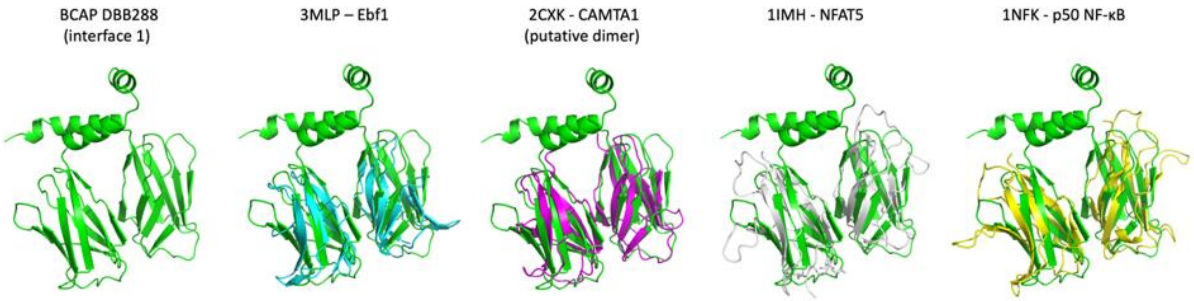

Figure 31. Structural comparison of BCAP and TIG^{TF} domain dimers.

Structural alignment of various TIG^{TF} domain dimers with the BCAP DBB domain (green): Ebf1 (teal, PDB:3MLP), CAMTA1 (pink, PDB:2CXK), NFAT5 (grey, PDB:1IMH), NF-κB p50 (yellow, PDB:1NFK).

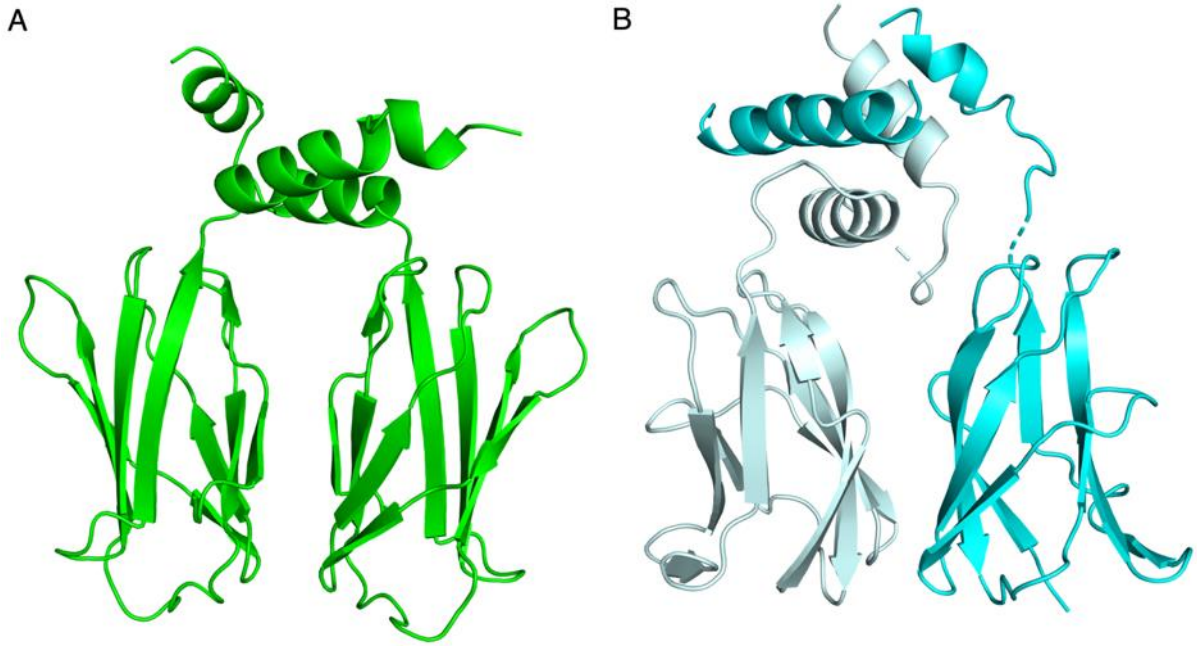

Figure 32. Comparison of the TIG-adjacent α-helical region in BCAP and Ebf1.
(A) Crystal structure of the TIG^{BCAP} dimer followed by 2 of 3 DBB α-helices. (B) Ebf1 TIG domain followed by its 'helix-loop-helix' motif.

3.2.11 Functional similarities between the DBB and TIG^{TF} domains

The striking structural similarities between the BCAP DBB domain and TIG^{TF} domains could indicate a certain level of functional conservation. In NF-κB and NFAT transcription factors, TIG domains fulfil the dual role of dimerisation and unspecific DNA binding (Ghosh, van Duyne et al. 1995, Stroud, Lopez-Rodriguez et al. 2002). In these structures, the TIG domain stabilises the interaction between DNA and the sequence specific DNA binding domains. TIG^{TF} domains make contact with the DNA phosphate backbone through two or three positively charged lysine and arginine residues located at the N-terminal TIG^{TF} loop region (Muller, Rey et al. 1995, Chen, Glover et al. 1998, Stroud, Lopez-Rodriguez et al. 2002).

The BCAP DBB domain similarly contains lysine and arginine residues in the BC-loop (Figure 33A). As these DNA binding residues are not conserved among TIG^{TF} domains, their functional relevance was further investigated.

The first step of this investigation was to confirm the cellular localisation of BCAP. Although characterised as cytosolic adaptor protein in DT40 cells, one study has shown nuclear localisation in HEK293 and U-2 osteosarcoma cells *via* immunofluorescence microscopy (Okada, Maeda et al. 2000, Thul, Akesson et al. 2017). In order to determine the subcellular localisation of BCAP in human

cells, THP-1 macrophages and Ramos B cells were fixed and analysed *via* immunofluorescence microscopy. Results indicate a clear cytosolic localisation of BCAP, independent of LPS stimulation in THP-1 cells or BCR stimulation in Ramos B cells (Figure 34). Cytosolic localisation of BCAP reduces the likelihood that BCAP interacts with genomic DNA in a physiological context.

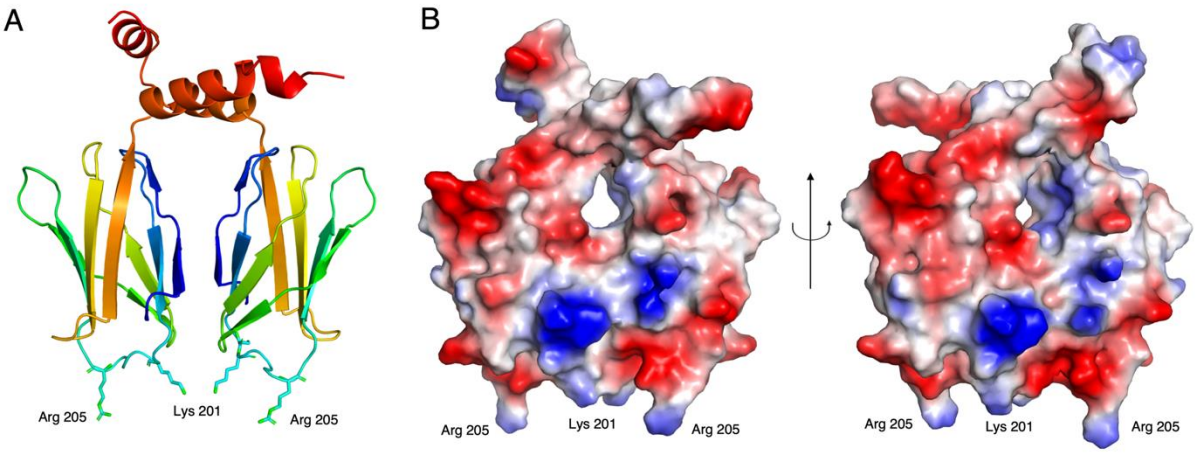

Figure 33. The BCAP DBB domain contains lysine and arginine residues that may participate in DNA binding.
(A) DBB288 structure with positively charged residues in the BC-loop highlighted as indicated. (B) Electrostatic charge representation of the DBB288 surface. Positively charged areas are coloured in blue, negatively charges areas in red.

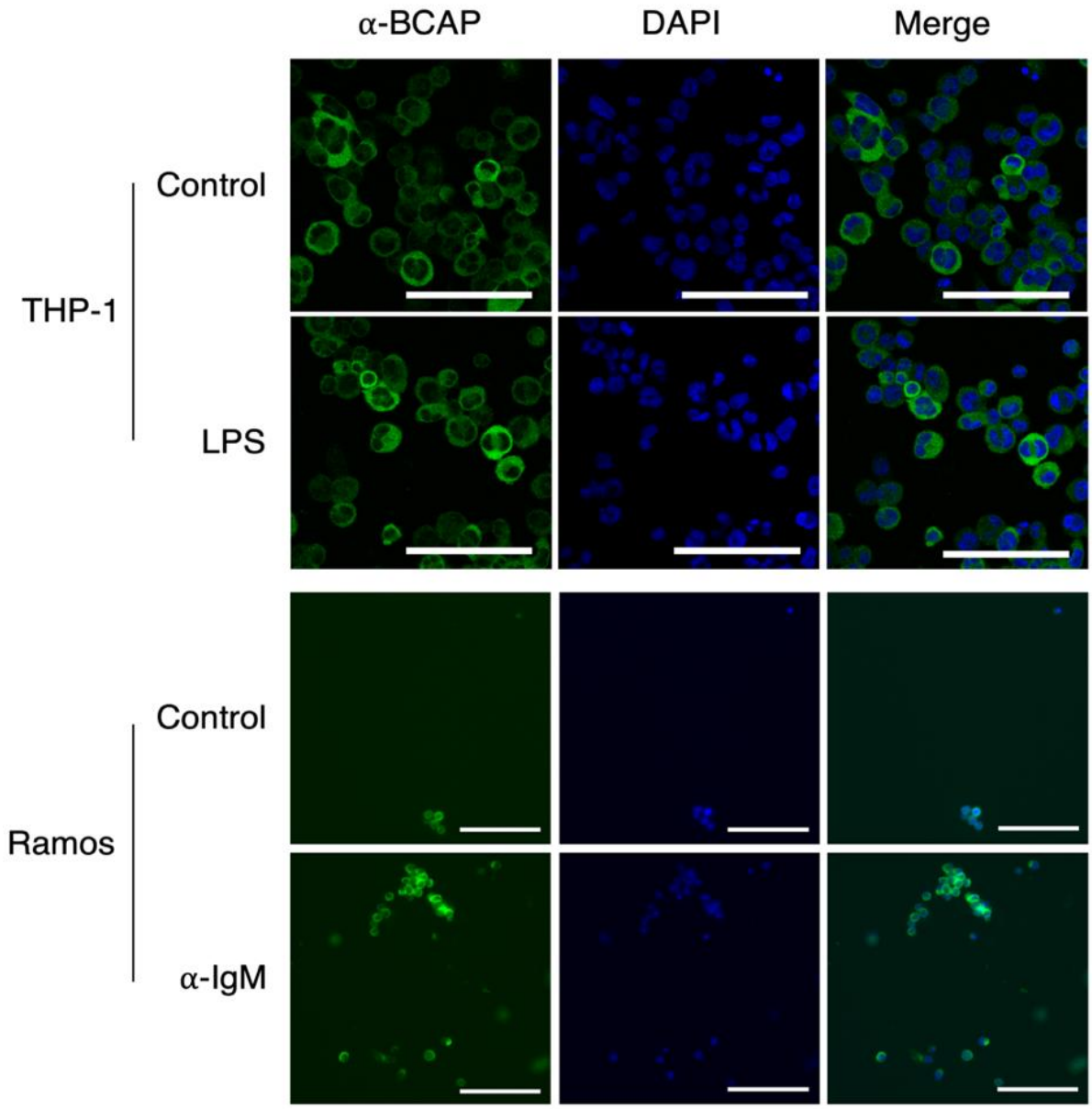

Figure 34. BCAP is an exclusively cytosolic protein in THP-1 and Ramos B cells.

Representative images of fixed (A) THP-1 cells analysed by confocal fluorescence microscopy. Cells were stimulated with 100 ng/ml LPS for 30 min. Images were obtained with the kind help of Helena Rannikmae (Department of Biochemistry, University of Cambridge). (B) Ramos B cell analysed by epifluorescence microscopy. Cells were stimulated with 5 µg/ml α-IgM for 15 min. (A) and (B) Nuclei strained with DAPI are represented in blue, endogenous BCAP immunostained with α-BCAP antibody is shown in green. Scale bar corresponds to 100 µm.

3.3 The BCAP interactome and the role of phosphorylation

3.3.1 Background

BCAP has been characterised in a number of cell types and species including chicken, mouse, and human. Across species, BCAP persistently appears as multiple bands on western blots (Okada, Maeda et al. 2000, MacFarlane, Yamazaki et al. 2008, Troutman, Hu et al. 2012). The bands corresponding to $BCAP_L$ migrate above the expected MW at 100 kDa and 110 kDa. Similarly, $BCAP_S$ migrates at 70 kDa and 80 kDa. Similar band shifts have not been observed upon BCAP expression in bacterial cells, suggesting that PTMs contribute to this phenomenon (Halabi 2015). This hypothesis is supported by the observation that BCAP is tyrosine phosphorylated *in vivo*, albeit on all four bands visible on western blot (Okada, Maeda et al. 2000, MacFarlane, Yamazaki et al. 2008, Troutman, Hu et al. 2012).

3.3.2 BCAP is hyperphosphorylated in mammalian cells

To investigate whether phosphorylation lies at the basis of this unusual migration pattern, endogenous BCAP from human macrophages and B cells was dephosphorylated. Λ-phosphatase treatment resulted in the elimination of the higher MW bands for both $BCAP_L$ and $BCAP_S$ (Figure 35B). Consequently, hyperphosphorylation is responsible for the upward shift of both BCAP isoforms. Further analysis of the phosphorylation sites by mass spectrometry was not feasible due to the low amounts of endogenous BCAP that could be isolated from human THP-1 macrophages (Figure 35A).

In order to increase the amount of BCAP available for further analysis, overexpression in Expi293F cells was used as a model system. Expression of $BCAP_L$ in Expi293F cells was conducted as described in Section 5.3.2. The purification strategy was identical to that of proteins expressed in *E. coli* with an initial nickel IMAC step, followed by TEV protease cleavage and gel filtration. During cell lysis and nickel IMAC, all buffers were supplemented with phosphatase inhibitors to preserve any phosphorylation present. Nickel IMAC resulted in a heterogeneous sample with multiple bands on SDS-PAGE (Figure 36A-B). However, further purification resulted in a relatively pure BCAP with two bands around 100 kDa and one contaminant around 70 kDa (Figure 36C-D), which was determined to be a degradation product by mass fingerprinting (data not shown).

Λ-phosphatase treatment of the purified $BCAP_L$ confirmed the presence of hyperphosphorylation in this expression system. Moreover, probing with antibodies on western

blot revealed the presence of phosphotyrosine and phosphoserine residues (Figure 35C). This demonstrates that BCAP expressed in Expi293F cells is a suitable proxy for endogenous BCAP from immune cells.

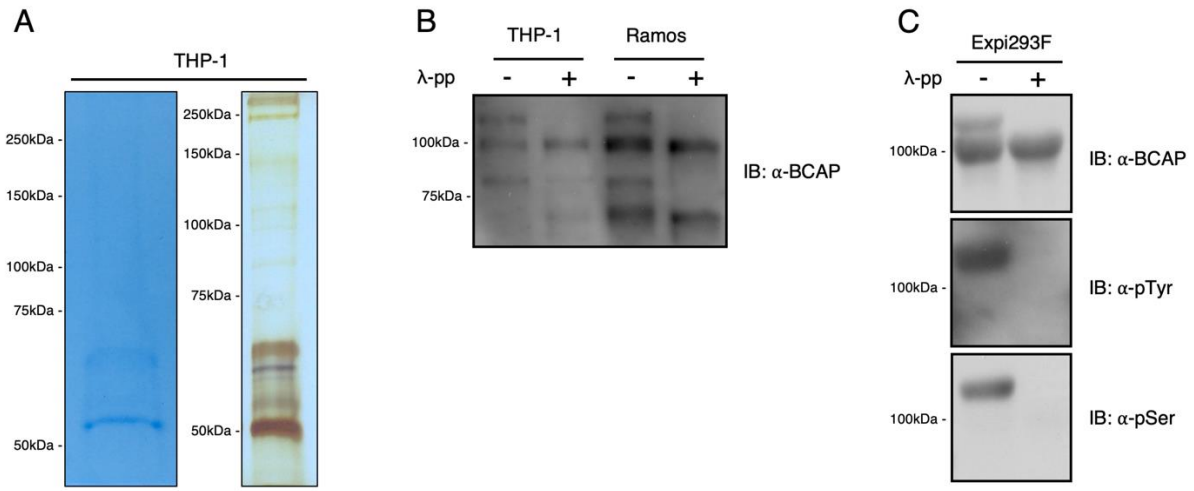

Figure 35. BCAP is hyperphosphorylated in B cell, macrophages and Expi293F cells.

(A) THP-1 macrophages were stimulated with 100 ng/ml LPS for 30 min. Following cell lysis, BCAP was immunoprecipitated using α-BCAP antibody and the resulting pulldown was analysed by SDS-PAGE. Samples were stained with Instant Blue Coomassie (left) and silver stain (right). (B) Lysates from THP-1 and Ramos cells were dephosphorylated with λ-phosphatase. (C) λ-phosphatase treatment of purified $BCAP_L$ overexpressed in Expi293F cells.

Further in-depth characterisation of the $BCAP_L$ phosphorylation pattern was conducted by mass spectrometry. Purified $BCAP_L$ was digested with various proteases and analysed by phosphopeptide mapping. A large abundance of phosphoserine residues was detected, with only few phosphothreonine and no phosphotyrosine residues (Figure 37). This is remarkable as western blot analysis clearly indicated the presence of tyrosine phosphorylation. *In silico* digestion with trypsin and chymotrypsin indicates that most tyrosine motifs in the C-terminal half of BCAP, including YxxM motifs, are part of very long peptides that are unlikely to be ionised. Therefore, the lack of tyrosine phosphorylation in this analysis might be a reflection of poor digestion patterns and inefficient ionisation. Unfortunately, alternative digestion with proteases Asp-N and Glu-C did not result in the detection of phosphotyrosine modifications. The abundance of serine and threonine phosphorylation suggests that these PTMs are the main contributor to BCAP hyperphosphorylation and the resulting band shift on SDS-PAGE.

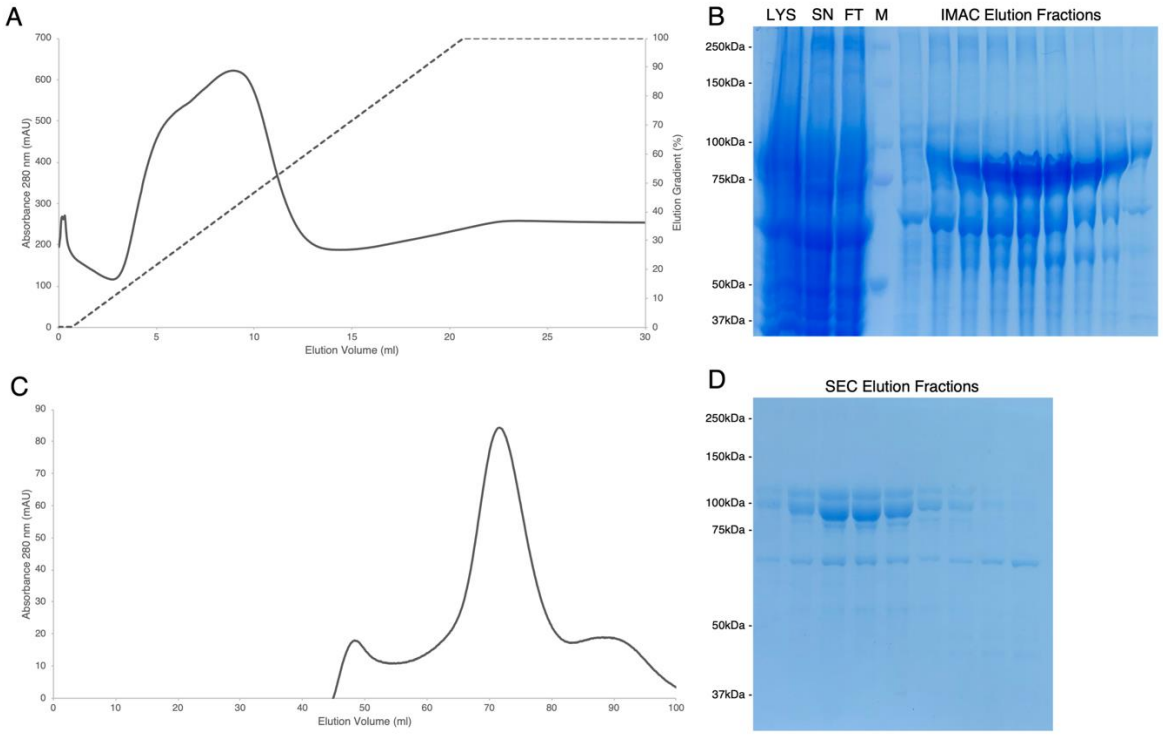

Figure 36. Purification of BCAP$_L$ *via* nickel affinity chromatography and gel filtration.

(A) Nickel IMAC elution profile of BCAP$_L$ from a 1 ml Chelating HP column. (B) SDS-PAGE was used to analyse the lysate (LYS), supernatant (SN), flowthrough (FT) and elution fractions from the BCAP$_L$ nickel IMAC purification. (C) Size exclusion chromatography of BCAP$_L$ using a HiLoad 16/600 Superdex 200. (D) SDS-PAGE analysis of BCAP$_L$ gel filtration peak elution fractions. M Indicates the marker.

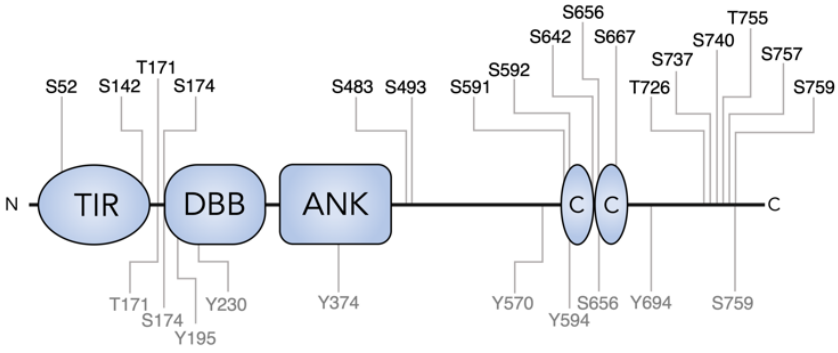

Figure 37. Phosphopeptide mapping reveals numerous BCAP phosphorylation sites.

Schematic depiction of BCAP containing all known phosphorylation sites determined by phosphopeptide mapping. Residues on top of the diagram represent phosphorylations that were discovered in this thesis. BCAP expressed in Expi293F cells was run on SDS-PAGE and separately digested with Asp-N, Glu-C, trypsin and chymotrypsin before mass spectrometry analysis. Grey residues below the diagram display previous results from our laboratory (Halabi 2015). BCAP was overexpressed in HEK293T cells and digested with both trypsin and chymotrypsin for analysis by mass spectrometry.

3.3.3 BCAP is phosphorylated by BTK and to a lesser extend SYK and LYN

As discussed in Section 1.14, the tyrosine kinases SYK, LYN and BTK have been suggested to phosphorylate BCAP. In order to resolve conflicting reports about these kinases, an *in vitro* kinase assay was conducted.

Purified $BCAP_L$ was dephosphorylated with λ-phosphatase and incubated with various non-receptor tyrosine kinases as described in Section 5.5.5. SYK, LYN and BTK were able to phosphorylate BCAP (Figure 38). BTK is the most efficient kinase, causing a significant shift in BCAP migration on western blot. Relative to BTK, phosphorylation by SYK and LYN was substantially lower. However, LYN phosphorylation of BCAP still resulted in a partial band shift when probed for tyrosine phosphorylation. In order to validate the specificity of the assay, other kinases were included in the experiments. TYK2 and ITK, a member of the TEC kinase family, were not able to phosphorylate BCAP under these conditions (Figure 38). Myelin basic protein (MyBP) was used to control for kinase catalytic activity (Figure 38).

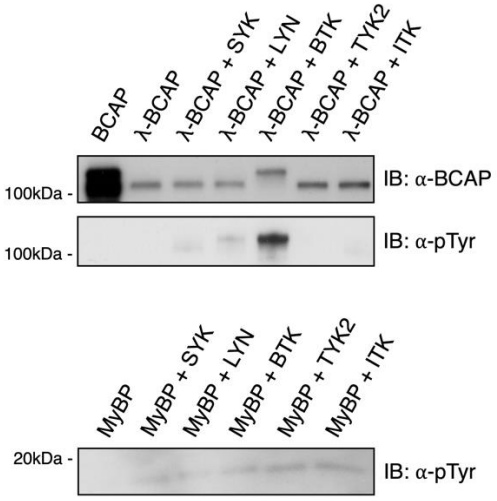

Figure 38. BCAP is phosphorylated by BTK, LYN and SYK.

(A) *In vitro* kinase assay of λ-phosphatase treated $BCAP_L$ (λ-BCAP) with 60 pmol SYK, LYN, BTK, TYK2 and ITK. Samples were incubated at 20 °C for 30 min. To control for kinase activity, myelin basic protein (MyBP) was similarly incubated with SYK, LYN, BTK, TYK2 and ITK. All samples were analysed by western blot for the presence of BCAP and phosphotyrosine modifications.

3.3.4 Virotrap screen reveals extensive nature of the BCAP interactome

In immune and Expi293F cells, hyperphosphorylation of BCAP may enable a multitude of interactions beyond the currently small BCAP interactome. In order to find novel BCAP interaction partners including potential serine kinases, a virotrap interaction screen was performed. The virotrap system takes advantage of the lentiviral budding machinery, where the viral p55 GAG protein is sufficient for budding and formation of virus-like particles (VLPs)

(Gheysen, Jacobs et al. 1989). When fusing a bait protein with GAG, the resulting VLPs can be used to co-purify bait protein interaction partners (Eyckerman, Titeca et al. 2016). This novel method preserves weak protein interactions by elimination of harsh lysis and washing steps. A virotrap interaction screen can therefore preserve and detect protein interactions that are not visible in other methods, although the use of HEK293T cells only presents a fraction of the total BCAP interactome in immune cells.

A BCAP virotrap experiment was conducted and the resulting hits were compared against a negative control containing *E. coli* dihydrofolate reductase protein (eDHFR). Analysis revealed numerous potential interaction partners listed in Figure 39A. The virotrap hits can roughly be divided into three groups. The first group contains SH2 and SH3 domain-containing proteins. The PI3K regulatory subunits p85α and p85β, Nck1 and Nck2 are known interaction partners of BCAP that interact *via* SH2 and SH3 domains (Figure 39A) (Okada, Maeda et al. 2000, Castello, Gaya et al. 2013). GRB2 and CRKL are novel SH2 and SH3 domain-containing adaptors proteins that play a role in immunity and B cells signalling (Sattler M. 1998, Engels, Konig et al. 2009). The SH2 domain of GRB2 has previously been predicted to interact with BCAP based on sequence specificity (Okada, Maeda et al. 2000). More specifically, the GRB2 SH2 domain recognises phosphorylated YxNx motifs such as BCAP ^{374}YPNT (Huang, Li et al. 2008). Additionally, previous mass spectrometry-based interaction studies found BCAP in a GRB2 interaction screen, suggesting an SH3 domain-dependent association (Bisson, James et al. 2011).

A second group of virotrap hits consists of proteins that were not previously linked to BCAP, BCR or TLR signalling. These include Annexin A6, CSNK1, CSNK2, PLSCR1, TOM1 and UEVLD (Figure 39A). Annexin A6 is a member of the annexin family of proteins that have been shown to play a role in the glucocorticoid-mediated innate immune response (Gerke and Moss 2002). Annexins are comprised of numerous annexin repeats that associate with and bend membranes in a calcium-dependent manner (Gerke and Moss 2002). Annexin A6 does not contain protein interaction domains that would enable a direct interaction with BCAP. However, other Annexin family proteins have been shown to interact with GRB2, and a similar association might take place in this virotrap screen (Alldridge and Bryant 2003).

Casein kinases, like CSNK1A1 and CSNK2A1 are ubiquitous serine and threonine kinases involved in numerous cellular functions including cell cycle progression, apoptosis, transcription, and viral infections (Venerando, Ruzzene et al. 2014). Casein kinases

phosphorylate substrates containing acidic residues in the vicinity of the target serine or threonine residue (Venerando, Ruzzene et al. 2014). BCAP contains numerous matching motifs, suggesting that BCAP may be a substrate of casein kinases (Appendix Table 1).

The phospholipid scramblase PLSCR1 was previously linked to IFN signalling, where it enhances the antiviral response (Dong, Zhou et al. 2004). Although no clear mechanism could be established for this link, PLSCR1 associates with DOCK2 in yeast two-hybrid assays, which may link the scramblase to the BCAP interactome (Rolland, Tasan et al. 2014). TOM1 is a membrane-associated protein that interacts with TOLLIP, which is a regulator of TLR signalling (Katoh, Imakagura et al. 2006). UEVLD is a poorly characterised protein that is proposed to function as a negative regulator of polyubiquitination (Kloor, Bork et al. 2002). For both proteins, no studies suggest a direct link to BCAP or other BCAP interaction partners.

The third group of virotrap hits contains many of the least significantly enriched proteins. Several proteins are part of the ESCRT-III complex and cytoskeleton associated proteins (Figure 39A). Since proteins of the ESCRT-III complex have previously been identified in virotrap screens and due to their role in viral budding, they are most likely artefacts and therefore are not further analysed (Hurley and Hanson 2010, Eyckerman, Titeca et al. 2016).

This initial virotrap setup compares BCAP overexpression to eDHFR control and represents the BCAP interactome in the absence of a stimulus. In order to increase the chance of detecting interaction partners that are activated by inflammatory signalling, a second virotrap screen was conducted, in which TLR4 signalling was induced. To this end, a constitutively active truncated TLR4 receptor (tTLR4, residues 569-839) was co-transfected with the GAG-BCAP bait construct (Figure 39B). A list of enriched proteins was obtained by comparing the relative enrichment of BCAP + tTLR4 to an eDHFR + tTLR4 control. Once again, a number of known interaction partners including p85 and NCK were significantly enriched in the BCAP-containing VLPs (Figure 39C-D). The potentially new interaction partners GRB2, CRKL and CSNKs were also enriched. The remaining proteins enriched in this virotrap screen are ESCRT-III complex associated proteins or ribosomal and nuclear proteins.

The enrichment of ribosomal and nuclear proteins may be an indication of cell death through excessive TLR4 signalling or cell stress. Cell death would result in the release of nuclear proteins into the medium, where they coat VLPs through unspecific interactions. And even though the ranked significance of adaptor proteins and CSNKs varied from the first virotrap screen, the quantitative difference in enrichment is not higher than in the initial experiment.

Overall, activation of NF-κB signalling in this virotrap screen did not result in the identification of additional interaction partners.

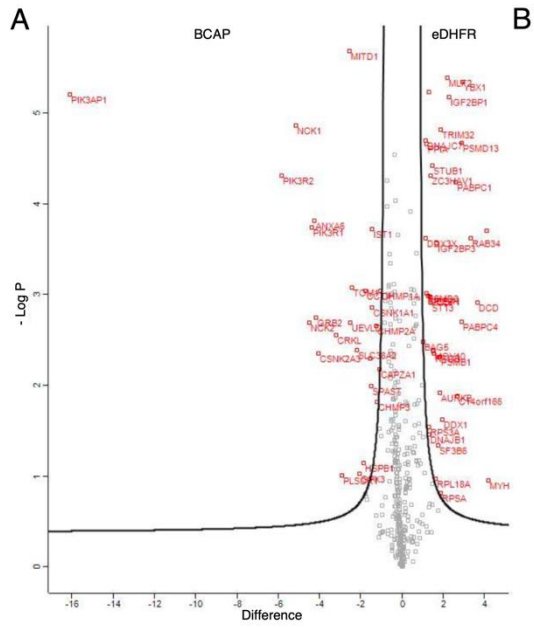

Figure 39. Virotrap interaction screen reveals novel BCAP interaction partners.

HEK293T cells were transfected with a GAG-BCAP fusion construct, tTLR4 and a pMD2.G - pcDNA3-FLAG-VSV-G mix to generate FLAG-VSV-G coated virus-like particles (VLPs). After purification and tryptic digest, the VLP contents were analysed by mass spectrometry. (A) Volcano plot of significant hits from the BCAP virotrap screen compared to the eDHFR control. (C) Volcano plot of virotrap his obtained by comparing BCAP + tTLR4 to eDHFR + tTLR4. (A) and (C) False discovery rates (FDR) = 0.05 and S0 = 1. (B) and (D) Overview of virotrap hits sorted according to their relative difference to the eDHFR control.

3.3.5 The role of casein kinases in BCAP phosphorylation

In order to test whether BCAP is a substrate of CSNK1A1 and CSNK2A1, an *in vitro* kinase assay was performed. The assay assessed the ability of CSNK1A1 and CSNK2A1 to phosphorylate BCAP in comparison to the serine kinase GSK-3. The results show that CSNK2A1 but not CSNK1A1 or GSK-3 phosphorylate BCAP (Figure 40). It is therefore likely that CSNK2A1 contributes to the abundance of serine and threonine phosphorylation on BCAP. The role of these phosphoserine and phosphothreonine modifications remains unknown and further research is required to elucidate any related potential mechanism of regulation.

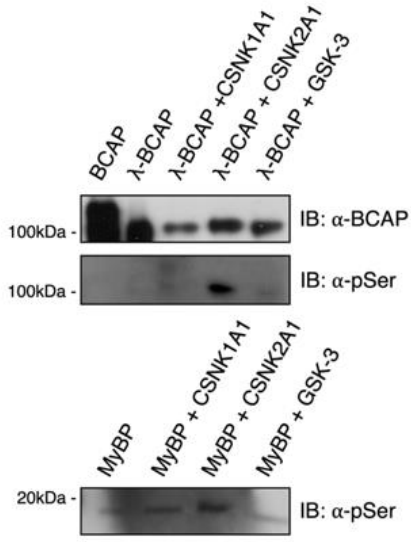

Figure 40. BCAP is phosphorylated by CSNK2A1 but not CSNK1A1.

(A) *In vitro* kinase assay of λ-phosphatase treated $BCAP_L$ (λ-BCAP) with 60 pmol CSNK1A1, CSNK2A1, and GSK-3. Samples were incubated at 20 °C for 30 min. (B) To control for kinase activity, myelin basic protein (MyBP) was similarly incubated with CSNK1A1, CSNK2A1, and GSK-3. All samples were analysed by western blot for the presence of BCAP and phosphoserine modifications.

3.3.6 Validation of the virotrap hits GRB2 and CRKL

Virotrap interaction screens are an unbiased method to discover novel protein-protein interaction. However, since the technique relies on the co-purification of proteins, virotrap hits can represent both direct and indirect protein interactions. In order to confirm that GRB2 and CRKL interact with BCAP directly, a Co-IP was performed. FLAG-GRB2, FLAG-CRKL and Myc-$BCAP_L$ constructs were transiently overexpressed in HEK293T cell. The results show that FLAG-GRB2 but not FLAG-CRKL was able to pull down Myc-$BCAP_L$ (Figure 41A). Moreover, BCAP Y374F mutation did not prevent this interaction. This result indicates that the ^{374}YPNT motif does not interact with the GRB2 SH2 domain, as previously proposed based on sequence specificity (Okada, Maeda et al. 2000). A *Phyre2* model (Kelley, Mezulis et al. 2015)

of the BCAP ANK domain also illustrates how the ^{374}YPTN motif is an unlikely binding site for the GRB2 SH2 domain (Figure 41B). Even though the Y374 is exposed at the surface of the protein, and potentially available for phosphorylation, the remaining residues of the motif are buried within the ANK fold. The ^{374}YPTN motif is therefore not immediately available for SH2 domain interactions, which require accessibility of all residues within the motif.

Overall these results suggest that the GRB2-BCAP association is a direct interaction, whereas the CRKL association is indirect. This hypothesis seems plausible given that CRKL has been reported to interact with p85 (Hartman, Wilson-Weekes et al. 2006, Liu, Chen et al. 2013). However, the BCAP-GRB2 interaction could not be validated in stimulated THP-1 macrophages and Ramos B cells (Figure 42). These results suggest that this interaction is not constitutive in these immune cells, and that it cannot be induced by TLR4 or BCR stimulation.

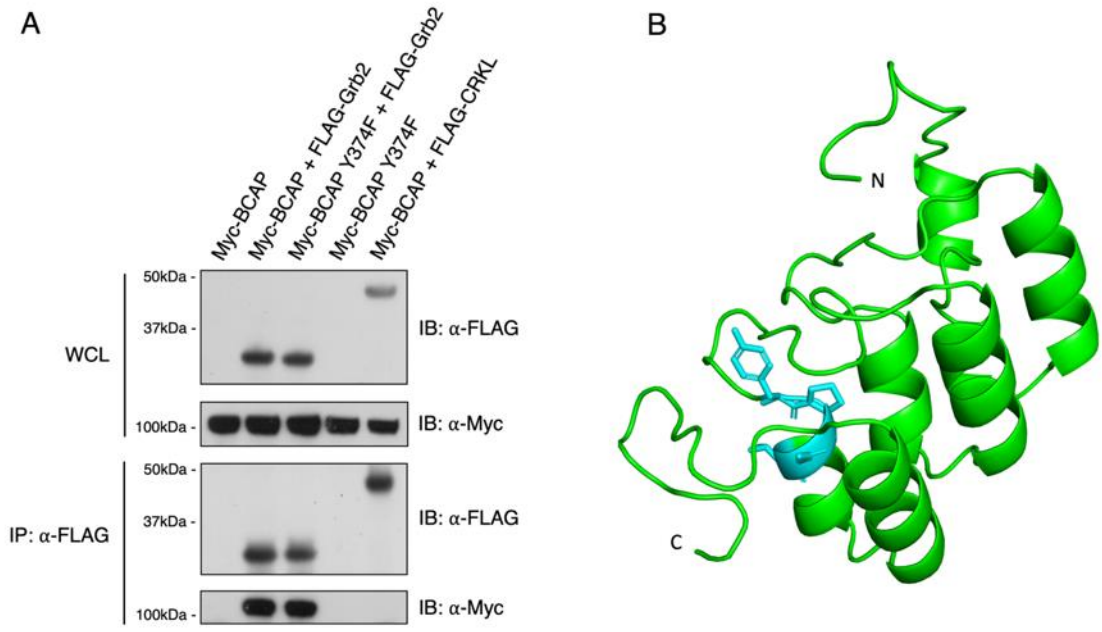

Figure 41. Co-immunoprecipitation in HEK293T cells reveals that GRB2 but not CRKL interacts with BCAP.
HEK293T cells were transiently transfected with Myc-BCAP$_L$, FLAG-GRB2, FLAG-CRKL, FLAG-BCAP$_L$, and Myc-CRKL. 24 h post-transfection, cells were lysed and subjected to immunoprecipitation with anti-FLAG antibody. Precipitates were split and assayed for precipitation of FLAG-tagged constructs or co-precipitation of Myc-tagged BCAP and CRKL by western blot. (B) Structural model of the BCAP ANK domain (*Phyre2* model). Residues of the ^{374}YPNT motif are highlighted in teal and represented as sticks.

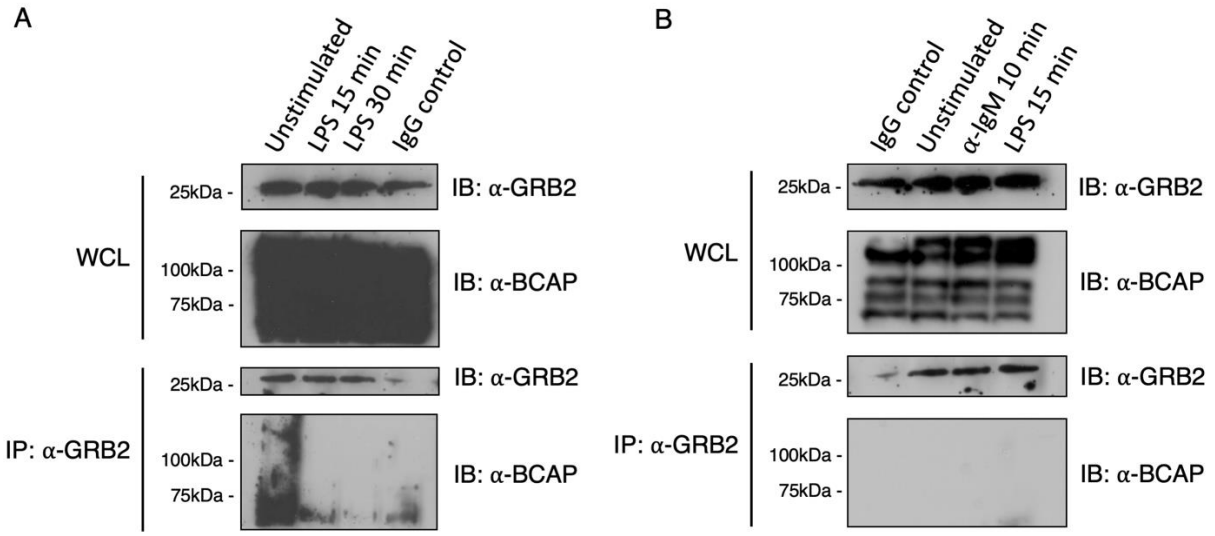

Figure 42. Co-immunoprecipitation in THP-1 and Ramos cells did not confirm the BCAP-GRB2 interaction.
(A) THP-1 cells were stimulated with 100 ng/ml LPS for 15 or 30 min. (B) Ramos cells were stimulated with 100 ng/ml LPS for 15 min or 5 µg/ml α-IgM for 10 min. (A) and (B) After lysis, lysates were subjected to a pulldown with α-GRB2 or a control IgG and subsequently probed for a BCAP interactions.

In order to obtain domain-level resolution of new and previously known interactions between BCAP and the SH domain-containing proteins GRB2, CRKL, p85 and PLC-γ2, an *in vitro* pulldown assay was performed. Purified GST-tagged bait proteins were purified by GST affinity purification and gel filtration as described in Section 5.4. GST fusion proteins were then immobilised on glutathione resin and purified BCAP was applied to the resin to probe for interactions. Full length GRB2, but not the GRB2 SH2 domain was able to pull down BCAP, independent of its phosphorylation state (Figure 43A). Consequently, the BCAP-GRB2 interaction is mediated by SH3 domains. This discovery supports the previous Co-IP results that ruled out ^{374}YPNT as a possible SH2 domain binding site.

A pulldown between BCAP and the p85 SH domains revealed an SH3 domain interaction in addition to a N-SH2 interaction (Figure 43B). Notably, a C-SH2 domain interaction could not be detected. The presence of the N-SH2 domain interaction was expected as BCAP was initially characterised as N-SH2 domain substrate (Okada, Maeda et al. 2000). The lack of a C-SH2 domain interaction could be attributed to missing phosphorylation of YxxM motifs, or a lower binding affinity of this domain. The C-SH2 domain has previously been shown to have a lower affinity for certain phosphotyrosine motifs than the N-SH2 domain (O'Brien, Rugman et al. 2000). *In vivo*, this lower C-SH2 domain affinity could be compensated for by avidity, through prior binding of SH3 and N-SH2 domains. The presence of an SH3 domain interaction between BCAP and PI3K is surprising, as several studies have shown that the *in situ* BCAP-p85

interaction relies on YxxM motifs (Aiba, Kameyama et al. 2008, Matsumura, Oyama et al. 2010). This paradox might be explained by SH3 domain regulation and competition between several SH3 domain interactions to occupy the BCAP proline-rich regions.

PLC-γ2 revealed a similar interaction mechanism to p85, with a robust SH3 domain interaction, an N-SH2 domain interaction and a weaker C-SH2 domain binding (Figure 43C). These extensive interactions suggest that BCAP and PLC-γ2 form a stable complex under physiological conditions. The presence of several PLC-γ2 and p85 SH2 domain interactions with BCAP in these assays also corroborates previous results suggesting that $BCAP_L$ contains tyrosine phosphorylation, even though this could not be confirmed by phosphopeptide mapping.

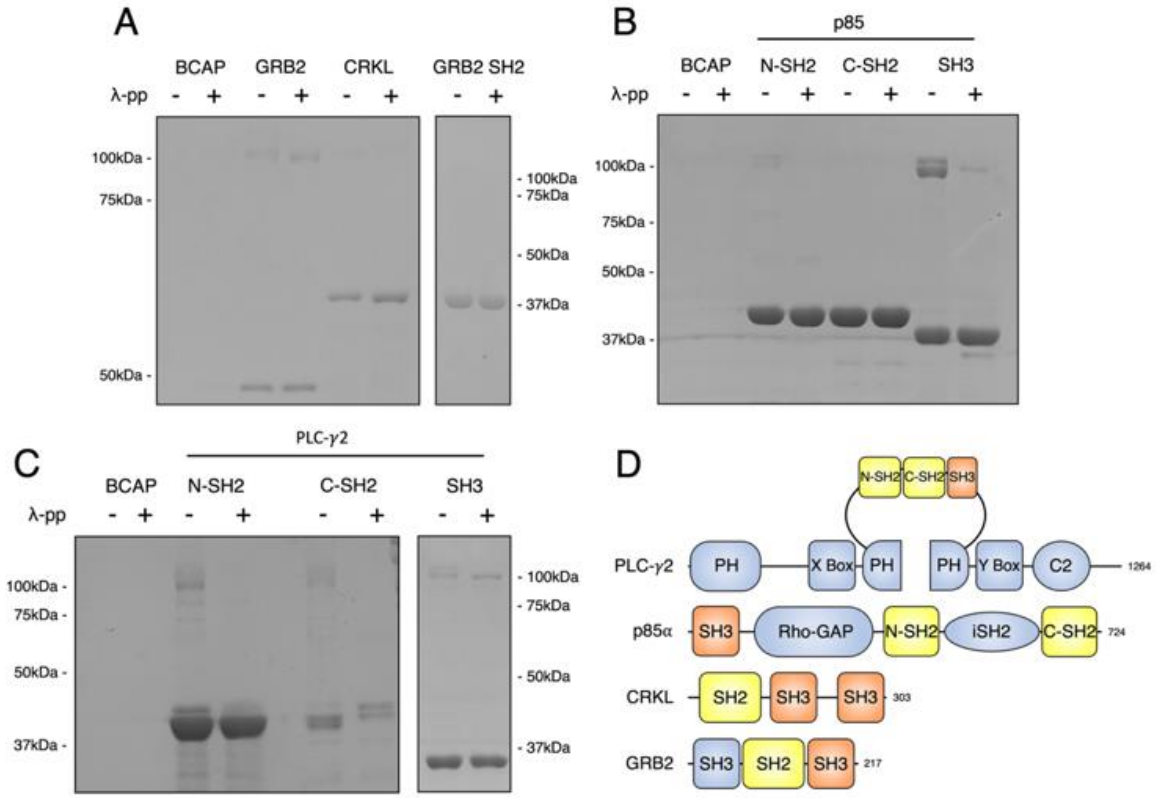

Figure 43. *In vitro* pulldown reveals novel SH3 domain interactions with BCAP.
Purified GST-tagged (A) GRB2, GRB2 SH2, CRKL, (B) p85 N-SH2, p85 cSH3, p85 SH3, (C) PLC-γ2 N-SH2, PLC-γ2 C-SH2, and PLC-γ2 SH3 were immobilised on glutathione resin. Purified $BCAP_L$ and dephosphorylated $BCAP_L$ were subsequently applied to the resin. After several wash steps, GST-tagged bait proteins were eluted from the resin and the eluent was probed for the presence of $BCAP_L$ on SDS-PAGE. (D) Schematic domain overview of SH2 and SH3 domain-containing proteins used in this pulldown experiment.

3.3.7 Limitations of the *in vitro* pulldown assay

The results presented in section 3.3.6 illustrate the *in vitro* capacity of various SH3 and SH3 domains to interact with BCAP. The results are in line with expected behaviour of phosphorylation-dependent SH2 domain binding and phosphorylation-independent SH3 domain binding. However, for the p85 SH3 domain interaction, the amounts of phosphorylated and de-phosphorylated BCAP varies significantly (Figure 43B). Although the SH3 domain interaction is not expected to be influenced by BCAP phosphorylation, such a decrease was not observed for the other SH3 domain interactions tested (Figure 43). Therefore, it cannot be ruled out that BCAP phosphorylation promotes p85 SH3 domain interactions with BCAP. In the absence of additional repeats of the experiment and without further investigation of this inconsistency, the results should be interpreted with caution.

3.3.8 Analysis of SH2 domain binding specificity *via* peptide arrays

While *in vitro* pulldowns revealed the SH2 and SH3 domain interactions, the precise binding sites on BCAP remain elusive. In order to analyse the SH2 domain interactions on a sequence specific level, a peptide array was used to identify relevant tyrosine motifs. Purified GST-tagged SH2 domains or full-length proteins were analysed for their affinity with peptides containing phosphorylated BCAP tyrosine motifs (Appendix Figure 1).

For the p85 SH2 domains, the peptide array showed a broader specificity than suggested by the literature. Next to interactions with YxxM motifs, numerous other motifs were bound by p85 (Figure 44A-B). This apparent broad specificity in peptide arrays has been previously described (Huang, Li et al. 2008), and is somewhat expected since secondary and tertiary structures are not accounted for in this technique. However, direct comparison between the four YxxM motifs reveals both p85 SH2 domains interact with the ^{459}YVEM peptide. Furthermore, the N-SH2 domain preferentially binds the ^{444}YESM motif, whereas the C-SH2 domain favours the ^{263}YTDM and ^{419}YESM motifs (Figure 44A).

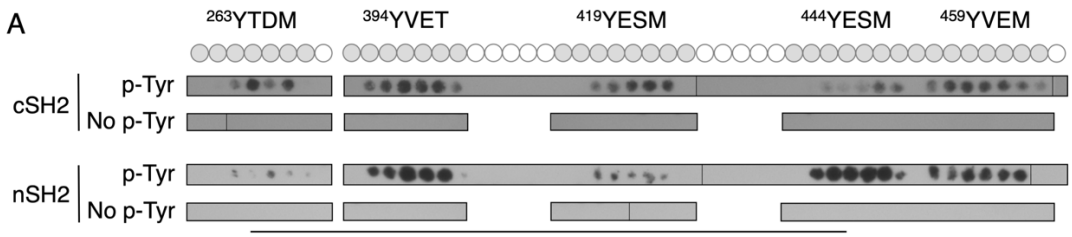

B

Domain	p-Tyr Motif	p85α N-SH2	p85α C-SH2	GRB2	CRKL	PLC-γ2 N-SH2	PLC-γ2 C-SH2
DBB domain	195YVIV*						
	230YTIS*	•	•		•		
	249YSGD						
	263YTDM		•			-	-
	292YNTE						
ANK domain	346YGLK			•		•	
	365YVSA			•			
	374YPNT*			•	•		
	394YVET	•	•			-	-
Tail domain	419YESM		•			-	-
	444YESM	•				-	-
	459YVEM	•	•				
	513YHTV						
	553YIFK				•		
	570YVSS		•				•
	595YDPF		•		•		
	694YESG		•	•	•		

Figure 44. Peptide arrays reveals binding sites for the p85 SH2 domains and other BCAP interaction partners.
Binding of SH2 domains to an array of 15-residue peptides containing unmodified and phosphorylated BCAP tyrosine motifs. (A) Binding of p85 SH2 domains to BCAP YxxM motifs. Phosphotyrosine containing peptides are indicated as full grey circles. (B) Binding of p85, GRB2, CRKL and PLC-γ2 SH2 domains to all tyrosine motifs in BCAP (excluding the TIR domain). Motifs with that have previously been shown to be phosphorylated are indicated in blue. (*) Indicates motifs are buried in the protein domain fold.

4 Discussion

4.1 An updated model of BCAP TLR signalling

The results from this thesis provide the first direct evidence for a human TIR domain interaction between $BCAP^{TIR}$ domain and MAL (Figure 8A). Previous studies made similar assertions while using TIR-DBB domains to show an interaction with MAL and MyD88 *via* co-immunoprecipitation (Troutman, Hu et al. 2012). Previous results in our laboratory indicated that human $BCAP_L$ interacts with MAL and MyD88 in a similar experimental setup (Halabi 2015). The $BCAP^{TIR}$ domain as a minimal requirement for heterotypic TIR domain interaction with MAL but not MyD88 (Figure 8) was unexpected since the $BCAP^{TIR}$ domain, like many TIR domains, was determined to be monomeric in solution (Xu, Tao et al. 2000, Khan, Brint et al. 2004, Nyman, Stenmark et al. 2008, Ohnishi, Tochio et al. 2009, Valkov, Stamp et al. 2011, Lin, Lu et al. 2012, Jang and Park 2014, Halabi, Sekine et al. 2017). It has been notoriously difficult to reconstitute TIR domain interactions *in vitro* using these monomeric TIR domains. Only recently, the nature of TIR domain interactions was revealed by Ve *et alia* (Ve, Vajjhala et al. 2017). Using Cryo-EM, they were able to show that the MAL^{TIR} and $MyD88^{TIR}$ domains form large filamentous structures. Although the physiological relevance of these large filaments is debatable, overexpression studies of MAL, MyD88 and ASC have shown that these filaments can assemble *in situ* (Avbelj, Wolz et al. 2014, Dick, Sborgi et al. 2016, Ve, Vajjhala et al. 2017). It is therefore likely that overexpression of MAL and MyD88 in HEK293T cells leads to the formation of TIR domain filaments. Consequently, the $BCAP^{TIR}$ domain is expected to be incorporated into MAL, but not MyD88 filaments (Figure 45A).

In order to further determine the domains required for BCAP signalling, various BCAP domain boundaries were tested for their ability to dampen TLR signalling using an NF-κB reporter assay. This type of NF-κB reporter assay is widely recognised as the gold standard to evaluate *in situ* NF-κB activation of TLR adaptor proteins including MAL, MyD88 and BCAP (Medzhitov, Preston-Hurlburt et al. 1998, Fitzgerald, Palsson-McDermott et al. 2001, Troutman, Hu et al. 2012).

However, the results from these NF-κB reporter assays should be interpreted with caution, since the physiological phenomenon underlying NF-κB activation in these assays is not fully understood. It is likely that MAL^{TIR} and $MyD88^{TIR}$ domain filaments are nucleation points for myddosome formation that eventually leads to NF-κB activation. When functionally evaluating

BCAP constructs with this assay, it is unlikely that the observed inhibition of NF-κB signalling is dependent on PI3K activation. PI3K-Akt signalling requires phosphorylated YxxM motifs, of which only one is present in the DBB domain of TIR-DBB constructs. Moreover, BCAP negative regulation of MAL NF-κB signalling is dependent on dimerisation through the third DBB α-helix, which does not affect the YxxM motif. It can therefore be concluded that BCAP NF-κB reporter assays measure the degree of steric inhibition of MAL^{TIR} and $MyD88^{TIR}$ domain filaments, rather than PI3K-dependent inhibition.

Results from the reporter assay suggest that the $BCAP^{TIR}$ domain does not inhibit MAL or MyD88-induced NF-κB signalling (Figure 9). In fact, the $BCAP^{TIR}$ domain strongly increases NF-κB signalling in both experiments. Inhibition of inflammatory signalling requires the full-length DBB domain in the context of MAL overexpression, and the TIR-TIG2α domains for MyD88 overexpression (Figure 9). This indicates that inhibition of MAL filaments requires DBB domain dimerisation, whereas disruption of MyD88 filaments only requires TIG2α domain association. Again, these findings are in contrast to a previous study that used similar TIR-DBB domains and $BCAP_S$ to conclude that the $BCAP^{TIR}$ domain is sufficient for the inhibition of inflammatory TLR signalling (Troutman, Hu et al. 2012). Despite slight differences in the minimal requirements for negative regulation of MAL and MyD88-induced NF-κB signalling, the results from Section 3.1 illustrate the crucial importance of the DBB domain.

The importance of DBB domain dimerisation was also reflected by *in vitro* experiments, where only dimeric BCAP constructs were able to inhibit MAL filament formation (Figure 11). Interestingly, BCAP was able to disrupt MAL^{TIR} domain oligomerisation at a 1:10 molar ratio, and in the absence of a stable complex during gel filtration. This could indicate that dimeric BCAP destabilises MAL oligomers in a transient manner.

The increase in NF-κB activity associated with $BCAP^{TIR}$ domain is inconsistent with the current understanding of BCAP as a negative regulator of TLR signalling (Figure 9). This phenomenon could be explained by the aforementioned incorporation in MAL^{TIR} domain filaments, where monomeric $BCAP^{TIR}$ domains act as neutral building blocks that increase total filament size and downstream myddosome formation (Figure 45A). Since the $BCAP^{TIR}$ domain does not associate with MyD88, the increase in MyD88-induced NF-κB signalling may be driven by an increase in MyD88 autoactivation. In this scenario, monomeric $BCAP^{TIR}$ domain engages in

transient TIR domain interactions with MyD88, which result in the release of MyD88^{TIR} domain auto-inhibition and therefore more efficient myddosome formation.

Together, these results suggest that the physiological phenomenon of BCAP negative regulation of TLR signalling is at least in part driven by steric inhibition of TIR signalosomes. BCAP would therefore play a pivotal role in controlling and regulating TIR domain filament formation in the context of TLR signalling (Figure 45B). This type of physical inhibition would take place in addition to the phosphoinositide metabolism and possible regulation by FoxO transcription factors (Aksoy, Taboubi et al. 2012, Ni, MacFarlane et al. 2012, Hamerman, Pottle et al. 2016). Moreover, this model of physical inhibition is the only mechanism to address BCAP negative regulation of endosomal TLR signalling, where PI3K activity has no apparent function.

The BCAP^{TIR} domain also plays an important role outside TLR signalling. Downstream of IL-1R and IL-18R in CD4^{+} T cells, BCAP engages in TIR domain interactions to activate the PI3K–mTOR pathway, which enhances Th17 and Th1 cell responses (Deason, Troutman et al. 2018). IL-1R signalling does not require MAL, but MyD88 myddosome formation drives downstream NF-κB activation (Slack, Schooley et al. 2000). In these IL-1R signalosomes, BCAP^{TIR} domain interaction with MyD88 would most likely rely on DBB domain dimerisation.

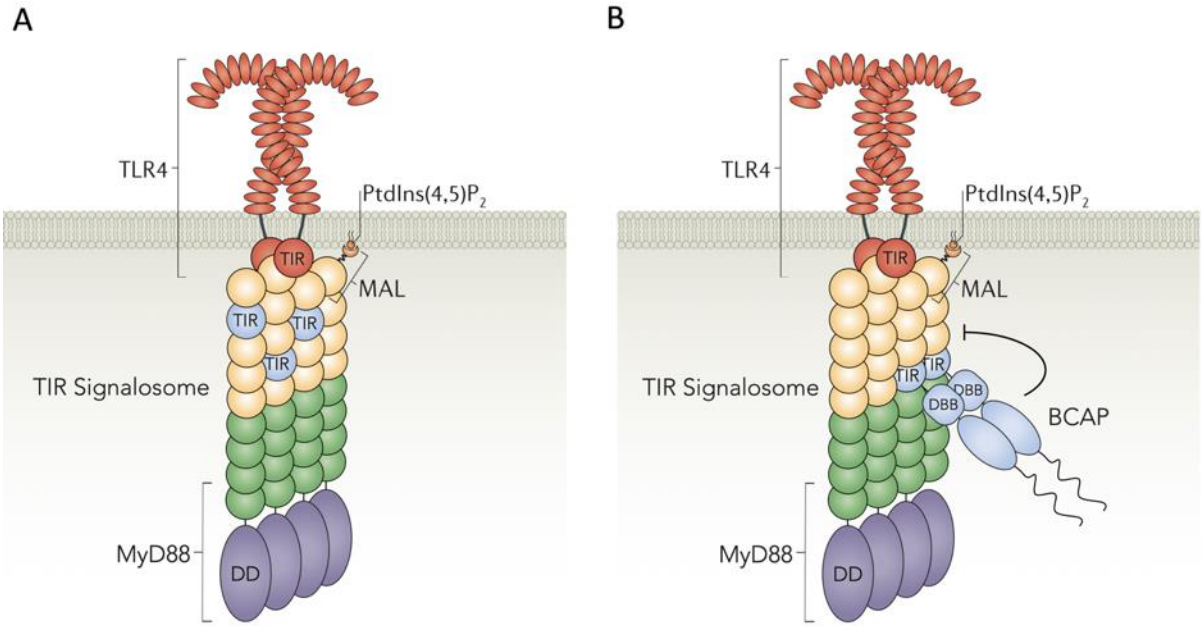

Figure 45. Dimeric BCAP regulates TIR domain signalosomes.

Schematic representation of the TLR4 signalosome. LPS binding (not shown) induces TLR4 dimerisation, resulting in the assembly of the TIR domain signalosome. Initial MAL and subsequently MyD88 recruitment lead to myddosome formation and downstream NF-κB signalling. (A) Monomeric BCAP^{TIR} domains (blue) interact with MAL without inhibiting TLR signalling. BCAP^{TIR} domains are incorporated in TIR signalosome, contributing to the overall size of the filament, leading to an increase in myddosome activation and downstream NF-κB signalling. (B) BCAP Dimerisation induces a conformational

shift and the TIR domains will counteract the assembly of the TIR signalosome, resulting in negative regulation of TLR signalling by steric inhibition.

This novel model for $BCAP^{TIR}$ domain interactions relies on a mechanism of indirect dimerisation. Although homotypic TIR domain dimerisation has never been observed for animal TIR domains, similar forms of indirect dimerisation have been described for other TLR adaptor proteins like SARM. The SARM domain architecture exhibits strong similarities to BCAP, with a C-terminal TIR domain preceded by two SAM oligomerisation domains (Carty, Goodbody et al. 2006). The N-terminal half of SARM contains two armadillo motifs, analogous to the BCAP ANK domain (Carty, Goodbody et al. 2006). In a physiological context, dimerisation by the TIR domain-adjacent SAM motifs induces TIR domain-dependent axonal degeneration (Gerdts, Summers et al. 2013).

Interestingly, SARM constructs lacking the TIR domain retain the ability to dimerise, but exhibit a dominant negative effect on axonal degeneration by full-length SARM (Gerdts, Summers et al. 2013). This is another point of similarity between BCAP and SARM, since $BCAP_L$ and $BCAP_S$ isoforms are present under physiological conditions. For BCAP however, indirect DBB domain dimerisation is based on the exclusive use of $BCAP_L$. Under physiological conditions, both BCAP isoforms have been shown to associate in Co-IP experiments (Halabi 2015), suggesting that BCAP forms heterodimers similar to SARM. These heterodimers can be expected to activate PI3K signalling and engage in MAL^{TIR} domain interactions without disrupting filament formation. Since $BCAP_L$ and $BCAP_S$ are expressed in similar quantities and given dimerisation is random, one can expect three distinct dimer populations that include $BCAP_L$ and $BCAP_S$ homodimers, as well as mixed heterodimers. Only $BCAP_L$ homodimers will disrupt TLR signalosomes, whereas heterodimers would act as neutral building blocks, similar to the $BCAP^{TIR}$ domain in MAL NF-κB reporter assays. $BCAP_S$ dimers lack the TIR domains required for association with TLR signalling.

The functional characterisation of the DBB domain has implications for related proteins. BCAP shares a high degree of sequence and structural similarity with the homolog BANK1 and the *D. melanogaster* protein Dof (Battersby, Csiszár et al. 2003). Secondary structure alignments exhibit an identical domain arrangement between the structured regions of BCAP and BANK1 (Appendix Figure 2). Based on this high level of sequence similarity, the N-terminal BANK1 domain has been suggested to represent an unannotated TIR domain (Halabi 2015). This is corroborated by the role of BANK1 in TLR7-mediated type I interferon production and TLR9-mediated IL-6 production (Wu, Kumar et al. 2013, Wu, Kumar et al. 2016). Therefore, BANK1

is likely involved in endosomal TLR signalling through TIR domain interactions. Given the functional characterisation of the BCAP DBB domain, it can be hypothesised that TIR^{BANK1} domain signalling is equally driven by DBB domain dimerisation. Dof is more distantly related to BCAP (16% sequence identity) and BANK1 (13.5% sequence identity). However, since the structure and therefore function of proteins is more conserved than the amino acid sequence, the conserved DBB domain likely functions as a dimerisation region in Dof fibroblast growth factor signalling.

4.2 Structure of the BCAP DBB domain

The work described in this thesis led to the determination of the first DBB domain crystal structure. Based on trypsin limited proteolysis of a larger DBB-ANK construct, DBB domain boundaries containing residues 179-288 were crystallised and a structure was solved at 3 Å (Figure 28). The structure revealed a TIG fold followed by two α-helices. Initially, the absence of the third DBB α-helix was concerning, since this α-helix drives BCAP dimerisation. However, structural similarity to other dimeric TIG^{TF} domains including NF-κB, NFAT and Ebf1 revealed that crystal contacts present in the DBB domain structure represent a physiological DBB dimer (Figure 31). The dimerisation interface includes the ABED β-sheet of the TIG fold, and the three C-terminal DBB α-helices. Structural alignments with TIG^{TF} domains reveal an unexpectedly high degree of structural similarity with RMSD values as low as 1.6 Å for TIG monomers and 2.3 Å to TIG dimers (Table 3). Given the DBB domain structure was solved with experimental phases, these low RMSD values are not biased by existing TIG structures. Comparison to other TIG^{TF}-like domains such as plexin family receptor-Ig domains did not yield meaningful alignments.

Besides the identification of a common dimerisation interface, further functional conservation was considered. TIG^{TF} domains assist sequence-specific DNA binding domains (DBDs) by making unspecific DNA backbone contacts *via* positively charged residues in the N-terminal TIG loops (Aravind and Koonin 1999). In this conformation, TIG^{TF} dimers have been described to 'sit on top' or 'hang above' the DNA helix (Stroud, Lopez-Rodriguez et al. 2002). The DNA-binding residues are not conserved among TFs, making it difficult to map this feature onto DBB domains. The BCAP DBB domain contains two positively charged residues (K201 and R205) that potentially enable DNA interactions. Since BCAP does not exhibit a nuclear localisation in macrophages and B cells, binding to nuclear DNA is unlikely. However, theoretically it remains a possibility that BCAP binds cytosolic viral DNA.

The combination of structural and functional approaches revealed the role of the BCAP DBB domain. This represents a significant step towards the full characterisation of BCAP. However, the structure and function of the C-terminal half of the protein remain largely unknown. As discussed in section 4.3, the C-terminal unstructured region of BCAP acts as a signalling platform for other protein interactions through SH2 and SH3 domain interactions. The ANK domain and coiled-coil region remain elusive structural features with no apparent function. It was proposed that the ANK domain might be involved in BCAP dimerisation (Halabi, Sekine et al. 2017), but experiments in this thesis show that the DBB α-helices are sufficient for self-association. ANK repeats can engage in protein interactions in multiple ways, and are involved in a wide range of functions such as signalling, cytoskeleton integrity, transcription and inflammatory responses (Mosavi, Cammett et al. 2004). This makes it nearly impossible to predict the BCAP ANK domain function, even though structure predictions like the *Phyre2* model in Figure 41 provide a starting point for further structural analysis. The structure and function of the BCAP coiled-coil region conserved among Dof, BANK1 and BCAP remain equally uncharacterised. Yeast two-hybrid experiments suggested self-association properties, but this could not be confirmed using other methods (Battersby, Csiszár et al. 2003).

4.3 The downstream BCAP interactome

In immune cells, endogenous BCAP exhibits an unusual migration pattern on SDS-PAGE. Firstly, BCAP isoforms each appear as two or three bands upwards of the expected molecular weight (Okada, Maeda et al. 2000). Secondly, the lower band of $BCAP_L$ migrates around 100 kDa, instead of the theoretical molecular weight of 90 kDa. The latter shift in migration is likely caused by the acidic nature of the protein ($BCAP_L$ pI 5.25; TIR domain pI 4.85). Protein acidity has previously been described to prevent saturation with SDS detergent molecules during SDS-PAGE (Matagne, Joris et al. 1991). The appearance of multiple protein bands on SDS-PAGE has been rarely discussed in previous studies. However, PTMs and the high proline content of BCAP have been suggested to contribute to this behaviour (Halabi 2015). Results from this thesis definitively show that this phenomenon is caused by phosphorylation (Figure 35). Similar to the reduced binding of SDS onto acidic proteins, the addition of numerous phosphate modifications likely limits SDS binding, resulting in a reduced total charge during SDS-PAGE. During the discovery of BCAP, the presence of tyrosine phosphorylation was shown by immunoblotting. However, since phosphotyrosines were present on all four BCAP bands, it could not be concluded that phosphorylation was causing the unusual band

pattern (Okada, Maeda et al. 2000). The new mass spectrometry data from BCAP expressed in Expi293F cells now reveals an enrichment of serine and threonine phosphorylation in the top-most band of BCAP (Figure 37). This suggests that serine and threonine phosphorylation is the major contributor to BCAP hyperphosphorylation, with only a minor role for tyrosine modifications.

The virotrap interaction screen contributed to the identification of a kinase responsible for part the hyperphosphorylation. Casein kinases were significantly enriched in the virotrap experiments and subsequent validation using *in vitro* kinase assays confirmed that CSNK2A1 is a BCAP kinase (Figure 40). The precise modification sites of CSNK2A1 phosphorylation remain elusive, and further research is required to investigate the regulatory functions of these phosphorylations.

Due to the importance of tyrosine phosphorylation for immune signalling, extensive phosphopeptide mapping was conducted with the aim of characterising BCAP tyrosine phosphorylation. Immunoblotting and *in vitro* binding of SH2 domains confirmed the presence of phosphotyrosine residues on BCAP expressed in Expi293F cells. However, protease digestion patterns and technical limitations of phosphoproteomics prevented the identification of any phosphorylation outside serine and threonine residues. A previous study in our laboratory had identified tyrosine phosphorylation by mass spectrometry and has shown that ^{195}YVIV, ^{230}YTIS, ^{374}YPNT, ^{570}YVSS, ^{594}YDPF, ^{694}YESG were phosphorylated in HEK293T cells (Figure 37) (Halabi 2015). And while HEK293T cells do not express tyrosine kinases like BTK (Thul, Akesson et al. 2017), this dataset provides a preliminary assessment of BCAP tyrosine phosphorylation.

To further investigate the kinases responsible for BCAP tyrosine phosphorylation, an *in vitro* kinase assay was used to compare the relative potential of LYN, SYK and BTK to phosphorylate BCAP. Conflicting reports have linked all three kinases to BCAP phosphorylation (Okada, Maeda et al. 2000, Inabe and Kurosaki 2002, Matsumura, Oyama et al. 2010, Halabi, Sekine et al. 2017). The *in vitro* kinase assay revealed that BCAP is more readily phosphorylated by BTK than LYN or SYK (Figure 38). Although inherent kinase activity cannot be fully accounted for in this experimental setup, the data clearly suggests that BTK plays a central role in BCAP hyperphosphorylation. LYN and SYK may still play a role in more specific BCAP phosphorylation, including phosphorylation of YxxM motifs. Overall these results confirm that BCAP is a substrate of numerous kinases, including the previously characterised c-Abl (Maruoka, Suzuki et al. 2005). The precise phosphorylation pattern likely

depends on context, for example, cell type, species and the local signalling environment that may differ between TLR, BCR and IL-1R signalling.

In order to discover novel BCAP interaction partners that may rely on BCAP hyperphosphorylation, a virotrap interaction screen was performed and a substantial list of potential interaction partners was obtained (Figure 39). Among the most significant hits were several known BCAP interaction partners, demonstrating the robust nature of the virotrap method. However, other important BCAP interaction partners were absent in this screen, including TIR domain adaptor proteins and PLC-γ2. TIR domain interactions might be affected by the N-terminal GAG-BCAP fusion used in this method. In tightly packed VLPs with lateral assembly of GAG fusion proteins, N-terminal TIR domain interactions are likely excluded during VLP budding. PLC-γ2 and other immune adaptors are absent due to the use of HEK293T cells, where expression of these proteins is limited or absent.

Validation through Co-IP in HEK293T cells and *in vitro* pulldown assays using purified proteins revealed that GRB2, but not CRKL, interacts with BCAP directly (Figure 41). The GRB2-BCAP interaction is SH3 domain-dependent, and does not involve SH2 domain interactions as previously hypothesised (Okada, Maeda et al. 2000). However, in THP-1 macrophages and Ramos B cells, this interaction was not constitutive (Figure 42). For the known interaction partners p85 and PLC-γ2, the *in vitro* pulldown revealed a combination of SH2 and SH3 domain interactions (Figure 43). Contrary to SH2 domains, SH3 domains do not require phosphorylation of the target sequence. Therefore, the p85 and PLC-γ2 SH3 domain interactions with BCAP may be constitutive. This suggestion may explain the strong interaction between BCAP and PLC-γ2 in HEK293T cells, and the constitutive association with p85 in macrophages and B cells (Aiba, Kameyama et al. 2008, Ni, MacFarlane et al. 2012, Halabi 2015).

These insights suggest a new model for BCAP interactions with p85 and PLC-γ2. Constitutive SH3 domain interactions may drive the formation of pre-formed but inactive complexes (Figure 46). Upon engagement in TLR or BCR signalosomes, BCAP tyrosine phosphorylation will induce rapid SH2 domain binding within the pre-formed complex. Initial N-SH2 domain interactions may further facilitate weaker C-SH2 domain binding. For p85, the peptide array data suggests that the N-SH2 domain preferentially binds the ^{444}YESM and ^{459}YVEM motifs, leaving the ^{419}YESM motif at an ideal distance for C-SH2 domain interactions (Fruman 2010). This sequential SH2 domain binding results in the release of auto-inhibition and activation of

p85 and PLC-γ2 (Yu, Wjasow et al. 1998, Gresset, Hicks et al. 2010, Burke, Vadas et al. 2011) (Figure 46).

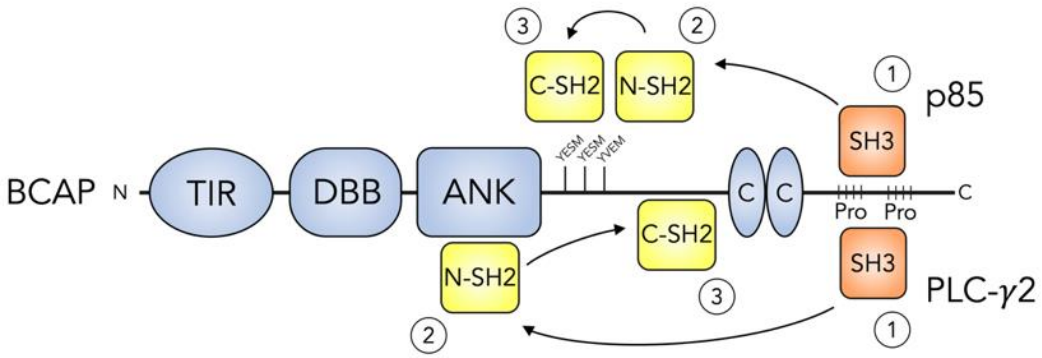

Figure 46. Constitutive SH3 domain interactions facilitate rapid SH2 domain binding upon BCAP tyrosine phosphorylation.

Stepwise binding model for the SH2 and SH3 domain-containing BCAP interaction partners p85 and PLC-γ2. The PI3K p85 or PLC-γ2 SH3 domains constitutively interact with BCAP proline-rich regions (Pro). The preformed complex can then rapidly engage in N-SH2 domain interaction upon BCAP tyrosine phosphorylation. High-affinity N-SH2 interactions facilitate the binding of lower-affinity C-SH2 domain interaction resulting in full activation of PI3K and PLC-γ2.

BCAP peptide array data provides an additional level of granularity by locating the specific tyrosine motifs involved in BCAP-SH2 domain interactions (Figure 44). TIR domain tyrosine motifs were not considered SH2 domain binding sites since previous studies have shown that BCAPs interacts with p85 (Okada, Maeda et al. 2000). Moreover, TIR domains engage in oligomeric TIR domain interactions and are therefore unlikely to be accessible for SH2 domain interactions. This *in vitro* binding assay showed a multitude of interaction motifs for p85, PLC-γ2, GRB2 and CRKL. Many of the interactions go beyond the SH2 domain specificity that was previously attributed to these domains (Huang, Li et al. 2008). And while these *in vitro* binding results do represent the physical binding potential of SH2 domains, the physiological relevance of these interactions is not obvious. Secondary and tertiary protein structure, as well as tyrosine phosphorylation has to be taken into account.

The central requirement for SH2 domain interactions is tyrosine phosphorylation. Existing data gives some evidence to suggest that ^{195}YVIV, ^{230}YTIS, ^{374}YPNT, ^{419}YESM, ^{444}YESM, ^{459}YVEM, ^{513}YHTV, ^{553}YIFK, ^{570}YVSS, ^{594}YDPF and ^{694}YESG can be phosphorylated *in situ* (Maruoka, Suzuki et al. 2005, Halabi 2015). The second requirement for physiological BCAP-SH2 domain interactions is surface accessibility of the full tyrosine motif (Songyang, Shoelson et al. 1993). The DBB domain structure sheds some light on the position of certain tyrosine motifs. The ^{263}YTDM motif is fully accessible in a short turn between the TIG domain

and first α-helix. The ^{195}YVIV and ^{230}YTIS motifs are buried in the ABED dimerisation β-sheet, while the tyrosine residues are exposed. Similar predictions can be made for an *in silico* structural model of the ANK domain. The ^{374}YPNT motif is buried in the α-helical core, while the tyrosine residue points outwards resulting in surface accessibility. However, the ^{346}YGLK, ^{365}YVSA and ^{394}YVET motifs are accessible at the protein surface of the ANK domain model.

These structure predictions reduce the total amount of potential tyrosine interaction motifs. The resulting SH2 domain interaction network with p85, PLC-γ2 and other adaptor proteins is likely highly dynamic and context dependent. Additional results from the Co-IP and *in vitro* pulldowns add multiple, possibly competing, SH3 domain interactions to the BCAP interactome. Further phosphopeptide mapping or other characterisation of tyrosine phosphorylation upon TLR, BCR and IL-1R receptor stimulation would be required to identify the role of specific motifs during signalling events.

Combined with previously characterised BCAP interactions, this virotrap screen and subsequent validation experiments substantially expand the BCAP interactome, revealing an extensive SH2 and SH3 domain network (Figure 47).

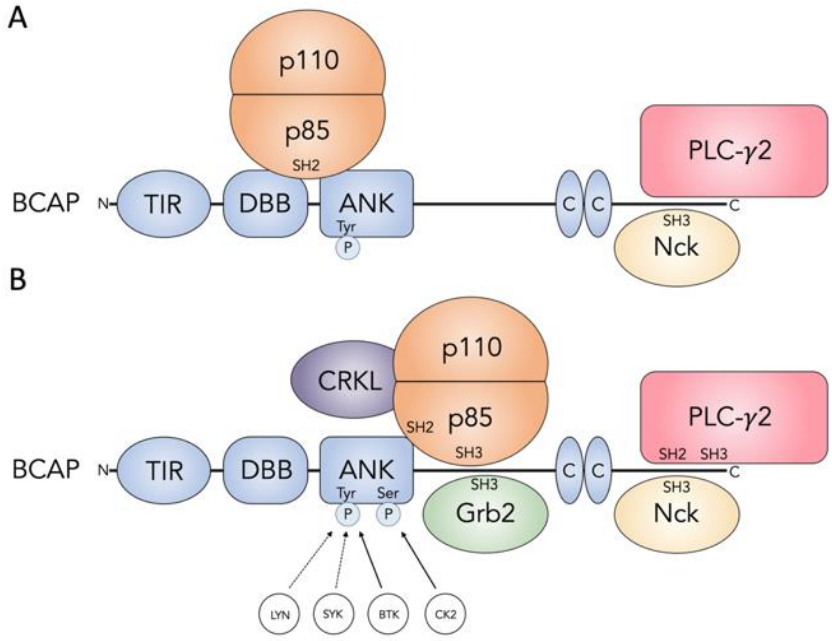

Figure 47. Overview of the BCAP SH2 and SH3 domain interactome.
(A) Overview of the SH2 and SH3 domain-containing interaction partners of BCAP as described in the literature. (B) Updated BCAP interactome representing novel GRB2 and CRKL associations and detailing individual SH2 and SH3 domains interactions on BCAP. The model also includes kinases responsible for serine phosphorylation and tyrosine phosphorylation, which is required for SH2 domain interactions.

4.4 The limitations of HEK293T cells for the study of immune adaptors.

HEK293-derived cell types like HEK293T and Expi293F cells are used in numerous experiments throughout this thesis, due to their robustness, easy maintenance and ease of transfections. However, as a model system for hematopoietic cells, where BCAP is predominantly found, HEK293 cells have important limitations. Specifically, the absence of potential interaction partners and the differences in BCAP phosphorylation have to be taken into account.

For the characterisation of BCAP interactions with TIR domain-containing adaptor proteins such as MAL and MyD88, HEK293T cells are commonly used as a model system since they contain an intact NF-κB signalling pathway. Therefore, overexpression of TLRs or the adaptors MAL, MyD88 and TRIF is sufficient to generate inflammatory signalling (Medzhitov, Preston-Hurlburt et al. 1998, Fitzgerald, Palsson-McDermott et al. 2001, Yamamoto, Sato et al. 2002). This makes HEK293T cells a suitable model system for studying the mechanism of TLR signalling including the TIR signalosome.

During the study of the wider BCAP interactome, the use of HEK293-derived cells is more limiting since their protein expression pattern is not representative for that of hematopoietic cells. For example, important tyrosine kinases like BTK, and to a lesser extent SYK and LYN, as well as known BCAP interaction partners like PLC-γ2 are not expressed in HEK293T cells. It can therefore not be assumed that the BCAP hyperphosphorylation pattern found in HEK cells is identical to that in macrophages or B cells. Since the virotrap technique is currently restricted to the use of HEK293T cells, the resulting findings can only be a subset of the BCAP interactome found in immune cells. Moreover, in order to make definitive statements about the role and mechanism of novel BCAP interaction partners such as GRB2, it is important to validate these interactions in HEK293 cells as well as macrophages and B cells as attempted in section 3.3.6.

4.5 Future directions

4.5.1 The role of BCAP in the TLR signalosome

The functional data set out in this thesis provides a novel model for the regulation of TLR signalling. However, the mechanism for $BCAP^{TIR}$ domain interactions with MAL and MyD88 could not be determined. Further biophysical and structural studies are required to characterise the incorporation of $BCAP^{TIR}$ domains into MAL and MyD88 filaments, and to unravel the

mechanism of steric inhibition. As described by Ve *et alia*, Cryo-EM and turbidity assays are powerful tools to characterise filament formation (Ve, Vajjhala et al. 2017). These tools could be relied upon when characterising these outstanding mechanisms.

Structural characterisation of the DBB domain revealed a strong conservation between TIG^{TF} domains and the BCAP DBB domain. A subsequent functional conservation could not be completely ruled out, and future investigation into the functional similarities between these two domains should include *in vitro* sequence-unspecific DNA binding assays that can definitively test the hypothesis of functional conservation.

4.5.2 Cryo-EM of BCAP and downstream protein complexes

This thesis sheds light on the function of the DBB domain, and the role of dimerisation in negative regulation of TLR signalling. DBB domain dimerisation likely induces conformational restraints on the relative orientation of $BCAP^{TIR}$ domains, resulting in disruption of MAL and MyD88 filaments. However, results in this study provide no structural data that could inform a precise mechanism for the model of indirect TIR domain dimerisation.

Efforts to crystallise dimeric BCAP constructs containing the TIR domain were not successful. BCAP remains a challenging target for further crystallisation studies due to its unstructured region and TIR domains that may adopt various conformations due to the long DBB linker region.

With recent advancements in cryo-EM (Cheng 2015), it is now conceivable to obtain a structural model of full-length BCAP including the C-terminal unstructured region. Such a model may capture several TIR domain conformations that could provide clues in search of a structural model for TIR signalosome regulation. Moreover, a cryo-EM model of BCAP would also provide a structure of the ANK domain and coiled-coil region, possibly revealing functional characteristics of these domains.

Since small proteins are more difficult targets for cryo-EM structure determination, it is not obvious that BCAP would be a suitable target from which an atomic model could be derived. The unstructured C-terminal region might not adopt a stable conformation, which would *de facto* reduce the protein region suitable for model building to an equivalent molecular weight of less than 150 kDa for a dimer. However, even a cryo-EM map with a resolution unsuitable for *de novo* model building could still provide valuable information as 3D structures are now available for the TIR, DBB and ANK domains of BCAP.

In order to determine whether dimeric full-length BCAP is a suitable target for future cryo-EM studies, preliminary data was collected using purified BCAP from Expi293F cells (Figure 48). While the quality of these images is not sufficient to obtain high quality 2D class averages required for a 3D model, these images demonstrate that BCAP can be imaged using cryo-EM. A thorough optimisation of buffer conditions and subsequent freezing in combination with high-end 300 kV cryo-EM equipment will likely lead to a model in which the existing domain structures can be fitted.

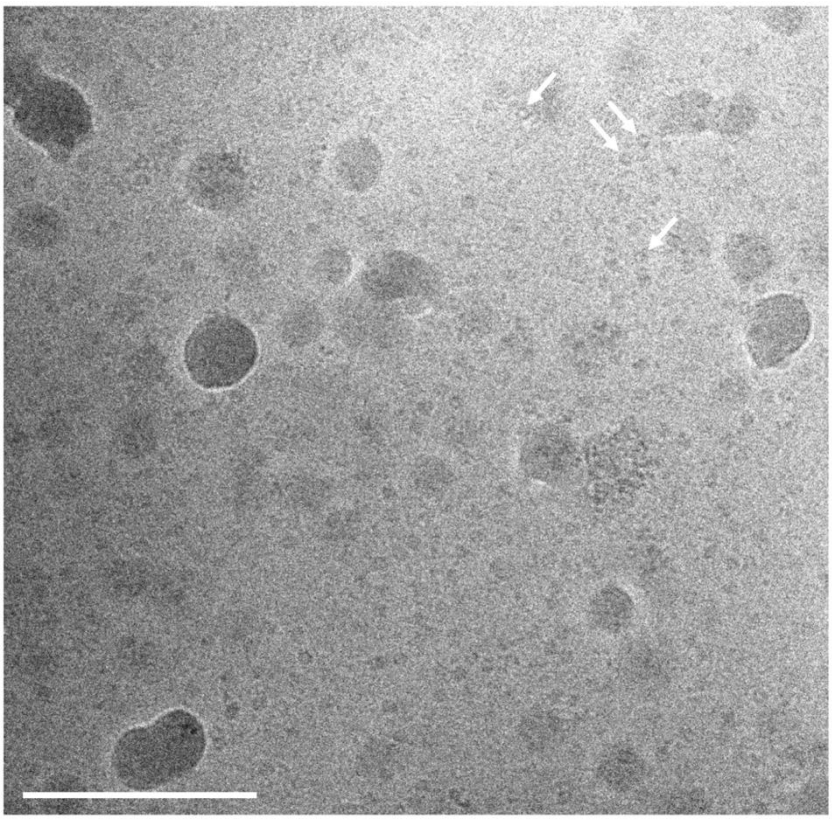

Figure 48. Preliminary cryo-EM images provide a proof of principle for future structural studies.
Purified $BCAP_L$ from Expi293F spotted onto graphene oxide grids at a concentration of 0.1 mg/ml before flash freezing in liquid ethane. Images were collected on a 150 kV JEM 1400+ (JEOL) cryo-EM. Samples preparation and data collection were conducted in collaboration with Sander Van der Verren (VIB/VUB Brussels, Belgium). Arrows highlight individual BCAP dimers. Scale bar corresponds to 80 nm.

Larger BCAP-PI3K and BCAP-PLC-γ2 complexes would be equally attractive targets for future cryo-EM studies, due to the medical relevance of these enzymes and the progress made in this thesis. Improvement in the production of phosphorylated $BCAP_L$ and structural models for the DBB and ANK domains make PI3K and PLC-γ2 complexes feasible targets. BCAP is increasingly being linked to signalling pathways outside of BCR and TLR signalling, making it an ever more important immune adaptor and a crucial regulator of enzymes like PI3K and PLC-γ2. Structures of these BCAP complexes would provide valuable insights into the precise regulation and activation of these enzymes.

Existing structures of PI3K again provide a reference for model building of these complexes (Huang, Mandelker et al. 2007). Preliminary results suggest that p85 can be successfully expressed in *E. Coli* as N-terminal GST fusion protein (data not shown). Moreover, full-length PI3K and PLC-γ2 are commercially available in quantities suitable for cryo-EM.

Structural studies of these complexes could be complemented with functional activity assays of PI3K and PLC-γ2 (Aksoy, Taboubi et al. 2012) in the presence of BCAP, to test the model of sequential SH domain binding proposed in this thesis. In particular, comparing the effect of phosphorylated and dephosphorylated BCAP on enzyme activity would be a possible avenue to verify the order and importance of SH2 and SH3 domain interactions.

4.5.3 Further characterisation of the BCAP interactome and phosphorylation.

The virotrap experiment conducted in this thesis marks an important step towards further characterisation of the BCAP interactome. However, as it was not possible to identify the physiological context in which the BCAP interactions with GRB2 and CRKL take place, further experiments are required to determine the precise signalling pathways and cellular context of these interactions. BCAP has recently been linked to IFN-α production and inflammasome activation through numerous previously unrelated adaptor proteins (Carpentier, Ni et al. 2019, Chu, Ni et al. 2019), suggesting that BCAP is a more versatile adaptor protein than previously conceived. In this context, the other hits from the virotrap screen that were not further validated in this thesis, including ANXA6 and PLSCR1, may turn out to be important links between seemingly unrelated pathways.

The initial characterisation of BCAP phosphorylation in this thesis is a starting point for further analysis of this important PTM. A combination of inhibitors and phosphopeptide mapping could help reveal precise phosphorylated tyrosine motifs and the role of serine phosphorylation in the context of BCR, TCR or TLR stimulation. Given the incomplete phosphopeptide mapping in this thesis, more specialised tools and protocols like titanium dioxide or antibody enrichment for delicate tyrosine phosphorylations should be considered.

5 Methods

5.1 Cloning

5.1.1 Primer oligonucleotides

Forward and reverse primer oligonucleotides for ligation-independent cloning (LIC) and restriction enzyme (RE) cloning were designed using the *Crystallisation Construct Designer 2* tool (Mooij, Mitsiki et al. 2009). Unless stated otherwise, primers used have a melting temperature of 65 °C. Primers were ordered from Sigma-Aldrich, and were purified by de-salting. Primers larger than 100 bp were purified using HPLC. Table 4 provides an overview of the primers used in this project.

Table 4. List of Primers used for cloning.

Construct Name	Forward Primer (5'-3')	Reverse Primer (5'-3')	Destination Vector
BCAP TIG (179-264)	TACTTCCAATCCAATGCCATGGTGGTGCAGCCGGACCGCATTCG	TTATCCACTTCCAATGTTAAGTATAATAGCTGATAACGGTTTCACACACCACTAAGTCTCC	pMCSG7
BCAP DBB (179-288)	TACTTCCAATCCAATGCCATGGTGGTGCAGCCGGACCGCATTCG	TTATCCACTTCCAATGTTATTTAAAGGCCTGACACATGAATTCCACAGG	pMCSG7
BCAP DBB (179-318)	TACTTCCAATCCAATGCCATGGTGGTGCAGCCGGACCGCATTCG	TTATCCACTTCCAATGTTATCCAAAGAGGTGCAGTCCGCTTGC	pMCSG7
BCAP DBB (179-316)	TACTTCCAATCCAATGCCATGGTGGTGCAGCCGGACCGCATTCG	TTATCCACTTCCAATGTTAGAGGTGCAGTCCGCTTGCAGG	pMCSG7
BCAP DBB (179-313)	TACTTCCAATCCAATGCCATGGTGGTGCAGCCGGACCGCATTCG	TTATCCACTTCCAATGTTATCCGCTTGCAGGGATATTGTTCTTCAG	pMCSG7
BCAP DBB (179-312)	TACTTCCAATCCAATGCCATGGTGGTGCAGCCGGACCGCATTCG	TTATCCACTTCCAATGTTAGCTTGCAGGGATATTGTTCTTCAGGG	pMCSG7
BCAP DBB (179-322)	TACTTCCAATCCAATGCCATGGTGGTGCAGCCGGACCGCATTCG	TTATCCACTTCCAATGTTACAGCTGGTTGATTCCAAAGAGGTGC	pMCSG7
BCAP DBB-ANK (179-370)	TACTTCCAATCCAATGCCATGGTGGTGCAGCCGGACCGCATTCG	TTATCCACTTCCAATGTTACTTGTTGGCCACGCTGTACGCCTGCAG	pMCSG7
BCAP DBB-ANK (179-396)	TACTTCCAATCCAATGCCATGGTGGTGCAGCCGGACCGCATTCG	TTATCCACTTCCAATGTTATTCCACATACTCGTCGATGAACTGCC	pMCSG7
BCAP DBB-ANK (179-398)	TACTTCCAATCCAATGCCATGGTGGTGCAGCCGGACCGCATTCG	TTATCCACTTCCAATGTTACACCGTTTCCACATACTCGTCGATG	pMCSG7
BCAP DBB-ANK (179-400)	TACTTCCAATCCAATGCCATGGTGGTGCAGCCGGACCGCATTCG	TTATCCACTTCCAATGTTACATGTCCACCGTTTCCACATACTCG	pMCSG7
BCAP DBB-ANK (179-402)	TACTTCCAATCCAATGCCATGGTGGTGCAGCCGGACCGCATTCG	TTATCCACTTCCAATGTTACTTGAGCATGTCCACCGTTTCCAC	pMCSG7
BCAP DBB-ANK (179-404)	TACTTCCAATCCAATGCCATGGTGGTGCAGCCGGACCGCATTCG	TTATCCACTTCCAATGTTAGTGACTCTTGAGCATGTCCACCG	pMCSG7
BCAP TIR-DBB-ANK (7-404)	TACTTCCAATCCAATGCCCCCAGAGGATGCGACATCCTCATC	TTATCCACTTCCAATGTTAGTGACTCTTGAGCATGTCCACCG	
BCAP ANK (333-467)	TACTTCCAATCCAATGCCGATGAAGAGCTGCCCACCCTGTTGCATTTTGC	TTATCCACTTCCAATGTTATGTACTGGCCTGAAGCATTTCAACATAGAGGTCTTCAG	pMCSG9
BCAP DBB (179-330) Strep	TACTTCCAATCCAATGCCATGGTGGTGCAGCCGGACCGCATTCG	TTATCCACTTCCAATGTTACTTTTCAAACTGCGGATGCGACCACATATTTGTCATCATATCTTCTTCTTCCAGCTGGTTGATTCCAAAGAG	pMCSG7
FLAG BCAP TIR (1-145)	ATGATGGGTACCATGGCAGCCTCAGGGGTGCCCAGAG	ATGATGGGATCCTTAGCCAGAATCTTCGGAAATGGCTTTTTTCACAGCTGC	pcDNA3.1(+)
FLAG BCAP TIR-TIG2α (1-288)	ATGATGGGTACCATGGCAGCCTCAGGGGTGCCCAGAG	ATGATGTCTAGATTATTTAAAGGCCTGACACATGAATTCCACAGGATTCGCG	pcDNA3.1(+)
FLAG BCAP TIR-DBB (1-311)	ATGATGGGTACCATGGCAGCCTCAGGGGTGCCCAGAG	ATGATGGGATCCTTATGCAGGGATATTGTTCTTCAGGGATTCGGTTAGCAG	pcDNA3.1(+)
FLAG BCAP TIR-DBB-ANK (1-426)	ATGATGGGTACCATGGCAGCCTCAGGGGTGCCCAGAG	ATGATGGGATCCTTAGGAAAGGTGGGCCATGGACTCGTACACAG	pcDNA3.1(+)
Myc BCAP TIR (1-145)	ATGATGGGATCCATGGCAGCCTCAGGGGTGCCCAGAG	ATGATGGGTACCTTAGCCAGAATCTTCGGAAATGGCTTTTTTCACAGCTGC	pcDNA3.1(+)
Myc BCAP TIR-DBB (1-311)	ATGATGGGATCCATGGCAGCCTCAGGGGTGCCCAGAG	ATGATGGGTACCTTATGCAGGGATATTGTTCTTCAGGGATTCGGTTAGCAG	pcDNA3.1(+)
Myc BCAP TIR-DBB-ANK (1-426)	ATGATGGGATCCATGGCAGCCTCAGGGGTGCCCAGAG	ATGATGGGTACCTTAGGAAAGGTGGGCCATGGACTCGTACACAG	pcDNA3.1(+)
Myc BCAP-L (Y374F)	GGTGTTGGGGAAGTGGCCATGCTTGTTGGC	GCCAACAAGCATGGCCACTTCCCCAACACC	pcDNA3.1(+)
His Avi BCAP-L (2-805)	ATGATGAAGCTTGCCGCCACCATGCATCATCACCATCACCACGCTGCTGGCCTGAACGACATCTTCGAGGCTCAGAAAATCGAATGGCACGAAGAGGATCTGTACTTTCAGAGCGCAGCCTCAGGGGTGCCC	ATGATGGGATCCCTAGCGTCCTCTGGGTGGAACAGGTG	pcDNA3.1(+)
GAG BCAP (1-805)	ATGATGGAATTCATGGCAGCCTCAGGGGTGCC	ATGATGTCTAGATTAGCGTCCTCTGGGTGGAACAGG	pMET7-Gag
FLAG-MyD88 (1-296)	ATGATGAAGCTTATGGCTGCAGGAGGTCCCGG	ATGATGGGATCCTTAGGGCAGGGACAAGGCCTTGG	pcDNA3.1(+)
MAL TIR (79-221) Strep	TACTTCCAATCCAATGCCAGTAGTCGCTGGAGCAAAGACTATGACGTCTGC	TTATCCACTTCCAATGTTACTTTTCAAACTGCGGATGCGACCAACTGAGTGTCTGCAGATAACGCATGACAGCTTCTTTG	pMCSG7
GRB2 (1-217)	TACTTCCAATCCAATGCCATGGAAGCCATCGCCAAATATGACTTCAAAGCTACTGC	TTATCCACTTCCAATGTTAGACGTTCCGGTTCACGGGGGTGACATAATTG	pMCSG10
GRB2 SH2 (86-179)	TACTTCCAATCCAATGCCTGGTTTTTTGGCAAAATCCCCAGAGCCAAGGCAG	TTATCCACTTCCAATGTTACTGTTCTATGTCCCGCAGGAATATCTGCTGGTTTC	pMCSG10
GRB2 Myc His (1-217)	ATGATGGGTACCGCCGCCACCATGGAACAAAAACTTATTTCTGAAGAAGATCTGGACTCCTCGGACCGCTCCGCCTG	ATGATGCTCGAGTTACTCGTTTTCATCTGGGTTTTGAGGGTCAAAGATTTTGACG	pCMV
p85α SH3 (39-121)	TACTTCCAATCCAATGCCATGAGTGCTGAGGGGTACCAGTAC	TTATCCACTTCCAATGTTACGAGATTTTTTTCCTTCCAATATATTCTACGTAAGTTC	pMCSG10
p85α nSH2 (359-478)	TACTTCCAATCCAATGCCGGTATGAATAACAATATGTCCTTACAAAATGCTGAATG	TTATCCACTTCCAATGTTAATCTTCTTTGACAACTTGATCCTGTTGGTATTTG	pMCSG10
p85α cSH2 (652-758)	TACTTCCAATCCAATGCCGAAGATTTGCCCCATCATGATGAGAAGAC	TTATCCACTTCCAATGTTATGCATATACTGGGTAGGCTAGTGTGAC	pMCSG10
p85α (1-724)	TACTTCCAATCCAATGCCATGAGTGCTGAGGGGTACCAGTACAGAGCG	TTATCCACTTCCAATGTTATCGCCTCTGCTGTGCATATACTGGGTAGGC	pMCSG10
PLC-γ2 nSH2 (534-634)	TACTTCCAATCCAATGCCCACAAGAAGGTGGAGAAGAGGACG	TTATCCACTTCCAATGTTAAGGGTCCGTGAGCCGCAGC	pMCSG10
PLC-γ2 cSH2 (649-734)	TACTTCCAATCCAATGCCGACAGCCTGAGCCGCGGAG	TTATCCACTTCCAATGTTAGGGGTAGCGCAGTCTCATCTTTCG	pMCSG10
PLC-γ2 SH3 (769-829)	TACTTCCAATCCAATGCCATGCCTCAGAGAACCGTGAAAGCTC	TTATCCACTTCCAATGTTAAGTTGAGATGTCCTCGACGTAGTTGG	pMCSG10
CRKL Myc (1-303)	ATGATGGGTACCCGCCACCATGTCCTCCGCCAGGTTCGACTCCTCGGACCGCTCCGCCTG	ATGATGGGTACCTTACAGATCCTCTTCAGAGATGAGTTTCTGCTCCTCGTTTTCATCTGGGTTTTGAGGGTCAAAGATTTTGACG	pcDNA3.1(+)
FLAG CRKL (2-303)	ATGATGGGATCCTCCTCCGCCAGGTTCGACTCCTCGGACCGCTCCGCCTG	ATGATGCTCGAGTTACTCGTTTTCATCTGGGTTTTGAGGGTCAAAGATTTTGACG	pcDNA3.1(+)

5.1.2 PCR for LIC and RE cloning

Gene amplification from plasmid DNA was performed using Vent DNA polymerase (NEB). PCR reactions contained the following reagents in a total volume of 50 µl: 100 ng template plasmid DNA, 0.5 µM forward and reverse primers, 200 µM dNTPs, 6 mM $MgSO_4$, 5% (v/v)

DMSO, 10X thermoPol reaction buffer (NEB) and 2 U Vent DNA polymerase (NEB). The thermocycler protocol is shown in Table 5. After PCR amplification, the PCR fragment was purified on agarose gel. These 1% agarose gels were cast with TEA buffer (40 mM TRIS, 20 mM acetic acid, 1 mM EDTA pH 8.3) and SYBR Safe DNA Gel Stain (Thermo Fisher Scientific), and subsequently run in TAE buffer at 100 V for 1 h. PCR products were extracted from the agarose gel using the QIAquick Extraction Kit (Qiagen).

Table 5. Thermocycler protocol for LIC and RE cloning.

98 °C	30 s	
98 °C	30 s	30 x
65 °C	30 s	
72 °C	1 min / kb	
72 °C	5 min	

5.1.3 Site-directed mutagenesis PCR

In order to substitute individual amino acids or to delete a region from a plasmid vector, the Quikchange II protocol (Agilent) was followed. Primers were designed using the *Quikchange Primer Design tool* (Agilent) and contained the appropriate overlap for base changes or deletions. A total reaction volume of 50 µl contained 10 ng template plasmid DNA, 125 ng forward and reverse primers, 100 µM dNTPs, 10X PfuUltra reaction buffer (Agilent) and 2.5 U PfuUltra HF DNA polymerase (Agilent). The thermocycler protocol used is shown in Table 6.

Table 6. Thermocycler protocol for site-directed mutagenesis.

95 °C	30 s	
95 °C	30 s	
55 °C	1 min	16 x
68 °C	1 min / kb	

5.1.4 Colony PCR

In order to confirm the presence of desired inserts in a newly cloned plasmid, a DreamTaq (Thermo Fisher Scientific) colony PCR protocol was used. Each PCR reaction comprised the following reagents in a total volume of 25 µl: material from a bacterial colony, 2X DreamTaq DNA Polymerase PCR Master Mix (Thermo Fisher Scientific) containing 1.25 U DreamTaq DNA Polymerase and 1 µM forward and reverse primers used in the cloning of the plasmid. The thermocycler protocol is shown in Table 7. PCR fragments were visualised on a 1% agarose gel.

Table 7. Thermocycler protocol for colony PCR.

95 °C	30 s	
95 °C	30 s	30 x
65 °C	30 s	
72 °C	1 min / kb	
72 °C	10 min	

Ligation-independent cloning (LIC)

LIC compatible pMCSG7, pMCSG9 and pMCSG10 vectors were used for protein expression in *E. coli*. These vector contain a N-terminal His-TEV$_{cs}$ and His-GST-TEV$_{cs}$ tags, respectively. The vectors were linearised by SspI (NEB) digestion according to the manufacturer's recommendation. The linearised vectors, and PCR fragments containing 'LIC overhang sequences' (Eschenfeldt, Lucy et al. 2009), were digested with T4 DNA polymerase to generate LIC overhangs. For each DNA sequence, a 50 µl digest contained 250 ng linearised vector or PCR fragment, 10X NEB buffer 2 (NEB), 2.5 mM dGTP (vector) or dCTP (PCR fragment), 5 mM DTT and 1 U/µl of T4 DNA polymerase (NEB). The reaction mixture was incubated at room temperature for 30 min followed by heat inactivation at 75 °C for 20 min. For a typical LIC ligation, 2 µl treated vector and PCR fragment were mixed and incubated at room temperature for 20 min prior to transformation into *E. coli* cells as described in section 5.1.6.

5.1.5 Restriction enzyme cloning

Constructs used for overexpression in mammalian cells were cloned using restriction enzymes. Primers were designed to overlap with a specific region of the gene of interest and to contain a restriction site that is compatible with the target plasmid. Depending on the use of the construct, various N-terminal and C-terminal epitope tags were included in the primer sequences (Table 4).

Vector and PCR fragment were purified on a 1% agarose gel as describe in section 5.1.2, after which they were digested with the appropriate restriction enzymes in a double digest. A typical 20 µl reaction contained 1 µg fragment of vector DNA, 10X CutSmart buffer (NEB) and 10 U of each restriction enzyme (NEB). Following another agarose gel purification and gel extraction step, the PCR fragment and vector were ligated using T4 DNA ligase (NEB) and transformed into *E. coli* cells as described in section 5.1.6.

5.1.6 Transformation of bacterial cells

To transform plasmid DNA into bacterial cells, 100 ng plasmid DNA was incubated with 50 µl chemically competent DH5α or Rosetta2(DE3) cells on ice for 5 min. The cells were subsequently subjected to a heat shock treatment at 42 °C for 60 s, followed by incubation on ice for 5 min. The cells were then supplemented with 350 µl SOC medium for recovery and incubated at 37 °C for 1 h with shaking. After recovery in SOC medium, transformed cells were spread onto agar plates (containing a combination of antibiotics at a final concentration of 100 mg/ml ampicillin, 350 mg/ml chloramphenicol, 50 mg/ml kanamycin or 50 µg/ml spectinomycin) for selection and incubated overnight at 37 °C.

For sequencing and plasmid DNA amplification, transformed bacterial cells were grown in 5 ml LB overnight at 37 °C. Cell were then harvested and plasmid DNA was extracted using the QIAprep Spin Miniprep Kit (Qiagen). For protein expression, a 5 ml culture was used to inoculate 1 l of main culture as described in section 5.3.1.

5.2 Cell biology techniques

5.2.1 Cells and routine cell culture

Mammalian cell tissue culture handling was conducted in a containment level 1 laboratory in a sterile tissue culture flow hood, with appropriate measures to ensure sterile conditions.

Human embryonic kidney 293 (HEK293) and HEK293 cell containing the viral SV40 T-antigen (HEK293T) were used for co-immunoprecipitation and NF-κB luciferase assays. The cell lines were obtained from the American Type Culture Collection (ATCC, USA), and were maintained in high-glucose Dulbecco's modified Eagle's medium (DMEM) (Sigma-Aldrich) supplemented with 2 mM glutamine, 100 U/ml penicillin, 100 µg/mL streptomycin and 10% (v/v) heat-inactivated foetal calf serum (FCS) at 37 °C with 5% CO_2. Passaging took place around 80-90% confluency, and cells were diluted no further than $4x10^4$ cells/ml before seeding in a new flask.

Expi293F suspension cells were made available by AstraZeneca (Cambridge, UK), for the purpose of $BCAP_L$ protein expression. Cells were maintained in vented 850 cm^2 roller bottles with Expi293 Medium (Gibco) at 140 rpm, 37 °C and 8% CO_2. In order to facilitate aeration, the culture volume in roller bottles did not exceed 1/3 of the total volume. Passaging took place every second day, and cells were seeded at a density of $5x10^5$ cells/ml.

THP-1 cells were obtained from Iain Fraser (National Institute for Allergy and Infectious Diseases, USA). Cells were maintained in RPMI 1640 medium (Invitrogen) supplemented with 10% FCS, L-glutamine, 100 U/ml penicillin and 100 mg/ml streptomycin at 37 °C and 5% CO_2. Cells were passaged every second day and diluted to $2x10^5$ cells/ml. Monocytic THP-1 cells were differentiated into macrophages using 10 ng/ml phorbol 12-myristate 13-acetate (PMA) (Sigma-Aldrich) for 12 h followed by 24 h in normal culturing conditions.

Ramos B cells were obtained from the American Type Culture Collection (ATCC) and cultured in RPMI medium (Invitrogen) supplemented with 10% FCS, L-glutamine, 100 U/ml penicillin and 100 mg/ml streptomycin at 37 °C and 5% CO_2. Cells were passaged every second day and diluted to $2x10^5$ cells/ml.

5.2.2 Co-immunoprecipitation of endogenous proteins

Ten million differentiated THP-1 macrophages or Ramos B cells were resuspended in HEPES lysis buffer (50 mM HEPES 150 mM NaCl, 2 mM EDTA, 10% glycerol, 0.5% NP-40 pH 7.5) supplemented with 5 mM sodium orthovanadate, 50 mM sodium fluoride, 60 mM β-glycerophosphate and 100X protease inhibitor cocktail (Calbiochem). In this buffer, the cells were lysed at 4 °C for 30 min while rotating. The lysate was subsequently cleared by centrifugation at 16000 × g for 10 min at 4 °C.

The lysate supernatant was pre-cleared with 20 µl protein A/G agarose beads (Santa Cruz Biotech) equilibrated in HEPES lysis buffer and incubated at 4 °C for 2 h while rotating. Then, 1-2 mg primary antibody was added to the lysates for overnight incubation at 4 °C. The next day, 25 µl protein A/G agarose beads equilibrated in HEPES lysis buffer, were added to the sample and incubated at 4 °C for 3 h while rotating. Samples were washed three times with 1 ml HEPES lysis buffer before boiling in the presence of 4X SDS-loading buffer. The samples were loaded onto SDS-PAGE for western blot analysis.

5.2.3 Co-immunoprecipitation of overexpressed proteins

HEK293T cells were seeded into 6-well plates at a density of $2x10^5$ per well. At 70-80% confluency 3 µg plasmid DNA was transiently transfected into each well with JetPEI (Polyplus Transfection SA) according to the manufacturer's recommendation. At 24 h post-transfection, cells were washed with PBS and lysed with 300 µl of HEPES lysis buffer (50 mM HEPES, 150 mM NaCl, 2 mM EDTA, 10% glycerol, 0.5% NP-40 pH 7.5), supplemented with 50 mM NaF, 5 mM orthovanadate, 60 mM β-glycerophoaphate and 100X protease inhibitor cocktail

(Calbiochem). Cells were lysed at 4 °C for 30 min while rotating, and the lysate was subsequently cleared by centrifugation at 16000 × g for 10 min at 4 °C.

Immunoprecipitation of overexpressed FLAG-tagged proteins was conducted by the addition of 10 µl EZview Red FLAG M2 beads (Sigma-Aldrich), equilibrated in HEPES lysis buffer. Samples were then incubated at 4 °C for 2 h while rotating. After three washes with 1 ml HEPES lysis buffer, samples were boiled in the presence of 4X SDS-loading buffer and loaded onto SDS-PAGE for western blot analysis.

5.2.4 NF-κB reporter assay

HEK293T cells were seeded into a 96-well plate at $1.5x10^4$ cells per well. At a confluency of 80%, JetPEI (Polyplus Transfection SA) was used to transiently transfect cells with the NF-κB reporter vector pBIIX-luc, pCMV-Renilla-luc, Myc-MAL, Myc-MyD88 and various BCAP constructs, totalling 100 ng DNA per well. At 24 h post-transfection, cells were lysed in 50 µl passive lysis buffer (Promega). The lysates were assayed for luciferase activity using the Dual-Glo luciferase kit (Promega) on a PHERAstar FS (BMG Labtech) plate reader with the kind help of Michael Scherm. Luciferase activity is represented as firefly luciferase signal relative to *Renilla* luciferase signal and normalised to cells transfected with empty vectors.

5.2.5 Fluorescence microscopy

THP-1 monocytes were seeded onto Falcon CultureSlides (Corning) and differentiated into macrophages as described in section 5.2.1. After 24 h, THP-1 macrophages were stimulated with 100 ng/ml LPS for 30 min and subsequently washed with PBS. Ramos B cells were stimulated with α-IgM for 10 min, pelleted by centrifugation at 1500 × g for 5 min and resuspended in PBS.

Immunostaining of THP-1 macrophages took place on the coverslips, whereas the Ramos cell were stained in suspension and spun down before applying subsequent buffer solutions. Immunostaining of both cell types was carried out at room temperature. Cells were fixed using 3.7% paraformaldehyde in PBS for 15 min, after which the cells were permeabilised with 0.1% triton x-100 in PBS for 5 min. After washing with PBS, cells were blocked in 0.25% (w/v) BSA in PBS for 30 min. Cell were immunostained with polyclonal α-BCAP antibody (diluted 1/200 in 2.5% (w/v) BSA in PBS) for 1 h. After washing twice with PBS, cells were incubated with Alexa Fluor-conjugated secondary antibody (diluted 1/2000 in 0.25% (w/v) BSA in PBS) for 1 h. After a final wash with PBS, 15 µl of DAPI-containing mounting medium (Vector Shield, H-1200) was applied to the cells before the coverslip with THP-1 cells was inversely mounted

onto a glass SuperFrost Plus glass slide (VWR International). Ramos B cells were resuspended in mounting medium and equally applied to a glass slide and covered with a coverslip. Glass slides were sealed with nail varnish and samples were dried away from daylight before imaging with on an EVOS M5000 (Invitrogen) epifluorescence microscope.

5.2.6 Western blotting

Proteins separated by SDS-PAGE were transferred to Hybond-C Nitrocellulose membrane (GE Healthcare) using the Bolt Mini Blot Module (Life Technologies). Transfer was conducted in transfer buffer (25 mM Tris, 192 mM glycine, 20% v/v methanol) at 12 V for 90 min. The nitrocellulose membrane was then blocked in 5% (w/v) BSA in TBS supplemented with 0.05% tween 20 (TBST) for a minimum of 45 min at room temperature. Overnight, membranes were incubated with primary antibodies diluted in blocking buffer containing 2.5% (w/v) in BSA TBST at 4 °C. Before and after incubation with secondary antibody, membranes were washed three times with TBST for 5 min. Blots were incubated with horseradish peroxidase-conjugated secondary antibody diluted in 2.5% (w/v) BSA TBST for 1 h at room temperature. Primary and secondary antibodies were diluted according to the manufacturer's recommendation. Protein bands were visualised using ECL reagent (GE Healthcare) and visualised on Hyperfilm ECL (GE Healthcare) using a mini-medical series developer (AFP Imaging).

5.3 Protein expression

5.3.1 Protein expression in *E. coli*

Rosetta2(DE3) cells were transformed with a plasmid containing the protein of interest as described in section 5.1.6. Overnight, 5 ml precultures were grown in LB medium with appropriate antibiotics. These precultures were used to inoculate 1 l auto-induction medium as described by (Studier 2005). Inoculated main cultures were grown at 37 °C with shaking (140 rpm) for 4 h, after which the temperature was reduced to 20 °C for protein expression overnight.

For selenomethionine incorporation during protein expression, precultures were grown overnight in LB medium, spun down and resuspended in M9 minimal medium. Precultures were then each used to inoculate 1 l of M9 minimal medium supplemented with 0.05 g selenomethionine (Sigma-Aldrich), 0.1 g lysine (Sigma-Aldrich), 0.1 g threonine (Sigma-Aldrich), 0.1 g phenylalanine (Sigma-Aldrich), 0.05 g leucine (Sigma-Aldrich), 0.05 g isoleucine (Sigma-Aldrich) and 0.05 g valine (Sigma-Aldrich). Main cultures were grown at

37 °C with shaking (140 rpm). At and OD600 0.6-0.7, cultures were induced with 1 mM IPTG and the temperature was reduced to 20 °C for protein expression overnight.

5.3.2 Protein expression in mammalian cells

A total volume of 225 ml Expi293F cells was seeded at a density of $2x10^5$ cells/ml. After reaching a density of $4.0x10^6$ cells/ml the following day, cells were transiently transfected with His-Avi-TEV_{cs}-BCAP. For each 225 ml culture bottle, 375 µg of plasmid DNA and 1.5 ml of 1 mg/ml PEI (Polysciences) were separately diluted in 12.5 ml of Expi293 Medium (Gibco), and subsequently mixed for 15 min at room temperature before adding to the cell culture. At 24 h post-transfection, fresh medium was added to increase the culture volume to 500 ml. Three days post-transfection, cells were harvested and pelleted as described in section 5.3.3.

5.3.3 Cell pellet harvesting and lysis

Bacterial and mammalian cell cultures were pelleted at 4000 rpm for 10 min at room temperature in a JLA8.100 rotor (Beckman Coulter). After discarding the supernatant, the resulting pellets were flash frozen in liquid nitrogen and stored at -80 °C.

For cell lysis, pellets were resuspended in 30 ml GST lysis buffer (PBS supplemented with 100X protease inhibitor cocktail (Calbiochem)) or nickel-NTA lysis buffer (50 mM TRIS, 250 mM NaCl, 30 mM Imidazole, 1 mM TCEP pH 7.5, supplemented with 100X protease inhibitor cocktail (Calbiochem)), according to the purification strategy. Lysis was performed on ice using a Vibra-Cell VCX130 ultra-sonicator (Sonics & Materials Inc) with an amplitude of 60% for a total of 1-2 min using an appropriate pulse cycle to limit heat generation. The cell lysate was cleared by centrifugation at 20000 × g and 4 °C for 30 min. The supernatant was captured and filtered using a 0.2 µm syringe filter.

5.4 Protein purification

5.4.1 Nickel affinity purification

Soluble His-tagged proteins extracted from bacterial or mammalian cultures were cleared as described in section 5.3.3 and loaded onto a 1 ml Chelating HP column (GE Healthcare) equilibrated in nickel-NTA buffer (50 mM TRIS, 250 mM NaCl, 30 mM imidazole, 1 mM TCEP pH 7.5). During the purification of $BCAP_L$ expressed in mammalian cells, all buffers were supplemented with 50 mM NaF, 5 mM orthovanadate and 60 mM β-glycerophoaphate to inhibit endogenous phosphatases. The column was washed with 5 column volumes of nickel-NTA washing buffer (50 mM TRIS, 1000 mM NaCl, 30 mM imidazole, 1 mM TCEP pH 7.5)

and subsequently eluted on an ÄKTA FPLC system (GE Healthcare). Elution was performed with a linear gradient of 20 column volumes from nickel-NTA binding buffer to nickel-NTA elution buffer (50 mM TRIS, 250 mM NaCl, 500 mM imidazole, 1 mM TCEP pH 7.5).

For TEV protease cleavage, the eluted His-tagged protein fractions were pooled and the volume was doubled using SEC buffer (20 mM TRIS, 100 mM NaCl, 1 mM TCEP pH 7.5) to reduce the imidazole concentration. Depending on the protein concentration, 1-5 µg of purified TEV protease was added to the His-tagged protein and incubated at 4 °C for 3 h. After TEV cleavage, the protease digest was cleared using a 0.2 µm syringe filter and the sample was loaded onto a 5 ml Chelating HP column (GE Healthcare) equilibrated in SEC buffer (20 mM TRIS, 100 mM NaCl, 1 mM TCEP pH 7.5). The flowthrough was collected for subsequent size exclusion chromatography.

5.4.2 GST affinity purification

Soluble GST fusion proteins were extracted from bacterial cells and cleared as described in section 5.3.3, before loading onto 2ml of Glutathione Sepharose 4B (GE Healthcare) equilibrated in PBS. The resin was washed using 10 column volumes of PBS and thereafter eluted using GST elution buffer (50 mM TRIS, 10 mM glutathione, 1 mM TCEP pH 8.0). Where required, TEV protease cleavage was performed as described in section 5.4.1. After elution from the Glutathione Sepharose 4B or TEV protease cleavage, protein samples were pooled for size exclusion chromatography.

5.4.3 Anion exchange chromatography

Samples were concentrated using a Vivaspin concentrator (Sartorius) to reduce the volume for subsequent ten-fold dilution in anion exchange loading buffer (50 mM TRIS, 20 mM NaCl, 2 mM DTT pH 8.0). The diluted sample was then loaded onto a 1 ml Q HP column (GE Healthcare) equilibrated in anion exchange loading buffer, followed by a 10 column volumes wash with anion exchange loading buffer. The protein was eluted on an ÄKTA FPLC system (GE Healthcare) using a 20 column volumes linear gradient of anion exchange elution buffer (50 mM TRIS, 1000 mM NaCl, 2 mM DTT pH 8.0).

5.4.4 Size exclusion chromatography

Pooled fractions from previous purification steps were concentrated using appropriate Vivaspin concentrators (Sartorius) to reduce the volume to less than 3% of the size exclusion column volume. The samples were subsequently cleared by centrifugation at 16000 × g for 10 min at 4 °C. Unless stated otherwise, samples were loaded onto a HiLoad 16/600 Superdex 200 prep

grade (GE Healthcare) equilibrated with SEC buffer (20 mM TRIS, 100 mM NaCl, 1 mM TCEP pH 7.5). For $BCAP_L$, the SEC buffer was supplemented with 5% glycerol. The gel filtration was performed using an ÄKTA FPLC system (GE Healthcare) at 1 ml/min. Relevant elution fractions were analysed on SDS-PAGE.

5.5 Protein biochemical analysis

5.5.1 SDS-PAGE

Proteins were analysed by 8-15% SDS-PAGE polyacrylamide gels (Table 8). Protein samples for SDS-PAGE were denatured in 4X SDS-loading buffer (10% (w/v) SDS, 20% (v/v) glycerol, 200 mM TRIS, 0.05% (w/v) bromophenol blue, 700 mM β-mercapto-ethanol pH 6.8) and boiled for 5 min prior to loading. Electrophoresis was performed at 200 V for 1 h in running buffer (25 mM Tris, 192 mM Glycine, 0.1% (w/v) SDS pH 8.3). Gels were stained using Instant Blue Coomassie (Expedeon) where no western blot analysis was conducted.

Table 8. Materials to cast SDS-PAGE gels.

Reagent (per gel)	8-15% Resolving gel	Stacking gel
40 % Acrylamide	1 - 1.9 ml	250 µl
MilliQ water	1.75 - 2.65 ml	1.45 ml
1.0 M Tris-HCl, pH 6.8	-	250 µl
1.5 M Tris-HCl, pH 8.8	1.25 ml	-
10% SDS	50 µl	20 µl
10% Ammonium persulfate	50 µl	20 µl
TEMED	2µl	2µl

5.5.2 Native-PAGE

For native-PAGE, 6% acrylamide gels were cast using TRIS CAPS running buffer (30 mM TRIS, 10 mM CAPS pH 9.4). Samples were mixed with 5X native-PAGE sample buffer (30 mM TRIS, 10 mM CAPS, 50% glycerol, 0.01% bromophenol blue pH 9.4) before loading. Gels were run in TRIS CAPS running buffer at 100 V for 2 h.

5.5.3 Lysine methylation

Proteins for lysine methylation were dialysed in HEPES buffer (20 mM HEPES, 100 mM NaCl, 1 mM TCEP pH 7.5) overnight to avoid the presence of free TRIS buffer amines. At a protein concentration of 1 mg/ml, 20 µl of 1M Borane dimethylamine complex and 40 µl of 1M formaldehyde were added per ml of protein solution. After 2 h incubation at 4 °C, another 10 µl of 1 M Borane dimethylamine complex was added for each ml of protein solution and incubated overnight at 4 °C. The methylation was terminated by buffer exchange *via* gel filtration on a

HiLoad 16/600 Superdex 200 prep grade (GE Healthcare) equilibrated with SEC buffer (20 mM TRIS, 100 mM NaCl, 1 mM TCEP pH 7.5).

5.5.4 GST pull-down assay

GST-tagged proteins were expressed in *E. coli* and purified as described in section 5.3.1 and section 5.4. For each pull-down 100 µl of Glutathione Sepharose 4B (GE Healthcare) was equilibrated in PBS. A total of 100 µg purified GST-GRB2, GST-CRKL, GST-GRB2-SH2, GS-p85-N-SH2, GST-p85-C-SH2, GST-p85-SH3, GST-PLC-γ2-SH2-1 and GST-PLC-γ2-SH3 were loaded onto the GST resin. After washing the columns with 300 µl PBS, 50 µg $BCAP_L$ and dephosphorylated $BCAP_L$ were applied to the columns and again washed with 300 µl PBS. This was followed by three further wash steps using 500 µl PBS. The samples were eluted from the GST resin with 100 µl GST elution buffer (50 mM TRIS, 10 mM glutathione, 1 mM TCEP pH 8.0), after which the samples were analysed by SDS-PAGE.

5.5.5 *In vitro* kinase assay

For *in vitro* kinase assays, 2 µg dephosphorylated $BCAP_L$ or 100 µg dephosphorylated myelin basic protein (Active Motif) was diluted in 500 µl kinase buffer (50 mM HEPES, 10 mM $MgCl_2$, 0.01% BRIJ35, 1 mM EGTA, 150 µM ATP pH 7.5). After adding 60 pmol SYK (Thermo Fisher Scientific), LYN (Thermo Fisher Scientific), BTK (Thermo Fisher Scientific), TYK2 (Thermo Fisher Scientific), ITK (Thermo Fisher Scientific), CSNK1A1 (Thermo Fisher Scientific) or CSNK2A1 (Thermo Fisher Scientific), the samples were incubated at 30 °C for 30 min. The reaction was stopped using SDS-loading buffer and samples were analysed on western blot.

5.5.6 Filament formation assay

The MAL^{TIR} domain was expressed and purified as described in section 5.3.1 and 5.3, respectively. Starting from a stock concentration of 10 µM, MAL and various BCAP constructs were mixed at a molar ration of 1:10. The protein mixture was then incubated at 30 °C for 1 h to induce filament formation of the MAL^{TIR} domain. Soluble and insoluble fractions were separated by centrifugation at 16000 × g for 10 min, and subsequently analysed by SDS-PAGE.

5.5.7 Virotrap interaction screen

For the BCAP and eDHFR bait constructs, a T75 flask was seeded with $1x10^7$ HEK293T cells. The next day, each flask was transiently transfected with 15 µg bait plasmid DNA using PEI (Polysciences). To ensure correct bait and VSV-G expression, 7.5 µg GAG-BCAP, 5.4 µg mock vector, and 2.1 µg of a 1/2 pMD2.G - pcDNA3-FLAG-VSV-G mix, were combined with

37.5 µg PEI for transfection. After 32 h, the cellular supernatant was harvested and cleared by centrifugation at 16000 × g for 10 min. The tagged VLPs were captured by adding a total of 100 µl MyOne Streptavidin T1 beads (Thermo Fisher Scientific) pre-loaded with 10 µl anti-FLAG BioM2-Biotin antibody (Sigma-Aldrich). After 2 h incubation, the bead-particle complexes were washed with virotrap washing buffer (20 mM Tris-HCl, 150 mM NaCl pH 7.5) and were eluted with 200 µg/ml FLAG peptide (Sigma-Aldrich) in virotrap washing buffer for 30 min at 37 °C. VLPs were lysed by addition of SDS at a final concentration of 0.1%. After 5 min, SDS was removed using HiPPR Detergent Removal Spin Columns (Thermo Fisher Scientific) followed by boiling and digestion with sequence-grade trypsin (Promega). After acidification through the addition of 1 µl of 10% trifluoroacetic acid, peptides were separated by nano-LC and directly analysed with a Q Exactive instrument (Thermo Scientific) operating in MS/MS mode as described before (Stes, Laga et al. 2014). Peptide MS Searches were performed using MaxQuant (Cox and Mann 2008) against human SWISSPROT database, which was complemented with the HIV-1, EGFP, VSV-G and FLAG-VSV-G protein sequences. FDR rates were obtained as described before (Eyckerman, Titeca et al. 2016).

5.5.8 Peptide arrays binding assay

PepSPOT array membranes (JPT) were briefly washed in methanol, followed a wash with TBS. Membranes were blocked with 5% (w/v) BSA in TBS buffer supplemented with 0.05% tween 20 (TBST) for 3 h at room temperature. After blocking, the membrane was incubated with 1-5 µg of recombinant SH2 domain protein in 5% (w/v) TBST at room temperature overnight. After a brief wash with TBST, the peptide array was blotted onto a PVDF membrane in a sequential semi-dry blotting process according to the manufacturer's recommendation. PVDF membranes were then visualised by western blotting.

Membranes were regenerated by three washing steps with regeneration buffer (62.5 mM TRIS, 2% (w/v) SDS, 100 mM 2-mercaptoethanol pH 6.7) for 30 min at 50 °C. This was followed by three 20 min washes with 10X PBS, three 20 min washes with TBST and three 10 min washes with TBS after which the blotting and western blot analysis were repeated to confirm full regeneration of the peptide array.

5.6 Protein biophysical analysis

5.6.1 Protein crystallisation

Commercial crystallisation screens were set up using a Mosquito crystallisation robot (TTP Labtech). In a sitting drop format using 96-well 2-drop MRC plates (Swissci), each well contained 200 nl protein solution and 100 or 200 nl of the crystallisation condition. Plates were stored at 19 °C in a Rock Imager (Formulatrix) for daily imaging and on demand UV absorbance imaging. Table 9 provides an overview of the commercial crystallisation screens used for various constructs.

Table 9. Overview of commercial crystallisation screens.

	JCSG-plus (Molecular Dimensions)	PACT premier (Molecular Dimensions)	Wizard Classic 1 & 2 (Rigaku Reagents)	Wizard Classic 3 & 4 (Rigaku Reagents	ProPlex (Molecular Dimensions)	PEG/Ion Screen (Hampton Research)	Morpheus (Molecular Dimensions)	Additive screen (Hampton Research)
DBB-ANK396	x	x	x			x		
DBB-ANK404	x	x		x	x			x
Methylated DBB-ANK4	x	x	x			x		
TIR-DBB-ANK404	x	x		x				
Mm404	x	x	x					
DBB-ANK370	x	x		x	x	x		
DBB288	x	x	x	x	x		x	x

Manual crystallisation screens were performed in 24-well VXD plates (Hampton Research). Each well contained 500 µl of the crystallisation solution and two hanging drop crystallisation conditions. Each drop contained 1 µl protein solution and 1 or 2 µl of the respective crystallisation condition. Drops were inspected daily.

For x-ray diffraction, protein crystals were fished using CryoLoops (Hampton Research) and briefly soaked in a droplet of cryoprotectant (crystallisation condition + 25% (v/v) glycerol, unless stated otherwise) before flash freezing in liquid nitrogen.

5.6.2 Crystallographic data processing and structure determination

Both the native and anomalous datasets were indexed and scaled using *XDS* (Kabsch 2010). *Aimless* (Evans 2011) was used to convert files into the mtz binary file format. Phases from the 4 Å SAD dataset were used by the *Phaser SAD pipeline* (McCoy, Grosse-Kunstleve et al. 2007)

to generate initial phases for the 3 Å native dataset. The initial automated model building was followed up by extensive manual modelling in *Coot* (Emsley, Lohkamp et al. 2010), with iterative refinement in *Phenix.refine* (Afonine, Grosse-Kunstleve et al. 2012).

Structural protein alignments between TIG^{BCAP} and TFs were performed using *secondary-structure matching (SSM)* (Krissinel and Henrick 2004).

5.6.3 SEC-MALS

At a concentration of 2 mg/ml, samples were injected onto a Superdex 200 Increase 10/300 GL column (GE Healthcare) equilibrated in SEC buffer (20 mM TRIS, 100 mM NaCl, 1 mM TCEP pH 7.5). At a constant flow rate of 0.5 ml/min, the gel filtration was in-line with a $DAWN8^{+}$ (Wyatt technology) and an Optilab T-rEX (Wyatt technology) equipped with a multi-angle static light scattering (MALS) detector and refractometer, respectively. Data analysis was performed using ASTRA (V6.1) (Wyatt technology), using a refractive index increment value (dn/dc) of 0.185 ml/g. Protein concentrations and molecular mass determination was performed relative to a known 2 ml/ml BSA solution standard (Thermo Fisher Scientific).

5.6.4 Mass spectrometry

For mass fingerprinting, samples were run on SDS-PAGE and stained with Instant Blue Coomassie (Expedeon). Protein bands were then cut out and stored in a 5% methanol solution for further tryptic digest and MALDI-TOF mass fingerprinting at the CCPcore mass spectrometry facility (University of Cambridge, Department of Biochemistry).

Purified $BCAP_L$ for phosphopeptide mapping and digestion with trypsin and Asp-N was similarly separated on SDS-PAGE and stored in a 5% methanol solution before protease digestion of the phosphorylated band. LC-MS/MS and data analysis were performed at the CCPcore mass spectrometry facility (University of Cambridge, Department of Biochemistry). $BCAP_L$ for protease digestion with Glu-C, trypsin and chymotrypsin was separated on SDS-PAGE after which both the phosphorylated and dephosphorylated bands were excised from the gel and frozen at -20 °C. These samples were analysed by LC-MS/MS at the VIB Proteomics Core (VIB, Ghent).

5.6.5 Cryo-electron microscopy

$BCAP_L$ was expressed in EXPI293F cells and purified as described in sections 5.3.2 and 5.4, respectively. Purified $BCAP_L$ was buffer exchanged into SEC buffer (20 mM TRIS, 100 mM NaCl, 1 mM TCEP pH 7.5) and diluted to 0.1 mg/ml. Of this protein solution, 3 µl was blotted

onto graphene oxide-coated R2/1 QuantiFoil grids (Electron Microscopy Sciences) for manual back blotting and flash freezing in liquid ethane on a CP3 plunger (Gatan). Images were collected on a 150 kV JEM 1400+ (JEOL) cryo-EM. Cryo-EM sample preparation and imaging were performed in collaboration with Sander Van der Verren (VIB/VUB Brussels, Belgium).

5.7 Plasmids and antibodies

The following plasmids used for cloning and protein overexpression were generated outside our laboratory. pGEX-2T CRKL was a gift from Nora Heisterkamp (Childrens Hospital of Los Angles, USA). pGEX GRB2 SH2-SH3 was a gift from Bruce Mayer (University of Connecticut Health Center, USA). PLC-γ2-V5 was a kind gift from Marta Alarcón Riquelme (University of Granada, Spain). pMET7-GAG was obtained from, Sven Eyckerman (VIB, Belgium). tTLR4 was a gift from Roman Jerala (University of Ljubljana, Slovenia). Myc-p85α was a gift from David Fruman (University of California, USA).

Table 10. List of antibodies.

Antibody	Product Number	Vendor
Anti-FLAG-tag	F1804	Sigma-Aldrich
Anti-FLAG BioM2-Biotin	F9291	Sigma-Aldrich
Anti-Myc-tag	2276	Cell Signaling Technology
Anti-His-tag	552565	BD Bioscience
Anti-GST-tag	MA4-004	Thermo Fisher Scientific
Anti-BCAP	AF4857	R&D Systems
Anti-beta-actin	ab8226	Abcam
Anti-phosphotyrosine	ab179530	Abcam
Anti-phosphoserine	ab9332	Abcam
Anti-IgM	109-006-129	Jackson ImmunoResearch
Anti-rabbit-HRP	A0545	Sigma-Aldrich
Anti-goat-HRP	A5720	Sigma-Aldrich
Anti-mouse-HRP IgG	A9044	Sigma-Aldrich
Alexa Fluor-conjugated secondary antibody	ab150129	Abcam

6 References

Afonine, P. V., R. W. Grosse-Kunstleve, N. Echols, J. J. Headd, N. W. Moriarty, M. Mustyakimov, T. C. Terwilliger, A. Urzhumtsev, P. H. Zwart and P. D. Adams (2012). "Towards automated crystallographic structure refinement with phenix.refine." Acta Crystallogr D Biol Crystallogr **68**(Pt 4): 352-367.

Aiba, Y., M. Kameyama, T. Yamazaki, T. F. Tedder and T. Kurosaki (2008). "Regulation of B-cell development by BCAP and CD19 through their binding to phosphoinositide 3-kinase." Blood **111**(3): 1497-1503.

Aki, D., Y. Minoda, H. Yoshida, S. Watanabe, R. Yoshida, G. Takaesu, T. Chinen, T. Inaba, M. Hikida, T. Kurosaki, K. Saeki and A. Yoshimura (2008). "Peptidoglycan and lipopolysaccharide activate PLCgamma2, leading to enhanced cytokine production in macrophages and dendritic cells." Genes Cells **13**(2): 199-208.

Aksoy, E., S. Taboubi, D. Torres, S. Delbauve, A. Hachani, M. A. Whitehead, W. P. Pearce, I. M. Berenjeno, G. Nock, A. Filloux, R. Beyaert, V. Flamand and B. Vanhaesebroeck (2012). "The p110delta isoform of the kinase PI(3)K controls the subcellular compartmentalization of TLR4 signaling and protects from endotoxic shock." Nat Immunol **13**(11): 1045-1054.

Alaidarous, M., T. Ve, L. W. Casey, E. Valkov, D. J. Ericsson, M. O. Ullah, M. A. Schembri, A. Mansell, M. J. Sweet and B. Kobe (2014). "Mechanism of bacterial interference with TLR4 signaling by Brucella Toll/interleukin-1 receptor domain-containing protein TcpB." J Biol Chem **289**(2): 654-668.

Alexopoulou, L., A. C. Holt, R. Medzhitov and R. A. Flavell (2001). "Recognition of double-stranded RNA and activation of NF-kappaB by Toll-like receptor 3." Nature **413**(6857): 732-738.

Alldridge, L. C. and C. E. Bryant (2003). "Annexin 1 regulates cell proliferation by disruption of cell morphology and inhibition of cyclin D1 expression through sustained activation of the ERK1/2 MAPK signal." Experimental Cell Research **290**(1): 93-107.

Andrejeva, J., K. S. Childs, D. F. Young, T. S. Carlos, N. Stock, S. Goodbourn and R. E. Randall (2004). "The V proteins of paramyxoviruses bind the IFN-inducible RNA helicase, mda-5, and inhibit its activation of the IFN-beta promoter." Proc Natl Acad Sci U S A **101**(49): 17264-17269.

Aravind, L. and E. V. Koonin (1999). "Gleaning non-trivial structural, functional and evolutionary information about proteins by iterative database searches." J Mol Biol **287**(5): 1023-1040.

Arbibe, L., J. P. Mira, N. Teusch, L. Kline, M. Guha, N. Mackman, P. J. Godowski, R. J. Ulevitch and U. G. Knaus (2000). "Toll-like receptor 2-mediated NF-kappa B activation requires a Rac1-dependent pathway." Nat Immunol **1**(6): 533-540.

Avbelj, M., O. O. Wolz, O. Fekonja, M. Bencina, M. Repic, J. Mavri, J. Kruger, C. Scharfe, M. Delmiro Garcia, G. Panter, O. Kohlbacher, A. N. Weber and R. Jerala (2014). "Activation of lymphoma-associated MyD88 mutations via allostery-induced TIR-domain oligomerization." Blood **124**(26): 3896-3904.

Baba, Y. and T. Kurosaki (2011). "Impact of Ca2+ signaling on B cell function." Trends Immunol **32**(12): 589-594.

Bae, Y. S., H. Y. Lee, Y. S. Jung, M. Lee and P. G. Suh (2017). "Phospholipase Cgamma in Toll-like receptor-mediated inflammation and innate immunity." Adv Biol Regul **63**: 92-97.

Battersby, A., A. Csiszár, M. Leptin and R. Wilson (2003). "Isolation of Proteins that Interact with the Signal Transduction Molecule Dof and Identification of a Functional Domain Conserved between Dof and Vertebrate BCAP." Journal of Molecular Biology **329**(3): 479-493.

Bernal-Quiros, M., Y. Y. Wu, M. E. Alarcon-Riquelme and C. Castillejo-Lopez (2013). "BANK1 and BLK act through phospholipase C gamma 2 in B-cell signaling." PLoS One **8**(3): e59842.

Bernoux, M., T. Ve, S. Williams, C. Warren, D. Hatters, E. Valkov, X. Zhang, J. G. Ellis, B. Kobe and P. N. Dodds (2011). "Structural and functional analysis of a plant resistance protein TIR domain reveals interfaces for self-association, signaling, and autoregulation." Cell Host Microbe **9**(3): 200-211.

Bin, L. H., L. G. Xu and H. B. Shu (2003). "TIRP, a novel Toll/interleukin-1 receptor (TIR) domain-containing adapter protein involved in TIR signaling." J Biol Chem **278**(27): 24526-24532.

Bissig, C. and J. Gruenberg (2013). "Lipid sorting and multivesicular endosome biogenesis." Cold Spring Harb Perspect Biol **5**(10): a016816.

Bisson, N., D. A. James, G. Ivosev, S. A. Tate, R. Bonner, L. Taylor and T. Pawson (2011). "Selected reaction monitoring mass spectrometry reveals the dynamics of signaling through the GRB2 adaptor." Nat Biotechnol **29**(7): 653-658.

Bonham, K. S., M. H. Orzalli, K. Hayashi, A. I. Wolf, C. Glanemann, W. Weninger, A. Iwasaki, D. M. Knipe and J. C. Kagan (2014). "A promiscuous lipid-binding protein diversifies the subcellular sites of toll-like receptor signal transduction." Cell **156**(4): 705-716.

Bovijn, C., A. S. Desmet, I. Uyttendaele, T. Van Acker, J. Tavernier and F. Peelman (2013). "Identification of binding sites for myeloid differentiation primary response gene 88 (MyD88) and Toll-like receptor 4 in MyD88 adapter-like (Mal)." J Biol Chem **288**(17): 12054-12066.

Brehin, A. C., I. Casademont, M. P. Frenkiel, C. Julier, A. Sakuntabhai and P. Despres (2009). "The large form of human 2',5'-Oligoadenylate Synthetase (OAS3) exerts antiviral effect against Chikungunya virus." Virology **384**(1): 216-222.

Brint, E. K., D. Xu, H. Liu, A. Dunne, A. N. McKenzie, L. A. O'Neill and F. Y. Liew (2004). "ST2 is an inhibitor of interleukin 1 receptor and Toll-like receptor 4 signaling and maintains endotoxin tolerance." Nat Immunol **5**(4): 373-379.

Brown, J., H. Wang, J. Suttles, D. T. Graves and M. Martin (2011). "Mammalian target of rapamycin complex 2 (mTORC2) negatively regulates Toll-like receptor 4-mediated inflammatory response via FoxO1." J Biol Chem **286**(52): 44295-44305.

Buchan, D. W. A. and D. T. Jones (2019). "The PSIPRED Protein Analysis Workbench: 20 years on." Nucleic Acids Research.

Burke, J. E., O. Vadas, A. Berndt, T. Finegan, O. Perisic and R. L. Williams (2011). "Dynamics of the phosphoinositide 3-kinase p110delta interaction with p85alpha and membranes reveals aspects of regulation distinct from p110alpha." Structure **19**(8): 1127-1137.

Carlsson, E., J. L. Ding and B. Byrne (2016). "SARM modulates MyD88-mediated TLR activation through BB-loop dependent TIR-TIR interactions." Biochim Biophys Acta **1863**(2): 244-253.

Carpentier, S. J., M. Ni, J. M. Duggan, R. G. James, B. T. Cookson and J. A. Hamerman (2019). "The signaling adaptor BCAP inhibits NLRP3 and NLRC4 inflammasome activation in macrophages through interactions with Flightless-1." Sci Signal **12**(581).

Carty, M., R. Goodbody, M. Schroder, J. Stack, P. N. Moynagh and A. G. Bowie (2006). "The human adaptor SARM negatively regulates adaptor protein TRIF-dependent Toll-like receptor signaling." Nat Immunol **7**(10): 1074-1081.

Castello, A., M. Gaya, J. Tucholski, T. Oellerich, K. H. Lu, A. Tafuri, T. Pawson, J. Wienands, M. Engelke and F. D. Batista (2013). "Nck-mediated recruitment of BCAP to the BCR regulates the PI(3)K-Akt pathway in B cells." Nat Immunol **14**(9): 966-975.

Catrysse, L., L. Vereecke, R. Beyaert and G. van Loo (2014). "A20 in inflammation and autoimmunity." Trends Immunol **35**(1): 22-31.

Chan, S. L., T. Mukasa, E. Santelli, L. Y. Low and J. Pascual (2010). "The crystal structure of a TIR domain from Arabidopsis thaliana reveals a conserved helical region unique to plants." Protein Sci **19**(1): 155-161.

Chen, L., J. N. Glover, P. G. Hogan, A. Rao and S. C. Harrison (1998). "Structure of the DNA-binding domains from NFAT, Fos and Jun bound specifically to DNA." Nature **392**(6671): 42-48.

Cheng, Y. (2015). "Single-Particle Cryo-EM at Crystallographic Resolution." Cell **161**(3): 450-457.

Chiang, C. Y., V. Veckman, K. Limmer and M. David (2012). "Phospholipase Cgamma-2 and intracellular calcium are required for lipopolysaccharide-induced Toll-like receptor 4 (TLR4) endocytosis and interferon regulatory factor 3 (IRF3) activation." J Biol Chem **287**(6): 3704-3709.

Chu, T., M. Ni, C. Chen, S. Akilesh and J. A. Hamerman (2019). "Cutting Edge: BCAP Promotes Lupus-like Disease and TLR-Mediated Type I IFN Induction in Plasmacytoid Dendritic Cells." J Immunol **202**(9): 2529-2534.

Chuang, T. H. and R. J. Ulevitch (2004). "Triad3A, an E3 ubiquitin-protein ligase regulating Toll-like receptors." Nat Immunol **5**(5): 495-502.

Couillault, C., N. Pujol, J. Reboul, L. Sabatier, J. F. Guichou, Y. Kohara and J. J. Ewbank (2004). "TLR-independent control of innate immunity in Caenorhabditis elegans by the TIR domain adaptor protein TIR-1, an ortholog of human SARM." Nat Immunol **5**(5): 488-494.

Cox, J. and M. Mann (2008). "MaxQuant enables high peptide identification rates, individualized p.p.b.-range mass accuracies and proteome-wide protein quantification." Nat Biotechnol **26**(12): 1367-1372.

De Matteis, M. A. and A. Godi (2004). "PI-loting membrane traffic." Nat Cell Biol **6**(6): 487-492.

Deason, K., T. D. Troutman, A. Jain, D. K. Challa, R. Mandraju, T. Brewer, E. S. Ward and C. Pasare (2018). "BCAP links IL-1R to the PI3K-mTOR pathway and regulates pathogenic Th17 cell differentiation." J Exp Med **215**(9): 2413-2428.

Dick, M. S., L. Sborgi, S. Ruhl, S. Hiller and P. Broz (2016). "ASC filament formation serves as a signal amplification mechanism for inflammasomes." Nat Commun **7**: 11929.

Diebold, S. S., T. Kaisho, H. Hemmi, S. Akira and C. Reis e Sousa (2004). "Innate antiviral responses by means of TLR7-mediated recognition of single-stranded RNA." Science **303**(5663): 1529-1531.

Dodds, P. N. and J. P. Rathjen (2010). "Plant immunity: towards an integrated view of plant-pathogen interactions." Nat Rev Genet **11**(8): 539-548.

Dong, B., Q. Zhou, J. Zhao, A. Zhou, R. N. Harty, S. Bose, A. Banerjee, R. Slee, J. Guenther, B. R. Williams, T. Wiedmer, P. J. Sims and R. H. Silverman (2004). "Phospholipid scramblase 1 potentiates the antiviral activity of interferon." J Virol **78**(17): 8983-8993.

Duggan, J. M., M. B. Buechler, R. M. Olson, T. M. Hohl and J. A. Hamerman (2017). "BCAP inhibits proliferation and differentiation of myeloid progenitors in the steady state and during demand situations." Blood **129**(11): 1503-1513.

Dunne, A., M. Ejdeback, P. L. Ludidi, L. A. O'Neill and N. J. Gay (2003). "Structural complementarity of Toll/interleukin-1 receptor domains in Toll-like receptors and the adaptors Mal and MyD88." J Biol Chem **278**(42): 41443-41451.

Eijkelenboom, A. and B. M. Burgering (2013). "FOXOs: signalling integrators for homeostasis maintenance." Nat Rev Mol Cell Biol **14**(2): 83-97.

Emsley, P., B. Lohkamp, W. G. Scott and K. Cowtan (2010). "Features and development of Coot." Acta Crystallogr D Biol Crystallogr **66**(Pt 4): 486-501.

Engelman, J. A., J. Luo and L. C. Cantley (2006). "The evolution of phosphatidylinositol 3-kinases as regulators of growth and metabolism." Nat Rev Genet **7**(8): 606-619.

Engels, N., L. M. Konig, C. Heemann, J. Lutz, T. Tsubata, S. Griep, V. Schrader and J. Wienands (2009). "Recruitment of the cytoplasmic adaptor Grb2 to surface IgG and IgE provides antigen receptor-intrinsic costimulation to class-switched B cells." Nat Immunol **10**(9): 1018-1025.

Enokizono, Y., H. Kumeta, K. Funami, M. Horiuchi, J. Sarmiento, K. Yamashita, D. M. Standley, M. Matsumoto, T. Seya and F. Inagaki (2013). "Structures and interface mapping of the TIR domain-containing adaptor molecules involved in interferon signaling." Proc Natl Acad Sci U S A **110**(49): 19908-19913.

Eschenfeldt, W. H., S. Lucy, C. S. Millard, A. Joachimiak and I. D. Mark (2009). "A family of LIC vectors for high-throughput cloning and purification of proteins." Methods Mol Biol **498**: 105-115.

Essen, L. O., O. Perisic, R. Cheung, M. Katan and R. L. Williams (1996). "Crystal structure of a mammalian phosphoinositide-specific phospholipase C delta." Nature **380**(6575): 595-602.

Essuman, K., D. W. Summers, Y. Sasaki, X. Mao, A. DiAntonio and J. Milbrandt (2017). "The SARM1 Toll/Interleukin-1 Receptor Domain Possesses Intrinsic NAD(+) Cleavage Activity that Promotes Pathological Axonal Degeneration." Neuron **93**(6): 1334-1343 e1335.

Evans, P. R. (2011). "An introduction to data reduction: space-group determination, scaling and intensity statistics." Acta Crystallogr D Biol Crystallogr **67**(Pt 4): 282-292.

Eyckerman, S., K. Titeca, E. Van Quickelberghe, E. Cloots, A. Verhee, N. Samyn, L. De Ceuninck, E. Timmerman, D. De Sutter, S. Lievens, S. Van Calenbergh, K. Gevaert and J. Tavernier (2016). "Trapping mammalian protein complexes in viral particles." Nat Commun **7**: 11416.

Falasca, M., S. K. Logan, V. P. Lehto, G. Baccante, M. A. Lemmon and J. Schlessinger (1998). "Activation of phospholipase C gamma by PI 3-kinase-induced PH domain-mediated membrane targeting." EMBO J **17**(2): 414-422.

Fan, W., H. Morinaga, J. J. Kim, E. Bae, N. J. Spann, S. Heinz, C. K. Glass and J. M. Olefsky (2010). "FoxO1 regulates Tlr4 inflammatory pathway signalling in macrophages." EMBO J **29**(24): 4223-4236.

Ferrao, R., H. Zhou, Y. Shan, Q. Liu, Q. Li, D. E. Shaw, X. Li and H. Wu (2014). "IRAK4 dimerization and trans-autophosphorylation are induced by Myddosome assembly." Mol Cell **55**(6): 891-903.

Fitzgerald, K. A., E. M. Palsson-McDermott, A. G. Bowie, C. A. Jefferies, A. S. Mansell, G. Brady, E. Brint, A. Dunne, P. Gray, M. T. Harte, D. McMurray, D. E. Smith, J. E. Sims, T. A. Bird and L. A. O'Neill (2001). "Mal (MyD88-adapter-like) is required for Toll-like receptor-4 signal transduction." Nature **413**(6851): 78-83.

Fitzgerald, K. A., D. C. Rowe, B. J. Barnes, D. R. Caffrey, A. Visintin, E. Latz, B. Monks, P. M. Pitha and D. T. Golenbock (2003). "LPS-TLR4 signaling to IRF-3/7 and NF-kappaB involves the toll adapters TRAM and TRIF." J Exp Med **198**(7): 1043-1055.

Fruman, D. A. (2010). "Regulatory subunits of class IA PI3K." Curr Top Microbiol Immunol **346**: 225-244.

Gay, N. J. and F. J. Keith (1991). "Drosophila Toll and IL-1 receptor." Nature **351**(6325): 355-356.

Gay, N. J., M. F. Symmons, M. Gangloff and C. E. Bryant (2014). "Assembly and localization of Toll-like receptor signalling complexes." Nat Rev Immunol **14**(8): 546-558.

Gentle, I. E., K. T. McHenry, A. Weber, A. Metz, O. Kretz, D. Porter and G. Hacker (2017). "TIR-domain-containing adapter-inducing interferon-beta (TRIF) forms filamentous structures, whose pro-apoptotic signalling is terminated by autophagy." FEBS J **284**(13): 1987-2003.

Gerdts, J., E. J. Brace, Y. Sasaki, A. DiAntonio and J. Milbrandt (2015). "SARM1 activation triggers axon degeneration locally via NAD(+) destruction." Science **348**(6233): 453-457.

Gerdts, J., D. W. Summers, Y. Sasaki, A. DiAntonio and J. Milbrandt (2013). "Sarm1-mediated axon degeneration requires both SAM and TIR interactions." J Neurosci **33**(33): 13569-13580.

Gerke, V. and S. E. Moss (2002). "Annexins: from structure to function." Physiol Rev **82**(2): 331-371.

Gheysen, D., E. Jacobs, F. de Foresta, C. Thiriart, M. Francotte, D. Thines and M. De Wilde (1989). "Assembly and release of HIV-1 precursor Pr55gag virus-like particles from recombinant baculovirus-infected insect cells." Cell **59**(1): 103-112.

Ghosh, G., G. van Duyne, S. Ghosh and P. B. Sigler (1995). "Structure of NF-kappa B p50 homodimer bound to a kappa B site." Nature **373**(6512): 303-310.

Girardin, S. E., R. Tournebize, M. Mavris, A. L. Page, X. Li, G. R. Stark, J. Bertin, P. S. DiStefano, M. Yaniv, P. J. Sansonetti and D. J. Philpott (2001). "CARD4/Nod1 mediates NF-kappaB and JNK activation by invasive Shigella flexneri." EMBO Rep **2**(8): 736-742.

Gresset, A., S. N. Hicks, T. K. Harden and J. Sondek (2010). "Mechanism of phosphorylation-induced activation of phospholipase C-gamma isozymes." J Biol Chem **285**(46): 35836-35847.

Guven-Maiorov, E., O. Keskin, A. Gursoy and R. Nussinov (2015). "A Structural View of Negative Regulation of the Toll-like Receptor-Mediated Inflammatory Pathway." Biophys J **109**(6): 1214-1226.

Guven-Maiorov, E., O. Keskin, A. Gursoy, C. VanWaes, Z. Chen, C. J. Tsai and R. Nussinov (2015). "The Architecture of the TIR Domain Signalosome in the Toll-like Receptor-4 Signaling Pathway." Sci Rep **5**: 13128.

Hacker, H., V. Redecke, B. Blagoev, I. Kratchmarova, L. C. Hsu, G. G. Wang, M. P. Kamps, E. Raz, H. Wagner, G. Hacker, M. Mann and M. Karin (2006). "Specificity in Toll-like receptor signalling through distinct effector functions of TRAF3 and TRAF6." Nature **439**(7073): 204-207.

Hacker, H., P. H. Tseng and M. Karin (2011). "Expanding TRAF function: TRAF3 as a tri-faced immune regulator." Nat Rev Immunol **11**(7): 457-468.

Hagman, J., M. J. Gutch, H. Lin and R. Grosschedl (1995). "EBF contains a novel zinc coordination motif and multiple dimerization and transcriptional activation domains." EMBO J **14**(12): 2907-2916.

Halabi, S. (2015). Involvement of B-cell adaptor for phosphoinositide 3-kinase in modulating crosstalk between the phosphoinositide 3-kinase, toll-like receptor, and phosphoilipase C[gamma]2 signalling pathways / Samer Halabi, 2015.

Halabi, S., E. Sekine, B. Verstak, N. J. Gay and M. C. Moncrieffe (2017). "Structure of the Toll/Interleukin-1 Receptor (TIR) Domain of the B-cell Adaptor That Links Phosphoinositide Metabolism with the Negative Regulation of the Toll-like Receptor (TLR) Signalosome." J Biol Chem **292**(2): 652-660.

Hamerman, J. A., J. Pottle, M. Ni, Y. He, Z. Y. Zhang and J. H. Buckner (2016). "Negative regulation of TLR signaling in myeloid cells--implications for autoimmune diseases." Immunol Rev **269**(1): 212-227.

Hartman, A. D., A. Wilson-Weekes, A. Suvannasankha, G. S. Burgess, C. A. Phillips, K. J. Hincher, L. D. Cripe and H. S. Boswell (2006). "Constitutive c-jun N-terminal kinase activity in acute myeloid leukemia derives from Flt3 and affects survival and proliferation." Exp Hematol **34**(10): 1360-1376.

Hasan, U., C. Chaffois, C. Gaillard, V. Saulnier, E. Merck, S. Tancredi, C. Guiet, F. Briere, J. Vlach, S. Lebecque, G. Trinchieri and E. E. M. Bates (2005). "Human TLR10 Is a Functional Receptor, Expressed by B Cells and Plasmacytoid Dendritic Cells, Which Activates Gene Transcription through MyD88." The Journal of Immunology **174**(5): 2942-2950.

Hauenstein, A. V., L. Zhang and H. Wu (2015). "The hierarchical structural architecture of inflammasomes, supramolecular inflammatory machines." Curr Opin Struct Biol **31**: 75-83.

Hedrick, S. M. (2009). "The cunning little vixen: Foxo and the cycle of life and death." Nat Immunol **10**(10): 1057-1063.

Heil, F., H. Hemmi, H. Hochrein, F. Ampenberger, C. Kirschning, S. Akira, G. Lipford, H. Wagner and S. Bauer (2004). "Species-specific recognition of single-stranded RNA via toll-like receptor 7 and 8." Science **303**(5663): 1526-1529.

Hemmi, H., O. Takeuchi, T. Kawai, T. Kaisho, S. Sato, H. Sanjo, M. Matsumoto, K. Hoshino, H. Wagner, K. Takeda and S. Akira (2000). "A Toll-like receptor recognizes bacterial DNA." Nature **408**(6813): 740-745.

Horng, T., G. M. Barton and R. Medzhitov (2001). "TIRAP: an adapter molecule in the Toll signaling pathway." Nat Immunol **2**(9): 835-841.

Horng, T. and R. Medzhitov (2001). "Drosophila MyD88 is an adapter in the Toll signaling pathway." Proc Natl Acad Sci U S A **98**(22): 12654-12658.

Hornung, V., A. Ablasser, M. Charrel-Dennis, F. Bauernfeind, G. Horvath, D. R. Caffrey, E. Latz and K. A. Fitzgerald (2009). "AIM2 recognizes cytosolic dsDNA and forms a caspase-1-activating inflammasome with ASC." Nature **458**(7237): 514-518.

Hou, F., L. Sun, H. Zheng, B. Skaug, Q. X. Jiang and Z. J. Chen (2011). "MAVS forms functional prion-like aggregates to activate and propagate antiviral innate immune response." Cell **146**(3): 448-461.

Hu, Z., Q. Zhou, C. Zhang, S. Fan, W. Cheng, Y. Zhao, F. Shao, H. W. Wang, S. F. Sui and J. Chai (2015). "Structural and biochemical basis for induced self-propagation of NLRC4." Science **350**(6259): 399-404.

Huang, C. H., D. Mandelker, O. Schmidt-Kittler, Y. Samuels, V. E. Velculescu, K. W. Kinzler, B. Vogelstein, S. B. Gabelli and L. M. Amzel (2007). "The structure of a human p110alpha/p85alpha complex elucidates the effects of oncogenic PI3Kalpha mutations." Science **318**(5857): 1744-1748.

Huang, H., L. Li, C. Wu, D. Schibli, K. Colwill, S. Ma, C. Li, P. Roy, K. Ho, Z. Songyang, T. Pawson, Y. Gao and S. S. Li (2008). "Defining the specificity space of the human SRC homology 2 domain." Mol Cell Proteomics **7**(4): 768-784.

Hughes, M. M., P. Lavrencic, R. C. Coll, T. Ve, D. G. Ryan, N. C. Williams, D. Menon, A. Mansell, P. G. Board, M. Mobli, B. Kobe and L. A. J. O'Neill (2017). "Solution structure of the TLR adaptor MAL/TIRAP reveals an intact BB loop and supports MAL Cys91 glutathionylation for signaling." Proc Natl Acad Sci U S A **114**(32): E6480-E6489.

Hurley, J. H. and P. I. Hanson (2010). "Membrane budding and scission by the ESCRT machinery: it's all in the neck." Nat Rev Mol Cell Biol **11**(8): 556-566.

Hyun, K. G., Y. Lee, J. Yoon, H. Yi and J. J. Song (2016). "Crystal structure of Arabidopsis thaliana SNC1 TIR domain." Biochem Biophys Res Commun **481**(1-2): 146-152.

Inabe, K. and T. Kurosaki (2002). "Tyrosine phosphorylation of B-cell adaptor for phosphoinositide 3-kinase is required for Akt activation in response to CD19 engagement." Blood **99**(2): 584-589.

Iwasaki, A. and R. Medzhitov (2015). "Control of adaptive immunity by the innate immune system." Nat Immunol **16**(4): 343-353.

Jang, T. H. and H. H. Park (2014). "Crystal structure of TIR domain of TLR6 reveals novel dimeric interface of TIR-TIR interaction for toll-like receptor signaling pathway." J Mol Biol **426**(19): 3305-3313.

Jiang, F., A. Ramanathan, M. T. Miller, G. Q. Tang, M. Gale, Jr., S. S. Patel and J. Marcotrigiano (2011). "Structural basis of RNA recognition and activation by innate immune receptor RIG-I." Nature **479**(7373): 423-427.

Jiang, S. H., V. Athanasopoulos, J. I. Ellyard, A. Chuah, J. Cappello, A. Cook, S. B. Prabhu, J. Cardenas, J. Gu, M. Stanley, J. A. Roco, I. Papa, M. Yabas, G. D. Walters, G. Burgio, K. McKeon, J. M. Byers, C. Burrin, A. Enders, L. A. Miosge, P. F. Canete, M. Jelusic, V. Tasic, A. C. Lungu, S. I. Alexander, A. R. Kitching, D. A. Fulcher, N. Shen, T. Arsov, P. A. Gatenby, J. J. Babon, D. F. Mallon, C. de Lucas Collantes, E. A. Stone, P. Wu, M. A. Field, T. D. Andrews, E. Cho, V. Pascual, M. C. Cook and C. G. Vinuesa (2019). "Functional rare and low frequency variants in BLK and BANK1 contribute to human lupus." Nat Commun **10**(1): 2201.

Jin, M. S., S. E. Kim, J. Y. Heo, M. E. Lee, H. M. Kim, S. G. Paik, H. Lee and J. O. Lee (2007). "Crystal structure of the TLR1-TLR2 heterodimer induced by binding of a tri-acylated lipopeptide." Cell **130**(6): 1071-1082.

Jin, T., A. Perry, P. Smith, J. Jiang and T. S. Xiao (2013). "Structure of the absent in melanoma 2 (AIM2) pyrin domain provides insights into the mechanisms of AIM2 autoinhibition and inflammasome assembly." J Biol Chem **288**(19): 13225-13235.

Kabsch, W. (2010). "Integration, scaling, space-group assignment and post-refinement." Acta Crystallogr D Biol Crystallogr **66**(Pt 2): 133-144.

Kagan, J. C., V. G. Magupalli and H. Wu (2014). "SMOCs: supramolecular organizing centres that control innate immunity." Nat Rev Immunol **14**(12): 821-826.

Kagan, J. C., T. Su, T. Horng, A. Chow, S. Akira and R. Medzhitov (2008). "TRAM couples endocytosis of Toll-like receptor 4 to the induction of interferon-beta." Nat Immunol **9**(4): 361-368.

Kaiser, W. J. and M. K. Offermann (2005). "Apoptosis Induced by the Toll-Like Receptor Adaptor TRIF Is Dependent on Its Receptor Interacting Protein Homotypic Interaction Motif." The Journal of Immunology **174**(8): 4942-4952.

Kang, J. Y., X. Nan, M. S. Jin, S. J. Youn, Y. H. Ryu, S. Mah, S. H. Han, H. Lee, S. G. Paik and J. O. Lee (2009). "Recognition of lipopeptide patterns by Toll-like receptor 2-Toll-like receptor 6 heterodimer." Immunity **31**(6): 873-884.

Kaplan-Turkoz, B., T. Koelblen, C. Felix, M. P. Candusso, D. O'Callaghan, A. C. Vergunst and L. Terradot (2013). "Structure of the Toll/interleukin 1 receptor (TIR) domain of the immunosuppressive Brucella effector BtpA/Btp1/TcpB." FEBS Lett **587**(21): 3412-3416.

Katoh, Y., H. Imakagura, M. Futatsumori and K. Nakayama (2006). "Recruitment of clathrin onto endosomes by the Tom1-Tollip complex." Biochem Biophys Res Commun **341**(1): 143-149.

Kawai, T., S. Sato, K. J. Ishii, C. Coban, H. Hemmi, M. Yamamoto, K. Terai, M. Matsuda, J. Inoue, S. Uematsu, O. Takeuchi and S. Akira (2004). "Interferon-alpha induction through Toll-like receptors involves a direct interaction of IRF7 with MyD88 and TRAF6." Nat Immunol **5**(10): 1061-1068.

Kelley, L. A., S. Mezulis, C. M. Yates, M. N. Wass and M. J. Sternberg (2015). "The Phyre2 web portal for protein modeling, prediction and analysis." Nat Protoc **10**(6): 845-858.

Khan, J. A., E. K. Brint, L. A. O'Neill and L. Tong (2004). "Crystal structure of the Toll/interleukin-1 receptor domain of human IL-1RAPL." J Biol Chem **279**(30): 31664-31670.

Kloor, M., P. Bork, A. Duwe, R. Klaes, M. von Knebel Doeberitz and R. Ridder (2002). "Identification and characterization of UEV3, a human cDNA with similarities to inactive E2 ubiquitin-conjugating enzymes." Biochim Biophys Acta **1579**(2-3): 219-224.

Kobayashi, K., L. D. Hernandez, J. E. Galan, C. A. Janeway, Jr., R. Medzhitov and R. A. Flavell (2002). "IRAK-M is a negative regulator of Toll-like receptor signaling." Cell **110**(2): 191-202.

Konno, H., T. Yamamoto, K. Yamazaki, J. Gohda, T. Akiyama, K. Semba, H. Goto, A. Kato, T. Yujiri, T. Imai, Y. Kawaguchi, B. Su, O. Takeuchi, S. Akira, Y. Tsunetsugu-Yokota and J. Inoue (2009). "TRAF6 establishes innate immune responses by activating NF-kappaB and IRF7 upon sensing cytosolic viral RNA and DNA." PLoS One **4**(5): e5674.

Kowalinski, E., T. Lunardi, A. A. McCarthy, J. Louber, J. Brunel, B. Grigorov, D. Gerlier and S. Cusack (2011). "Structural basis for the activation of innate immune pattern-recognition receptor RIG-I by viral RNA." Cell **147**(2): 423-435.

Kozyrev, S. V., A. K. Abelson, J. Wojcik, A. Zaghlool, M. V. Linga Reddy, E. Sanchez, I. Gunnarsson, E. Svenungsson, G. Sturfelt, A. Jonsen, L. Truedsson, B. A. Pons-Estel, T. Witte, S. D'Alfonso, N. Barizzone, M. G. Danieli, C. Gutierrez, A. Suarez, P. Junker, H. Laustrup, M. F. Gonzalez-Escribano, J. Martin, H. Abderrahim and M. E. Alarcon-Riquelme (2008). "Functional variants in the B-cell gene BANK1 are associated with systemic lupus erythematosus." Nat Genet **40**(2): 211-216.

Krissinel, E. and K. Henrick (2004). "Secondary-structure matching (SSM), a new tool for fast protein structure alignment in three dimensions." Acta Crystallogr D Biol Crystallogr **60**(Pt 12 Pt 1): 2256-2268.

Kurosaki, T. and S. Tsukada (2000). "BLNK: connecting Syk and Btk to calcium signals." Immunity **12**(1): 1-5.

Laird, M. H., S. H. Rhee, D. J. Perkins, A. E. Medvedev, W. Piao, M. J. Fenton and S. N. Vogel (2009). "TLR4/MyD88/PI3K interactions regulate TLR4 signaling." J Leukoc Biol **85**(6): 966-977.

Latty, S. L., J. Sakai, L. Hopkins, B. Verstak, T. Paramo, N. A. Berglund, E. Cammarota, P. Cicuta, N. J. Gay, P. J. Bond, D. Klenerman and C. E. Bryant (2018). "Activation of Toll-like receptors nucleates assembly of the MyDDosome signaling hub." Elife **7**.

Li, J., T. McQuade, A. B. Siemer, J. Napetschnig, K. Moriwaki, Y. S. Hsiao, E. Damko, D. Moquin, T. Walz, A. McDermott, F. K. Chan and H. Wu (2012). "The RIP1/RIP3 necrosome forms a functional amyloid signaling complex required for programmed necrosis." Cell **150**(2): 339-350.

Liaunardy-Jopeace, A., C. E. Bryant and N. J. Gay (2014). "The COP II adaptor protein TMED7 is required to initiate and mediate the delivery of TLR4 to the plasma membrane." Sci Signal **7**(336): ra70.

Liew, F. Y., D. Xu, E. K. Brint and L. A. O'Neill (2005). "Negative regulation of toll-like receptor-mediated immune responses." Nat Rev Immunol **5**(6): 446-458.

Lin, S. C., Y. C. Lo and H. Wu (2010). "Helical assembly in the MyD88-IRAK4-IRAK2 complex in TLR/IL-1R signalling." Nature **465**(7300): 885-890.

Lin, Z., J. Lu, W. Zhou and Y. Shen (2012). "Structural insights into TIR domain specificity of the bridging adaptor Mal in TLR4 signaling." PLoS One **7**(4): e34202.

Liu, C. H., T. C. Chen, C. H. Chen, C. Y. Kao and C. Y. Huang (2013). "Differential network biology reveals a positive correlation between a novel protein-protein interaction and cancer cells migration." Conf Proc IEEE Eng Med Biol Soc **2013**: 2700-2703.

Liu, L., I. Botos, Y. Wang, J. N. Leonard, J. Shiloach, D. M. Segal and D. R. Davies (2008). "Structural basis of toll-like receptor 3 signaling with double-stranded RNA." Science **320**(5874): 379-381.

Loiarro, M., E. Volpe, V. Ruggiero, G. Gallo, R. Furlan, C. Maiorino, L. Battistini and C. Sette (2013). "Mutational analysis identifies residues crucial for homodimerization of myeloid differentiation factor 88 (MyD88) and for its function in immune cells." J Biol Chem **288**(42): 30210-30222.

Lu, A., Y. Li, F. I. Schmidt, Q. Yin, S. Chen, T. M. Fu, A. B. Tong, H. L. Ploegh, Y. Mao and H. Wu (2016). "Molecular basis of caspase-1 polymerization and its inhibition by a new capping mechanism." Nat Struct Mol Biol **23**(5): 416-425.

Lu, A., V. G. Magupalli, J. Ruan, Q. Yin, M. K. Atianand, M. R. Vos, G. F. Schroder, K. A. Fitzgerald, H. Wu and E. H. Egelman (2014). "Unified polymerization mechanism for the assembly of ASC-dependent inflammasomes." Cell **156**(6): 1193-1206.

MacFarlane, A. W. t., T. Yamazaki, M. Fang, L. J. Sigal, T. Kurosaki and K. S. Campbell (2008). "Enhanced NK-cell development and function in BCAP-deficient mice." Blood **112**(1): 131-140.

Man, S. M., L. J. Hopkins, E. Nugent, S. Cox, I. M. Gluck, P. Tourlomousis, J. A. Wright, P. Cicuta, T. P. Monie and C. E. Bryant (2014). "Inflammasome activation causes dual recruitment of NLRC4 and NLRP3 to the same macromolecular complex." Proc Natl Acad Sci U S A **111**(20): 7403-7408.

Martinez-Bueno, M., N. Oparina, M. G. Dozmorov, M. C. Marion, M. E. Comeau, G. Gilkeson, D. Kamen, M. Weisman, J. Salmon, J. W. McCune, J. B. Harley, R. Kimberly, J. A. James, J. Merrill, C. Montgomery, C. D. Langefeld and M. E. Alarcon-Riquelme (2018). "Trans-Ethnic Mapping of BANK1 Identifies Two Independent SLE-Risk Linkage Groups Enriched for Co-Transcriptional Splicing Marks." Int J Mol Sci **19**(8).

Maruoka, M., J. Suzuki, S. Kawata, K. Yoshida, N. Hirao, S. Sato, S. P. Goff, T. Takeya, K. Tani and T. Shishido (2005). "Identification of B cell adaptor for PI3-kinase (BCAP) as an Abl interactor 1-regulated substrate of Abl kinases." FEBS Lett **579**(14): 2986-2990.

Matagne, A., B. Joris and J. M. Frere (1991). "Anomalous behaviour of a protein during SDS/PAGE corrected by chemical modification of carboxylic groups." Biochem J **280 (Pt 2)**: 553-556.

Matsumura, T., M. Oyama, H. Kozuka-Hata, K. Ishikawa, T. Inoue, T. Muta, K. Semba and J. Inoue (2010). "Identification of BCAP-(L) as a negative regulator of the TLR signaling-induced production of IL-6 and IL-10 in macrophages by tyrosine phosphoproteomics." Biochem Biophys Res Commun **400**(2): 265-270.

McCoy, A. J., R. W. Grosse-Kunstleve, P. D. Adams, M. D. Winn, L. C. Storoni and R. J. Read (2007). "Phaser crystallographic software." J Appl Crystallogr **40**(Pt 4): 658-674.

Medzhitov, R., P. Preston-Hurlburt and C. A. Janeway, Jr. (1997). "A human homologue of the Drosophila Toll protein signals activation of adaptive immunity." Nature **388**(6640): 394-397.

Medzhitov, R., P. Preston-Hurlburt, E. Kopp, A. Stadlen, C. Chen, S. Ghosh and C. A. Janeway, Jr. (1998). "MyD88 is an adaptor protein in the hToll/IL-1 receptor family signaling pathways." Mol Cell **2**(2): 253-258.

Mellett, M., P. Atzei, R. Bergin, A. Horgan, T. Floss, W. Wurst, J. J. Callanan and P. N. Moynagh (2015). "Orphan receptor IL-17RD regulates Toll-like receptor signalling via SEFIR/TIR interactions." Nat Commun **6**: 6669.

Meyers, B. C., M. Morgante and R. W. Michelmore (2002). "TIR-X and TIR-NBS proteins: two new families related to disease resistance TIR-NBS-LRR proteins encoded in Arabidopsis and other plant genomes." Plant J **32**(1): 77-92.

Meylan, E., K. Burns, K. Hofmann, V. Blancheteau, F. Martinon, M. Kelliher and J. Tschopp (2004). "RIP1 is an essential mediator of Toll-like receptor 3-induced NF-kappa B activation." Nat Immunol **5**(5): 503-507.

Miggin, S. M., E. Palsson-McDermott, A. Dunne, C. Jefferies, E. Pinteaux, K. Banahan, C. Murphy, P. Moynagh, M. Yamamoto, S. Akira, N. Rothwell, D. Golenbock, K. A. Fitzgerald and L. A. O'Neill (2007). "NF-kappaB activation by the Toll-IL-1 receptor domain protein MyD88 adapter-like is regulated by caspase-1." Proc Natl Acad Sci U S A **104**(9): 3372-3377.

Monie, T. P., C. E. Bryant and N. J. Gay (2009). "Activating immunity: lessons from the TLRs and NLRs." Trends Biochem Sci **34**(11): 553-561.

Mooij, W. T., E. Mitsiki and A. Perrakis (2009). "ProteinCCD: enabling the design of protein truncation constructs for expression and crystallization experiments." Nucleic Acids Res **37**(Web Server issue): W402-405.

Mosavi, L. K., T. J. Cammett, D. C. Desrosiers and Z. Y. Peng (2004). "The ankyrin repeat as molecular architecture for protein recognition." Protein Sci **13**(6): 1435-1448.

Motshwene, P. G., M. C. Moncrieffe, J. G. Grossmann, C. Kao, M. Ayaluru, A. M. Sandercock, C. V. Robinson, E. Latz and N. J. Gay (2009). "An oligomeric signaling platform formed by the Toll-like receptor signal transducers MyD88 and IRAK-4." J Biol Chem **284**(37): 25404-25411.

Muller, C. W., F. A. Rey, M. Sodeoka, G. L. Verdine and S. C. Harrison (1995). "Structure of the NF-kappa B p50 homodimer bound to DNA." Nature **373**(6512): 311-317.

Murray, D. and B. Honig (2002). "Electrostatic control of the membrane targeting of C2 domains." Mol Cell **9**(1): 145-154.

Nandety, R. S., J. L. Caplan, K. Cavanaugh, B. Perroud, T. Wroblewski, R. W. Michelmore and B. C. Meyers (2013). "The role of TIR-NBS and TIR-X proteins in plant basal defense responses." Plant Physiol **162**(3): 1459-1472.

Ni, M., A. W. t. MacFarlane, M. Toft, C. A. Lowell, K. S. Campbell and J. A. Hamerman (2012). "B-cell adaptor for PI3K (BCAP) negatively regulates Toll-like receptor signaling through activation of PI3K." Proc Natl Acad Sci U S A **109**(1): 267-272.

Nimma, S., T. Ve, S. J. Williams and B. Kobe (2017). "Towards the structure of the TIR-domain signalosome." Curr Opin Struct Biol **43**: 122-130.

Nyman, T., P. Stenmark, S. Flodin, I. Johansson, M. Hammarstrom and P. Nordlund (2008). "The crystal structure of the human toll-like receptor 10 cytoplasmic domain reveals a putative signaling dimer." J Biol Chem **283**(18): 11861-11865.

O'Brien, R., P. Rugman, D. Renzoni, M. Layton, R. Handa, K. Hilyard, M. D. Waterfield, P. C. Driscoll and J. E. Ladbury (2000). "Alternative modes of binding of proteins with tandem SH2 domains." Protein Sci **9**(3): 570-579.

Ohnishi, H., H. Tochio, Z. Kato, K. E. Orii, A. Li, T. Kimura, H. Hiroaki, N. Kondo and M. Shirakawa (2009). "Structural basis for the multiple interactions of the MyD88 TIR domain in TLR4 signaling." Proc Natl Acad Sci U S A **106**(25): 10260-10265.

Ohto, U., K. Fukase, K. Miyake and Y. Satow (2007). "Crystal structures of human MD-2 and its complex with antiendotoxic lipid IVa." Science **316**(5831): 1632-1634.

Okada, T., A. Maeda, A. Iwamatsu, K. Gotoh and T. Kurosaki (2000). "BCAP: the tyrosine kinase substrate that connects B cell receptor to phosphoinositide 3-kinase activation." Immunity **13**(6): 817-827.

Okkenhaug, K. (2013). "Signaling by the phosphoinositide 3-kinase family in immune cells." Annu Rev Immunol **31**: 675-704.

Oshiumi, H., M. Matsumoto, K. Funami, T. Akazawa and T. Seya (2003). "TICAM-1, an adaptor molecule that participates in Toll-like receptor 3-mediated interferon-beta induction." Nat Immunol **4**(2): 161-167.

Ouyang, X., H. Negishi, R. Takeda, Y. Fujita, T. Taniguchi and K. Honda (2007). "Cooperation between MyD88 and TRIF pathways in TLR synergy via IRF5 activation." Biochem Biophys Res Commun **354**(4): 1045-1051.

Pagan, A. J., M. Pepper, H. H. Chu, J. M. Green and M. K. Jenkins (2012). "CD28 promotes CD4+ T cell clonal expansion during infection independently of its YMNM and PYAP motifs." J Immunol **189**(6): 2909-2917.

Park, B. S., D. H. Song, H. M. Kim, B. S. Choi, H. Lee and J. O. Lee (2009). "The structural basis of lipopolysaccharide recognition by the TLR4-MD-2 complex." Nature **458**(7242): 1191-1195.

Pawelczyk, T. and A. Matecki (1999). "Phospholipase C-delta3 binds with high specificity to phosphatidylinositol 4,5-bisphosphate and phosphatidic acid in bilayer membranes." Eur J Biochem **262**(2): 291-298.

Pei, J., B. H. Kim and N. V. Grishin (2008). "PROMALS3D: a tool for multiple protein sequence and structure alignments." Nucleic Acids Res **36**(7): 2295-2300.

Peng, J., Q. Yuan, B. Lin, P. Panneerselvam, X. Wang, X. L. Luan, S. K. Lim, B. P. Leung, B. Ho and J. L. Ding (2010). "SARM inhibits both TRIF- and MyD88-mediated AP-1 activation." Eur J Immunol **40**(6): 1738-1747.

Poltorak, A., X. He, I. Smirnova, M. Y. Liu, C. Van Huffel, X. Du, D. Birdwell, E. Alejos, M. Silva, C. Galanos, M. Freudenberg, P. Ricciardi-Castagnoli, B. Layton and B. Beutler (1998). "Defective LPS signaling in C3H/HeJ and C57BL/10ScCr mice: mutations in Tlr4 gene." Science **282**(5396): 2085-2088.

Rana, R. R., P. Simpson, M. Zhang, M. Jennions, C. Ukegbu, A. M. Spear, Y. Alguel, S. J. Matthews, H. S. Atkins and B. Byrne (2011). "Yersinia pestis TIR-domain protein forms dimers that interact with the human adaptor protein MyD88." Microb Pathog **51**(3): 89-95.

Rana, R. R., M. Zhang, A. M. Spear, H. S. Atkins and B. Byrne (2013). "Bacterial TIR-containing proteins and host innate immune system evasion." Med Microbiol Immunol **202**(1): 1-10.

Rao, S., X. Liu, B. D. Freedman and E. M. Behrens (2013). "Spleen tyrosine kinase (Syk)-dependent calcium signals mediate efficient CpG-induced exocytosis of tumor necrosis factor alpha (TNFalpha) in innate immune cells." J Biol Chem **288**(18): 12448-12458.

Rawlings, D. J., M. A. Schwartz, S. W. Jackson and A. Meyer-Bahlburg (2012). "Integration of B cell responses through Toll-like receptors and antigen receptors." Nat Rev Immunol **12**(4): 282-294.

Reikine, S., J. B. Nguyen and Y. Modis (2014). "Pattern Recognition and Signaling Mechanisms of RIG-I and MDA5." Front Immunol **5**: 342.

Reuten, R., D. Nikodemus, M. B. Oliveira, T. R. Patel, B. Brachvogel, I. Breloy, J. Stetefeld and M. Koch (2016). "Maltose-Binding Protein (MBP), a Secretion-Enhancing Tag for Mammalian Protein Expression Systems." PLoS One **11**(3): e0152386.

Rhee, S. H., H. Kim, M. P. Moyer and C. Pothoulakis (2006). "Role of MyD88 in phosphatidylinositol 3-kinase activation by flagellin/toll-like receptor 5 engagement in colonic epithelial cells." J Biol Chem **281**(27): 18560-18568.

Rolland, T., M. Tasan, B. Charloteaux, S. J. Pevzner, Q. Zhong, N. Sahni, S. Yi, I. Lemmens, C. Fontanillo, R. Mosca, A. Kamburov, S. D. Ghiassian, X. Yang, L. Ghamsari, D. Balcha, B. E. Begg, P. Braun, M. Brehme, M. P. Broly, A. R. Carvunis, D. Convery-Zupan, R. Corominas, J. Coulombe-Huntington, E. Dann, M. Dreze, A. Dricot, C. Fan, E. Franzosa, F. Gebreab, B. J. Gutierrez, M. F. Hardy, M. Jin, S. Kang, R. Kiros, G. N. Lin, K. Luck, A. MacWilliams, J. Menche, R. R. Murray, A. Palagi, M. M. Poulin, X. Rambout, J. Rasla, P. Reichert, V. Romero, E. Ruyssinck, J. M. Sahalie, A. Scholz, A. A. Shah, A. Sharma, Y. Shen, K. Spirohn, S. Tam, A. O. Tejeda, S. A. Trigg, J. C. Twizere, K. Vega, J. Walsh, M. E. Cusick, Y. Xia, A. L. Barabasi, L. M. Iakoucheva, P. Aloy, J. De Las Rivas, J. Tavernier, M. A. Calderwood, D. E. Hill, T. Hao, F. P. Roth and M. Vidal (2014). "A proteome-scale map of the human interactome network." Cell **159**(5): 1212-1226.

Rueda, B., P. Gourh, J. Broen, S. K. Agarwal, C. Simeon, N. Ortego-Centeno, M. C. Vonk, M. Coenen, G. Riemekasten, N. Hunzelmann, R. Hesselstrand, F. K. Tan, J. D. Reveille, S. Assassi, F. J. Garcia-Hernandez, P. Carreira, M. Camps, A. Fernandez-Nebro, P. Garcia de la Pena, T. Nearney, D. Hilda, M. A. Gonzalez-Gay, P. Airo, L. Beretta, R. Scorza, T. R. Radstake, M. D. Mayes, F. C. Arnett and J. Martin (2010). "BANK1 functional variants are associated with susceptibility to diffuse systemic sclerosis in Caucasians." **69**(4): 700-705.

Saitoh, S. (2009). "Chaperones and transport proteins regulate TLR4 trafficking and activation." Immunobiology **214**(7): 594-600.

Santos-Sierra, S., S. D. Deshmukh, J. Kalnitski, P. Kuenzi, M. P. Wymann, D. T. Golenbock and P. Henneke (2009). "Mal connects TLR2 to PI3Kinase activation and phagocyte polarization." EMBO J **28**(14): 2018-2027.

Sarkar, S. N., K. L. Peters, C. P. Elco, S. Sakamoto, S. Pal and G. C. Sen (2004). "Novel roles of TLR3 tyrosine phosphorylation and PI3 kinase in double-stranded RNA signaling." Nat Struct Mol Biol **11**(11): 1060-1067.

Sattler M., S. R. (1998). "Role of the adapter protein CRKL in signal transduction of normal hematopoietic and BCR/ABL-transformed cells." Leukemia **12**(5): 637-644.

Sborgi, L., F. Ravotti, V. P. Dandey, M. S. Dick, A. Mazur, S. Reckel, M. Chami, S. Scherer, M. Huber, A. Bockmann, E. H. Egelman, H. Stahlberg, P. Broz, B. H. Meier and S. Hiller (2015). "Structure and assembly of the mouse ASC inflammasome by combined NMR spectroscopy and cryo-electron microscopy." Proc Natl Acad Sci U S A **112**(43): 13237-13242.

Shi, J., T. Cinek, K. E. Truitt and J. B. Imboden (1997). "Wortmannin, a phosphatidylinositol 3-kinase inhibitor, blocks antigen-mediated, but not CD3 monoclonal antibody-induced, activation of murine CD4+ T cells." J Immunol **158**(10): 4688-4695.

Shi, J., Y. Zhao, K. Wang, X. Shi, Y. Wang, H. Huang, Y. Zhuang, T. Cai, F. Wang and F. Shao (2015). "Cleavage of GSDMD by inflammatory caspases determines pyroptotic cell death." Nature **526**(7575): 660-665.

Shimazu, R., S. Akashi, H. Ogata, Y. Nagai, K. Fukudome, K. Miyake and M. Kimoto (1999). "MD-2, a molecule that confers lipopolysaccharide responsiveness on Toll-like receptor 4." J Exp Med **189**(11): 1777-1782.

Singh, M. D., M. Ni, J. M. Sullivan, J. A. Hamerman and D. J. Campbell (2018). "B cell adaptor for PI3-kinase (BCAP) modulates CD8(+) effector and memory T cell differentiation." J Exp Med **215**(9): 2429-2443.

Slack, J. L., K. Schooley, T. P. Bonnert, J. L. Mitcham, E. E. Qwarnstrom, J. E. Sims and S. K. Dower (2000). "Identification of two major sites in the type I interleukin-1 receptor cytoplasmic region responsible for coupling to pro-inflammatory signaling pathways." J Biol Chem **275**(7): 4670-4678.

Snyder, G. A., D. Deredge, A. Waldhuber, T. Fresquez, D. Z. Wilkins, P. T. Smith, S. Durr, C. Cirl, J. Jiang, W. Jennings, T. Luchetti, N. Snyder, E. J. Sundberg, P. Wintrode, T. Miethke and T. S. Xiao (2014). "Crystal structures of the Toll/Interleukin-1 receptor (TIR) domains from the Brucella protein TcpB and host adaptor TIRAP reveal mechanisms of molecular mimicry." J Biol Chem **289**(2): 669-679.

Song, S., C. Chew, B. M. Dale, D. Traum, J. Peacock, T. Yamazaki, R. Clynes, T. Kurosaki and S. Greenberg (2011). "A requirement for the p85 PI3K adapter protein BCAP in the protection of macrophages from apoptosis induced by endoplasmic reticulum stress." J Immunol **187**(2): 619-625.

Songyang, Z., S. E. Shoelson, M. Chaudhuri, G. Gish, T. Pawson, W. G. Haser, F. King, T. Roberts, S. Ratnofsky, R. J. Lechleider and et al. (1993). "SH2 domains recognize specific phosphopeptide sequences." Cell **72**(5): 767-778.

Sparks, A. B., J. E. Rider, N. G. Hoffman, D. M. Fowlkes, L. A. Quillam and B. K. Kay (1996). "Distinct ligand preferences of Src homology 3 domains from Src, Yes, Abl, Cortactin, p53bp2, PLCgamma, Crk, and Grb2." Proc Natl Acad Sci U S A **93**(4): 1540-1544.

Srivastava, S., L. Di, O. Zhdanova, Z. Li, S. Vardhana, Q. Wan, Y. Yan, R. Varma, J. Backer, H. Wulff, M. L. Dustin and E. Y. Skolnik (2009). "The class II phosphatidylinositol 3 kinase C2beta is required for the activation of the K+ channel KCa3.1 and CD4 T-cells." Mol Biol Cell **20**(17): 3783-3791.

Stes, E., M. Laga, A. Walton, N. Samyn, E. Timmerman, I. De Smet, S. Goormachtig and K. Gevaert (2014). "A COFRADIC protocol to study protein ubiquitination." J Proteome Res **13**(6): 3107-3113.

Stroud, J. C., C. Lopez-Rodriguez, A. Rao and L. Chen (2002). "Structure of a TonEBP-DNA complex reveals DNA encircled by a transcription factor." Nat Struct Biol **9**(2): 90-94.

Studier, F. W. (2005). "Protein production by auto-induction in high-density shaking cultures." Protein Expression and Purification **41**(1): 207-234.

Su, D., G. M. Coudriet, D. Hyun Kim, Y. Lu, G. Perdomo, S. Qu, S. Slusher, H. M. Tse, J. Piganelli, N. Giannoukakis, J. Zhang and H. H. Dong (2009). "FoxO1 links insulin resistance to proinflammatory cytokine IL-1beta production in macrophages." Diabetes **58**(11): 2624-2633.

Summers, D. W., D. A. Gibson, A. DiAntonio and J. Milbrandt (2016). "SARM1-specific motifs in the TIR domain enable NAD+ loss and regulate injury-induced SARM1 activation." Proc Natl Acad Sci U S A **113**(41): E6271-E6280.

Thul, P. J., L. Akesson, M. Wiking, D. Mahdessian, A. Geladaki, H. Ait Blal, T. Alm, A. Asplund, L. Bjork, L. M. Breckels, A. Backstrom, F. Danielsson, L. Fagerberg, J. Fall, L. Gatto, C. Gnann, S. Hober, M. Hjelmare, F. Johansson, S. Lee, C. Lindskog, J. Mulder, C. M. Mulvey, P. Nilsson, P. Oksvold, J. Rockberg, R. Schutten, J. M. Schwenk, A. Sivertsson, E. Sjostedt, M. Skogs, C. Stadler, D. P. Sullivan, H. Tegel, C. Winsnes, C. Zhang, M. Zwahlen, A. Mardinoglu, F. Ponten, K. von Feilitzen, K. S. Lilley, M. Uhlen and E. Lundberg (2017). "A subcellular map of the human proteome." Science **356**(6340).

Toshchakov, V. U., S. Basu, M. J. Fenton and S. N. Vogel (2005). "Differential Involvement of BB Loops of Toll-IL-1 Resistance (TIR) Domain-Containing Adapter Proteins in TLR4- versus TLR2-Mediated Signal Transduction." The Journal of Immunology **175**(1): 494-500.

Treiber, N., T. Treiber, G. Zocher and R. Grosschedl (2010). "Structure of an Ebf1:DNA complex reveals unusual DNA recognition and structural homology with Rel proteins." Genes Dev **24**(20): 2270-2275.

Troutman, T. D., W. Hu, S. Fulenchek, T. Yamazaki, T. Kurosaki, J. F. Bazan and C. Pasare (2012). "Role for B-cell adapter for PI3K (BCAP) as a signaling adapter linking Toll-like receptors (TLRs) to serine/threonine kinases PI3K/Akt." Proc Natl Acad Sci U S A **109**(1): 273-278.

Vajjhala, P. R., T. Ve, A. Bentham, K. J. Stacey and B. Kobe (2017). "The molecular mechanisms of signaling by cooperative assembly formation in innate immunity pathways." Mol Immunol **86**: 23-37.

Valkov, E., A. Stamp, F. Dimaio, D. Baker, B. Verstak, P. Roversi, S. Kellie, M. J. Sweet, A. Mansell, N. J. Gay, J. L. Martin and B. Kobe (2011). "Crystal structure of Toll-like receptor adaptor MAL/TIRAP reveals the molecular basis for signal transduction and disease protection." Proc Natl Acad Sci U S A **108**(36): 14879-14884.

van Meer, G., D. R. Voelker and G. W. Feigenson (2008). "Membrane lipids: where they are and how they behave." Nat Rev Mol Cell Biol **9**(2): 112-124.

Vanhaesebroeck, B., J. Guillermet-Guibert, M. Graupera and B. Bilanges (2010). "The emerging mechanisms of isoform-specific PI3K signalling." Nat Rev Mol Cell Biol **11**(5): 329-341.

Ve, T., P. R. Vajjhala, A. Hedger, T. Croll, F. DiMaio, S. Horsefield, X. Yu, P. Lavrencic, Z. Hassan, G. P. Morgan, A. Mansell, M. Mobli, A. O'Carroll, B. Chauvin, Y. Gambin, E. Sierecki, M. J. Landsberg, K. J. Stacey, E. H. Egelman and B. Kobe (2017). "Structural basis of TIR-domain-assembly formation in MAL- and MyD88-dependent TLR4 signaling." Nat Struct Mol Biol **24**(9): 743-751.

Venerando, A., M. Ruzzene and L. A. Pinna (2014). "Casein kinase: the triple meaning of a misnomer." Biochem J **460**(2): 141-156.

Verstak, B., C. J. Arnot and N. J. Gay (2013). "An alanine-to-proline mutation in the BB-loop of TLR3 Toll/IL-1R domain switches signalling adaptor specificity from TRIF to MyD88." J Immunol **191**(12): 6101-6109.

Vyncke, L., C. Bovijn, E. Pauwels, T. Van Acker, E. Ruyssinck, E. Burg, J. Tavernier and F. Peelman (2016). "Reconstructing the TIR Side of the Myddosome: a Paradigm for TIR-TIR Interactions." Structure **24**(3): 437-447.

Waldhuber, A., G. A. Snyder, F. Rommler, C. Cirl, T. Muller, T. S. Xiao, C. Svanborg and T. Miethke (2016). "A Comparative Analysis of the Mechanism of Toll-Like Receptor-Disruption by TIR-Containing Protein C from Uropathogenic Escherichia coli." Pathogens **5**(1).

Walter, T. S., C. Meier, R. Assenberg, K. F. Au, J. Ren, A. Verma, J. E. Nettleship, R. J. Owens, D. I. Stuart and J. M. Grimes (2006). "Lysine methylation as a routine rescue strategy for protein crystallization." Structure **14**(11): 1617-1622.

Wang, C., L. Deng, M. Hong, G. R. Akkaraju, J. Inoue and Z. J. Chen (2001). "TAK1 is a ubiquitin-dependent kinase of MKK and IKK." Nature **412**(6844): 346-351.

Weis, W. I., M. E. Taylor and K. Drickamer (1998). "The C-type lectin superfamily in the immune system." Immunol Rev **163**: 19-34.

West, A. P., G. S. Shadel and S. Ghosh (2011). "Mitochondria in innate immune responses." Nat Rev Immunol **11**(6): 389-402.

Williams, S. J., K. H. Sohn, L. Wan, M. Bernoux, P. F. Sarris, C. Segonzac, T. Ve, Y. Ma, S. B. Saucet, D. J. Ericsson, L. W. Casey, T. Lonhienne, D. J. Winzor, X. Zhang, A. Coerdt, J. E. Parker, P. N. Dodds, B. Kobe and J. D. Jones (2014). "Structural basis for assembly and function of a heterodimeric plant immune receptor." Science **344**(6181): 299-303.

Wong, Y. H., T. Y. Lee, H. K. Liang, C. M. Huang, T. Y. Wang, Y. H. Yang, C. H. Chu, H. D. Huang, M. T. Ko and J. K. Hwang (2007). "KinasePhos 2.0: a web server for identifying protein kinase-specific phosphorylation sites based on sequences and coupling patterns." Nucleic Acids Res **35**(Web Server issue): W588-594.

Wu, J., L. Sun, X. Chen, F. Du, H. Shi, C. Chen and Z. J. Chen (2013). "Cyclic GMP-AMP is an endogenous second messenger in innate immune signaling by cytosolic DNA." Science **339**(6121): 826-830.

Wu, Y. Y., R. Kumar, M. S. Haque, C. Castillejo-Lopez and M. E. Alarcon-Riquelme (2013). "BANK1 controls CpG-induced IL-6 secretion via a p38 and MNK1/2/eIF4E translation initiation pathway." J Immunol **191**(12): 6110-6116.

Wu, Y. Y., R. Kumar, R. Iida, H. Bagavant and M. E. Alarcon-Riquelme (2016). "BANK1 Regulates IgG Production in a Lupus Model by Controlling TLR7-Dependent STAT1 Activation." PLoS One **11**(5): e0156302.

Xu, H., X. He, H. Zheng, L. J. Huang, F. Hou, Z. Yu, M. J. de la Cruz, B. Borkowski, X. Zhang, Z. J. Chen and Q. X. Jiang (2014). "Structural basis for the prion-like MAVS filaments in antiviral innate immunity." Elife **3**: e01489.

Xu, Y., X. Tao, B. Shen, T. Horng, R. Medzhitov, J. L. Manley and L. Tong (2000). "Structural basis for signal transduction by the Toll/interleukin-1 receptor domains." Nature **408**(6808): 111-115.

Yamamoto, M., S. Sato, H. Hemmi, S. Uematsu, K. Hoshino, T. Kaisho, O. Takeuchi, K. Takeda and S. Akira (2003). "TRAM is specifically involved in the Toll-like receptor 4-mediated MyD88-independent signaling pathway." Nat Immunol **4**(11): 1144-1150.

Yamamoto, M., S. Sato, K. Mori, K. Hoshino, O. Takeuchi, K. Takeda and S. Akira (2002). "Cutting Edge: A Novel Toll/IL-1 Receptor Domain-Containing Adapter That Preferentially Activates the IFN- Promoter in the Toll-Like Receptor Signaling." The Journal of Immunology **169**(12): 6668-6672.

Yamazaki, T. and T. Kurosaki (2003). "Contribution of BCAP to maintenance of mature B cells through c-Rel." Nat Immunol **4**(8): 780-786.

Yamazaki, T., K. Takeda, K. Gotoh, H. Takeshima, S. Akira and T. Kurosaki (2002). "Essential immunoregulatory role for BCAP in B cell development and function." J Exp Med **195**(5): 535-545.

Yokoyama, K., I. H. Su Ih, T. Tezuka, T. Yasuda, K. Mikoshiba, A. Tarakhovsky and T. Yamamoto (2002). "BANK regulates BCR-induced calcium mobilization by promoting tyrosine phosphorylation of IP(3) receptor." EMBO J **21**(1-2): 83-92.

Yoneyama, M., M. Kikuchi, T. Natsukawa, N. Shinobu, T. Imaizumi, M. Miyagishi, K. Taira, S. Akira and T. Fujita (2004). "The RNA helicase RIG-I has an essential function in double-stranded RNA-induced innate antiviral responses." Nat Immunol **5**(7): 730-737.

Yoon, S. I., O. Kurnasov, V. Natarajan, M. Hong, A. V. Gudkov, A. L. Osterman and I. A. Wilson (2012). "Structural basis of TLR5-flagellin recognition and signaling." Science **335**(6070): 859-864.

Yu, J., C. Wjasow and J. M. Backer (1998). "Regulation of the p85/p110alpha phosphatidylinositol 3'-kinase. Distinct roles for the n-terminal and c-terminal SH2 domains." J Biol Chem **273**(46): 30199-30203.

Yu, Q., K. Qu and Y. Modis (2018). "Cryo-EM Structures of MDA5-dsRNA Filaments at Different Stages of ATP Hydrolysis." Mol Cell **72**(6): 999-1012 e1016.

Zanoni, I., R. Ostuni, L. R. Marek, S. Barresi, R. Barbalat, G. M. Barton, F. Granucci and J. C. Kagan (2011). "CD14 controls the LPS-induced endocytosis of Toll-like receptor 4." Cell **147**(4): 868-880.

Zhang, L., S. Chen, J. Ruan, J. Wu, A. B. Tong, Q. Yin, Y. Li, L. David, A. Lu, W. L. Wang, C. Marks, Q. Ouyang, X. Zhang, Y. Mao and H. Wu (2015). "Cryo-EM structure of the activated NAIP2-NLRC4 inflammasome reveals nucleated polymerization." Science **350**(6259): 404-409.

Zhang, X., M. Bernoux, A. R. Bentham, T. E. Newman, T. Ve, L. W. Casey, T. M. Raaymakers, J. Hu, T. I. Croll, K. J. Schreiber, B. J. Staskawicz, P. A. Anderson, K. H. Sohn, S. J. Williams, P. N. Dodds and B. Kobe (2017). "Multiple functional self-association interfaces in plant TIR domains." Proc Natl Acad Sci U S A **114**(10): E2046-E2052.

7 Acknowledgements

I am thankful to AstraZeneca for the generous PhD studentship and the excellent scientific support from Jon Read and David Fisher.

I would like to thank Nick for giving me all the space and scientific freedom I could have hoped for.

Thanks to the members of the lab for helping with numerous experiments and scientific discussions.

But most of all, thanks to Amanda for believing in me, and making the last few years one big exciting adventure.

8 Appendix

Appendix Table 1. KinasePhos CSNK2 prediction BCAP of phosphorylation.

Position	Target Residue	Kinase	Sequence	SVM score
52	S	CSNK2	GPEA**S**FSAE	0.562
54	S	CSNK2	EASF**S**AEDL	0.879
72	S	CSNK2	VVLL**S**AELV	0.549
149	S	CSNK2	SGCD**S**VTDT	0.586
213	S	CSNK2	EAEF**S**PEDS	0.887
592	S	CSNK2	RPQS**S**IYDP	0.730
720	S	CSNK2	TDST**S**STAS	0.653
740	S	CSNK2	LSVS**S**GMEG	0.895

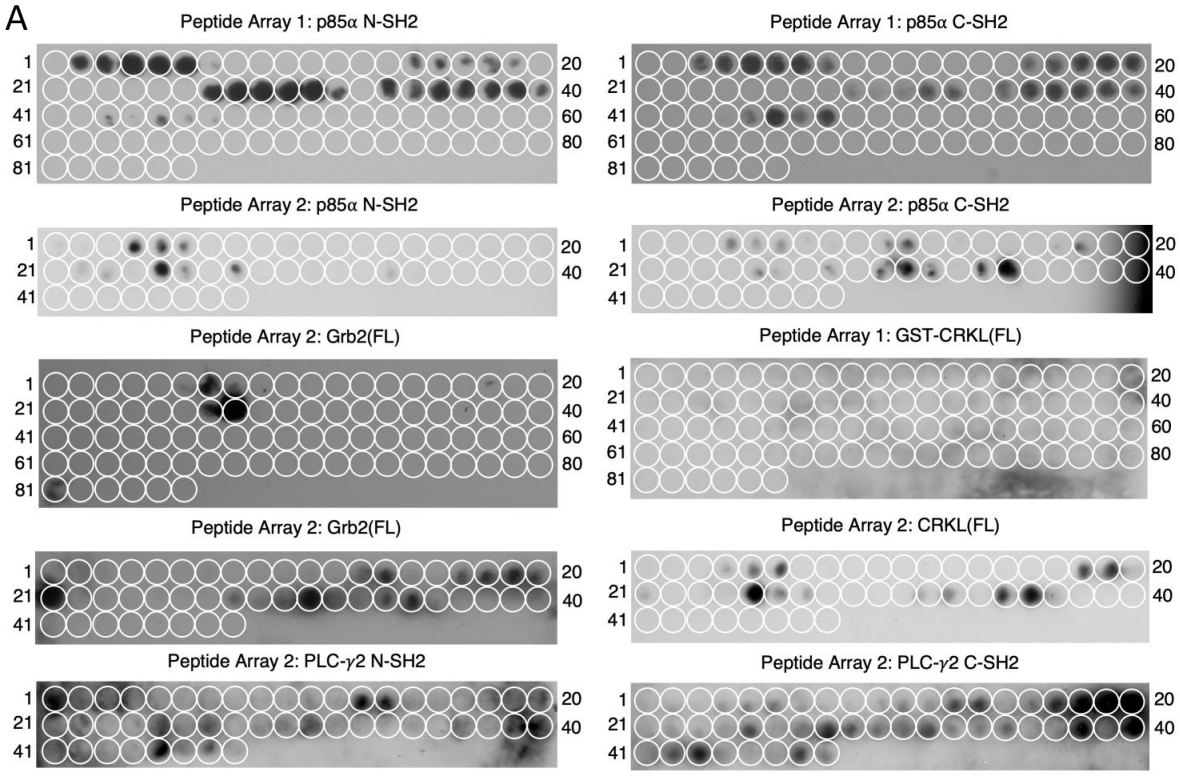

B Peptide Array 1

1 KHGFRDLRQFIDE-pY-V	23 LSTDLLMKCSLNPGC	45 ETVISY-pY-TDMEEIGN	67 LNPGCDEDLYESMAA
2 GFRDLRQFIDE-pY-VET	24 TDLLMKCSLNPGCDE	46 VCETVISY-pY-TDMEEI	68 PGCDEDLYESMAAFV
3 RDLRQFIDE-pY-VETVD	25 LLMKCSLNPGCDEDL	47 SY-pY-TDMEEIGNLLSN	69 CDEDLYESMAAFVPA
4 LRQFIDE-pY-VETVDML	26 MKCSLNPGCDEDL-pY-E	48 -pY-YTDMEEIGNLLSNAA	70 EDLYESMAAFVPAAT
5 QFIDE-pY-VETVDMLKS	27 CSLNPGCDEDL-pY-ESM	49 DMEEIGNLLSNAANP	71 LYESMAAFVPAATED
6 IDE-pY-VETVDMLKSHI	28 LNPGCDEDL-pY-ESMAA	50 KHGFRDLRQFIDEYV	72 ESMAAFVPAATEDLY
7 E-pY-VETVDMLKSHIKE	29 PGCDEDL-pY-ESMAAFV	51 GFRDLRQFIDEYVET	73 MAAFVPAATEDLYVE
8 VETVDMLKSHIKEEL	30 CDEDL-pY-ESMAAFVPA	52 RDLRQFIDEYVETVD	74 AFVPAATEDLYVEML
9 TVDMLKSHIKEELMH	31 EDL-pY-ESMAAFVPAAT	53 LRQFIDEYVETVDML	75 VPAATEDLYVEMLQA
10 DMLKSHIKEELMHGE	32 L-pY-ESMAAFVPAATED	54 QFIDEYVETVDMLKS	76 AATEDLYVEMLQAST
11 LKSHIKEELMHGEEA	33 ESMAAFVPAATEDL-pY-	55 IDEYVETVDMLKSHI	77 TEDLYVEMLQASTSN
12 SHIKEELMHGEEADA	34 MAAFVPAATEDL-pY-VE	56 EYVETVDMLKSHIKE	78 DLYVEMLQASTSNPI
13 IKEELMHGEEADAV-pY-	35 AFVPAATEDL-pY-VEML	57 IKEELMHGEEADAVY	79 YVEMLQASTSNPIPG
14 EELMHGEEADAV-pY-ES	36 VPAATEDL-pY-VEMLQA	58 EELMHGEEADAVYES	80 GDLVVCETVISYYTD
15 LMHGEEADAV-pY-ESMA	37 AATEDL-pY-VEMLQAST	59 LMHGEEADAVYESMA	81 LVVCETVISYYTDME
16 HGEEADAV-pY-ESMAHL	38 TEDL-pY-VEMLQASTSN	60 HGEEADAVYESMAHL	82 VCETVISYYTDMEEI
17 EEADAV-pY-ESMAHLST	39 DL-pY-VEMLQASTSNPI	61 EEADAVYESMAHLST	83 ETVISYYTDMEEIGN
18 ADAV-pY-ESMAHLSTDL	40 -pY-VEMLQASTSNPIPG	62 ADAVYESMAHLSTDL	84 VISYYTDMEEIGNLL
19 AV-pY-ESMAHLSTDLLM	41 EMLQASTSNPIPGDG	63 AVYESMAHLSTDLLM	85 SYYTDMEEIGNLLSN
20 -pY-ESMAHLSTDLLMKC	42 GDLVVCETVISY-pY-TD	64 YESMAHLSTDLLMKC	86 YTDMEEIGNLLSNAA
21 SMAHLSTDLLMKCSL	43 LVVCETVISY-pY-TDME	65 MKCSLNPGCDEDLYE	
22 AHLSTDLLMKCSLNP	44 VCETVISY-pY-TDMEEI	66 CSLNPGCDEDLYESM	

Peptide Array 2

1 IRCGAETTV-pY-VIVRC	13 PTLLHFAAK-pY-GLKNL	25 AHQLPDNEP-pY-IFKVF	37 GAETTVYVIVRCKLD
2 GAETTV-pY-VIVRCKLD	14 HFAAK-pY-GLKNLTALL	26 LPDNEP-pY-IFKVFAEK	38 KVENEYTISVKAPNL
3 TV-pY-VIVRCKLDDRVA	15 AK-pY-GLKNLTALLLTC	27 EP-pY-IFKVFAEKSQER	39 NVSLKIYSGDLVVCE
4 RMEAKVENE-pY-TISVK	16 LTCPGALQA-pY-SVANK	28 KSQERPGNF-pY-VSSES	40 AFKIVPYNTETLDKL
5 KVENE-pY-TISVKAPNL	17 PGALQA-pY-SVANKHGH	29 ERPGNF-pY-VSSESIRK	41 HFAAKYGLKNLTALL
6 NE-pY-TISVKAPNLSSG	18 QA-pY-SVANKHGHYPNT	30 NF-pY-VSSESIRKGPPV	42 PGALQAYSVANKHGH
7 SSGNVSLKI-pY-SGDLV	19 YSVANKHGH-pY-PNTIA	31 WRDRPQSSI-pY-DPFAG	43 ANKHGHYPNTIAEKH
8 NVSLKI-pY-SGDLVVCE	20 ANKHGH-pY-PNTIAEKH	32 RPQSSI-pY-DPFAGMKT	44 GQEEDVYHTVDDDEA
9 KI-pY-SGDLVVCETVIS	21 GH-pY-PNTIAEKHGFRD	33 SI-pY-DPFAGMKTPGQR	45 LPDNEPYIFKVFAEK
10 MCQAFKIVP-pY-NTETL	22 CHLGQEEDV-pY-HTVDD	34 LPAKVEFGV-pY-ESGPR	46 ERPGNFYVSSESIRK
11 AFKIVP-pY-NTETLDKL	23 GQEEDV-pY-HTVDDDEA	35 KVEFGV-pY-ESGPRKSV	47 RPQSSIYDPFAGMKT
12 VP-pY-NTETLDKLLTES	24 DV-pY-HTVDDDEAFSVD	36 GV-pY-ESGPRKSVIPPR	48 KVEFGVYESGPRKSV

Appendix Figure 1. Overview of peptide array results.

(A) Peptide arrays were incubated with 1-5 µg of recombinant SH2 domain protein as indicated. Protein binding was visualised by immunoblotting with ANTI-GST antibody. (B) Sequence overview of peptide arrays used in (A).

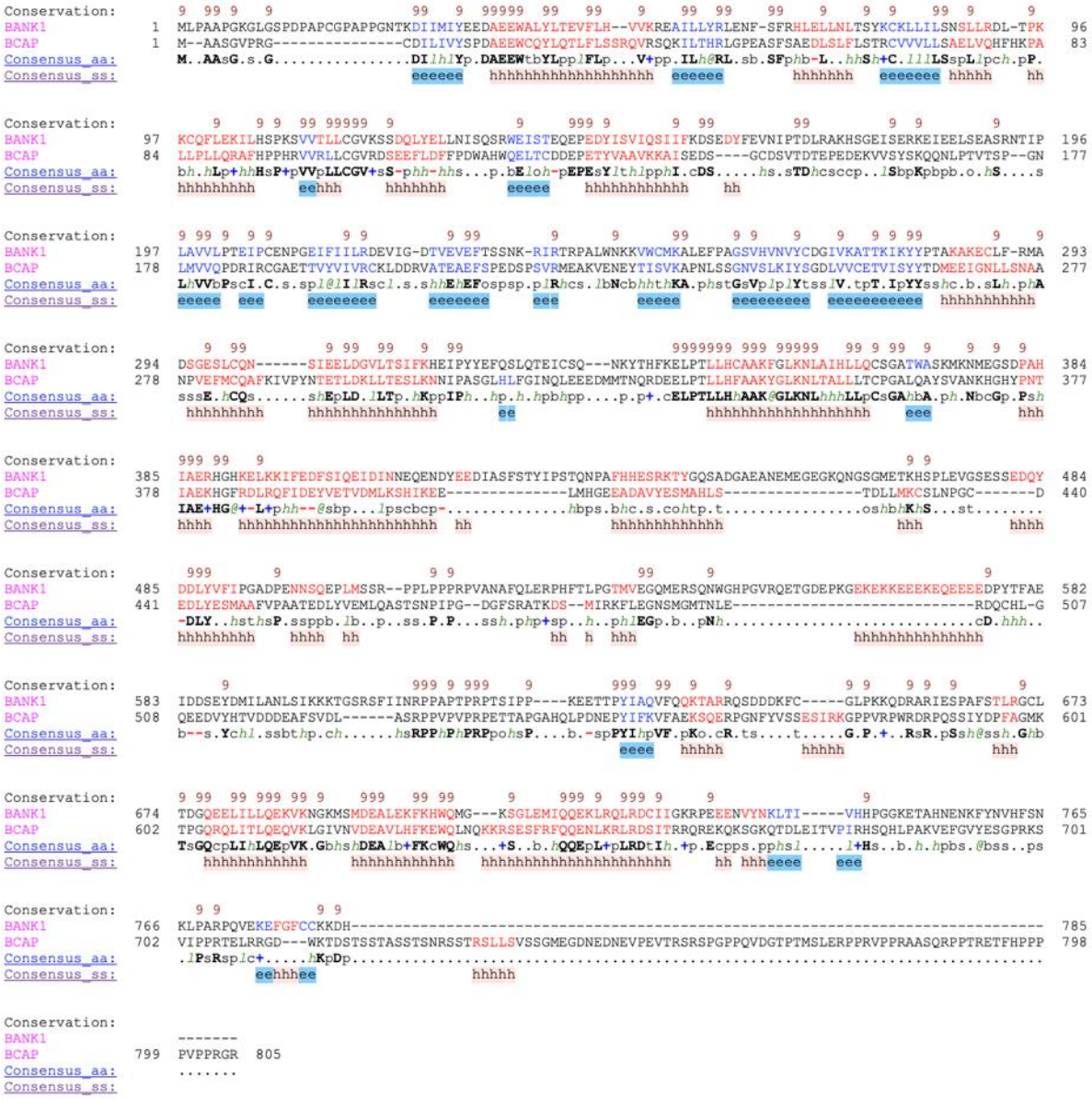

Appendix Figure 2. Secondary structure-based sequence alignment of BCAP and BANK1 illustrates a similar domain architecture.

PROMALS3D (Pei, Kim et al. 2008) secondary structure alignment of BCAP and BANK1. α-Helix and β-strand signatures are coloured in red and blue, respectively. Conserved secondary structure elements are indicated by a 'e' for β-strands and 'h' for α-helices. Amino acids conservation is indicated by a range of symbols ranging from a '.' for no conservation to capitalised and bold letters for sequence identity.